Biological Applications of Weak Polyelectrolyte Multilayers

by

Michael C. Berg

B.S., Chemical Engineering
Virginia Polytechnic Institute and State University, 2000

SUBMITTED TO THE CHEMICAL ENGINEERING DEPARTMENT IN PARTIAL FULFILLMENT OF THE REQUIREMENTS FOR THE DEGREE OF

Doctor of Philosophy in Chemical Engineering

at the
MASSACHUSETTS INSTITUTE OF TECHNOLOGY

MARCH 2005
[June 2005]

Signature of Author: _____
Chemical Engineering Department
March 8, 2005

Certified by: _____
Paula T. Hammond
Professor of Chemical Engineering
Thesis Supervisor

Certified by: _____
Michael F. Rubner
Professor of Materials Science and Engineering
Thesis Supervisor

Accepted by: _____
Daniel Blankschtein
Professor of Chemical Engineering
Chairman, Committee for Graduate Students

Biological Applications of Weak Polyelectrolyte Multilayers

by

Michael C. Berg

Submitted to the Chemical Engineering Department
On February 1, 2005 in Partial Fulfillment of the
Requirements for the Degree of Doctor of Philosophy
in Chemical Engineering

ABSTRACT

This thesis research focused on biological applications of ultra-thin weak polyelectrolyte multilayers with specific emphasis on cell patterning, drug delivery, and antibacterial coatings. All of these very different applications were studied using three different polymers – polyacrylic acid (PAA), poly(allylamine hydrochloride) (PAH), polyacrylamide (PAAm).

The first part of this thesis focuses on patterning polyelectrolyte multilayers found to resist mammalian cell adhesion, with ligands that promote specific interactions for adhesion. It was found that by patterning PAH on polyelectrolyte multilayers, the patterned functional group density and thickness could be tuned through ink pH adjustment. By changing the surface density of amine groups in the PAH patterns, the ligand density could also be altered using specific chemistry to attach peptides containing the tri-peptide sequence, RGD, which is known to promote cell adhesion in a number of cell types. The RGD density in the patterned regions determined the number of cells attached and the amount of cytoskeletal protein organization.

The second part is an evaluation of porous polyelectrolyte multilayers as a delivery system for controlled release of small molecule drugs. The loading and releasing properties of porous PAH/PAA multilayers were investigated using the two drugs, ketoprofen and cytochalasin D. It was determined that the amount of drug released was proportional to the number of porous layers. Nanoporous films showed zero-order release, whereas microporous films displayed Fickian diffusion. The efficacy of the released drugs was checked by monitoring the effect of released cytochalasin D on fibroblasts' division.

In the final part of this thesis, the antibacterial properties of both silver-loaded polyelectrolyte multilayers and superhydrophobic multilayers are examined. It was found that silver loaded multilayers killed bacteria to an extent greater than 99.99% for both airborne and waterborne models. Superhydrophobic films showed excellent anti-fouling properties for proteins, mammalian cells, and bacteria.

Thesis Supervisors: Paula T. Hammond, Associate Professor of Chemical Engineering
Michael F. Rubner, TDK Professor of Polymer Materials Science and Engineering

TABLE OF CONTENTS

LIST OF FIGURES AND TABLES

ACKNOWLEDGEMENTS

First, I would like to thank my thesis advisors, Prof. Paula T. Hammond and Prof. Michael F. Rubner. I have learned a great deal from both, and have become a much better scientist and writer by being a part of their research groups. Both gave me room to grow and come up with my own ideas, but were always there to help at the right time. I enjoyed working with both over my time at MIT, and have always felt that their personalities made my research not only interesting and rewarding, but a great deal of fun. Paula's warmth and friendliness always gave me confidence even when research was not going so well, and Michael's enthusiasm and energy made me feel like I could do anything.

I also would like to thank the rest of my thesis committee, Prof. Robert E. Cohen and Prof. James L. Sherley. Bob's helpfulness and good humor made me feel always welcome in his office. James's expertise made him a valuable resource especially with any "biology" questions, and he made me feel like I was a part of his group.

I would not have been able to complete this thesis without the help and support of my past and current fellow lab members. I would like to thank the Hammond group: Dr. Mitch Anthamatten, Dr. Dean Delongchamp, Dr. Dave Dewitt, Dr. Tarek Farhat, Shoshana Gourdin, LaShanda James-Korley, Dr. Xuiping Jiang, Mark Johnson, Heejae Kim, Ilsoon Lee, Dr. Geoff Lowman, Jodie Lutkenhaus, LaRuth McAfee, Andy Miller, Phuong Nguyen, Juhyun Park, Greg Pollock, Dr. Cathy Santini, Kris Stokes, Marriane Terrot, Dr. Lu Tian, Dr. Hiro Tokuhisa, Dr. Kris van Hege, Eric Verploegen, Ryan Waletko, Kris Wood, Dr. J.-S. Wu, Dr. Pil Yoo, Dr. Bruce Yu, Nicole Zacharia, and Dr. Haipeng Zheng. From the Rubner group, I would like to thank Dr. Hyunku Ahn, Fevzi Cebeci, Dr. Jeeyoung Choi, Anita Chung, Dr. Jeri'ann Hiller, Koji Itano, Daeyeon Lee, Dr. Zifeng Li, Dr. Jonas Mendelsohn, Dr. Takehiro Nishikawa, Adam Nolte, Prof. Masahiro Rikukawa, Dr. Hartmut Ruddman, Dr. Saturo Shimada, Dr. Nobuaki Takane, Dr. Tom Wang, Aleks White, Dr. Zhizoung Wu, Dr. Sung Yun Yang, Dr. Lei Zhai, Toshi, , Xiaxio In addition, I would like to thank the undergraduates that I had the pleasure to work with: Danielle Jensen, Yushan Kim, and Jack Milwid. In addition to my fellow group members in the Hammond and Rubner labs, I would also like to thank the Griffith lab, especially Ada Au, Lily Koo, Ley Richardson, and Kirsty Smith for their help and advice with cell culture. In addition, thanks to Dr. Shuguang Zhang and Dr. Carlos Semino for space to perform cell culture. The research in this thesis would also have not been possible without funding from the DuPont-MIT Alliance (DMA).

I would also like to thank my friends and fellow graduate students at MIT that shared a lot of good times over the years and quite a few pints of Guinness: Brian Baynes, Steve Fox, Kyle Jensen, Jeremy Johnson, Kathyrn Miller, Joe Moritz, Prem Pavoor, Mike Raab, Greg Randall, and Greg Zugates. Also, I would like to thank all of my friends from Delaware and Virginia Tech including Pri Chakkavarthi, Joe Fulcher, Adam Gayzik, Erik Johnson, Monte Marcum, Todd Smith, John Reynolds, Jason Soules, and Brad Turner. In addition, I would like to thank the Philadelphia Eagles, Flyers, Phillies, and Sixers for inspiring me to strive for excellence.

Finally and most importantly, this thesis would not have been possible without the love and support of my family. My parents, Donna and Cliff Berg, and my sister, Jennifer Berg, have always been there for me and believed in me. I would especially like to thank Janice Lansita for her love and support over the last few years; I could not have made it through without her.

Chapter 1 Introduction

1.1. Introductory Remarks

Polyelectrolyte multilayers have become a very highly studied class of materials over the past decade. This chapter serves to introduce important concepts about these thin polymer films before delving into the applications explored in this thesis. First, an overview of layer-by-layer polyelectrolyte multilayers will be presented, which will focus on the development of the research area and important concepts in the field. Second, the importance of a subset of these materials, weak polyelectrolyte multilayers, will be examined. Particular interest will be paid to the effect of assembly pH along with applications of these films, especially the use of polyelectrolyte multilayers as biomaterials. The emphasis of this discussion will be on relevant background information for the applications discussed in later chapters of this thesis. Finally, the objectives and outline of this thesis will be presented. In addition to this background section, each chapter has its own introduction that will give a more specific background to the specific subject matter of the chapter.

1.2. General Introduction

1.2.1. Layer-by-Layer Polyelectrolyte Multilayers

Since polyelectrolyte multilayers were first introduced by Decher et al. over a decade ago[1, 2], the amount of interest paid to these ultra-thin polymer films has grown exponentially.

The major reasons for this interest are their ease of processing, variety of materials which can be incorporated into their assembly, and the versatility of the technique. Polyelectrolyte multilayers are assembled using a layer-by-layer assembly process that is shown graphically in Figure 1-1. In a typical process, a substrate is dipped into the first polyelectrolyte solution for a long enough time to allow the polyelectrolyte to adsorb to the surface. After rinsing off loosely bound polymer, the substrate is then dipped into a polyelectrolyte solution of opposite charge. This second polyelectrolyte adsorbs to the surface due to electrostatic attraction and actually overcompensates for the surface charge[3] resulting in a reversal of the surface charge. The process is repeated until the desired number of layers is deposited. Each step results in a reversal of surface charge allowing the next layer to be deposited. The multilayers can be applied using any method that allows the polyelectrolyte solution to come into contact with the substrate, with the most common methods including dip-coating[1], deposition on colloids[4], or spin-coating[5, 6].

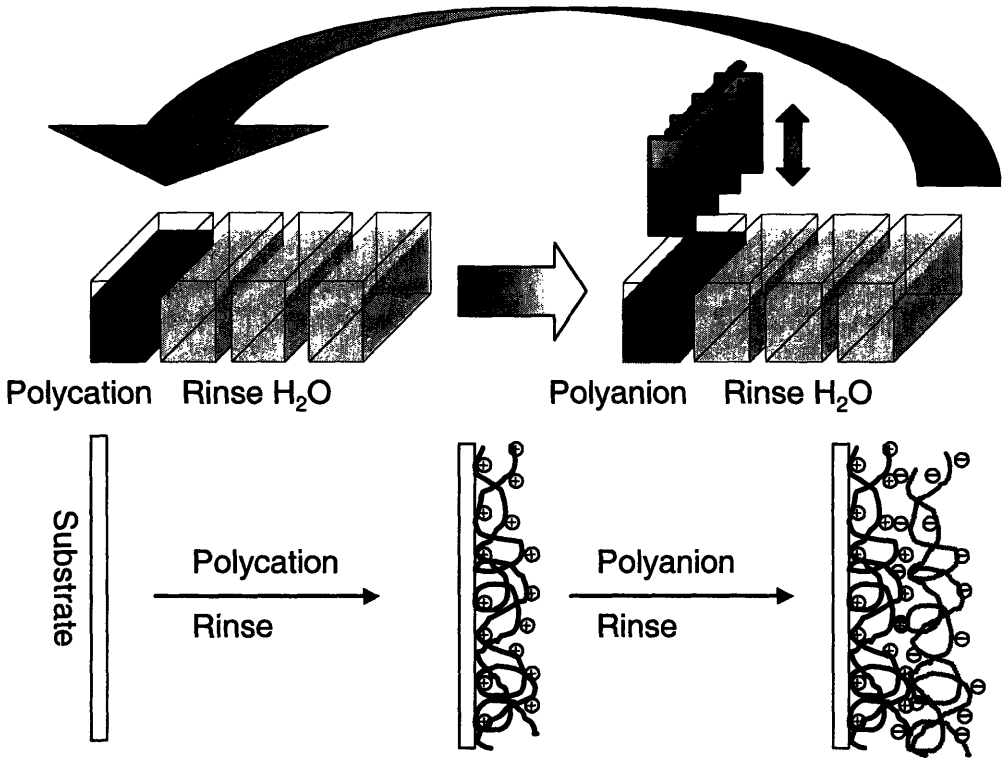

Figure 1-1. Assembly process for layer-by-layer polyelectrolyte multilayer films formed by alternately dipping a substrate in a polycation and a polyanion solution.

In addition to model polyelectrolytes, many different materials can be incorporated into polyelectrolyte multilayers including proteins[7], DNA[8], dyes[9, 10], light emitting polymers[11, 12], and inorganics[13, 14]. Also, the buildup of these thin films is not limited to electrostatic interactions. Hydrogen bonding[15-18], van der Waals forces[19], and biomolecular interactions[20] have been explored as well. Hydrogen-bonded multilayers will be discussed in detail in a later section due to their relevance to this thesis.

Polyelectrolyte multilayer assembly compared to other self-assembly techniques such as self-assembled monolayers (SAMs) or Langmuir-Blodgett films is much more versatile. Besides the variety of materials that can be incorporated into the films, a wide range of substrates can be employed including polymers, metals, and glass. With other techniques, the substrate is often limited to a specific surface that interacts with the deposited molecules. An example of this is

thiol-containing SAMs that require a gold surface for deposition. In addition, polyelectrolyte multilayers are not limited to simple changes in the surface properties of the material. The interior of the films can be used for many different applications as well including their use as nanoreactors[21, 22] and light emitting devices[11, 12].

1.2.2. pH Tunable Weak Polyelectrolyte Multilayers

Polyelectrolyte multilayers made from weak polyelectrolytes have the advantage that their properties can be tuned by simple pH adjustments. For this reason, the pH of weak polyelectrolyte solutions is an extremely important parameter when assembling the films. Unlike strong polyelectrolytes, which remain charged over the entire pH range, the degree of ionization of weak polyelectrolytes depends greatly on solution pH. The Henderson-Hasselbach equation modified to account for polyelectrolytes[23] explains the relationship between these two variables:

$$pH = pK_0 + \log\frac{\alpha}{1-\alpha} + 0.434[\Delta Fe(\alpha, Cs)/RT] \qquad (1.1)$$

where pK_0 is the intrinsic ionization constant, α is the degree of ionization, ΔFe is the extra work required to add or remove a proton due to neighboring charge groups, Cs is the ionic strength of the solution, R is the gas constant, and T is temperature. The Rubner group has shown that the incremental thickness of adsorbed weak polyelectrolyte layers changes greatly with the degree of ionization[24, 25]. These thickness differences affect the bulk and surface characteristics of the film. Shiratori et al. produced a matrix of polyelectrolyte multilayer films using two model weak polyelectrolytes, poly(allylamine hydrochloride) (PAH) and polyacrylic acid (PAA). Figure 1-2 shows their chemical structures. PAH is a weak polycation in which the charge density along the polymer chain decreases as the solution pH increases. PAA, a weak polyanion, increases in

charge density as the solution pH increases. The solution pKa (pH where 50% of polyelectrolyte's repeat units are charged) of PAH is approximately 8.8[26-28], and the solution pKa for PAA is approximately 6.5[27, 28]. The pKa's of both PAA and PAH can change when incorporated into polyelectrolyte multilayers[27].

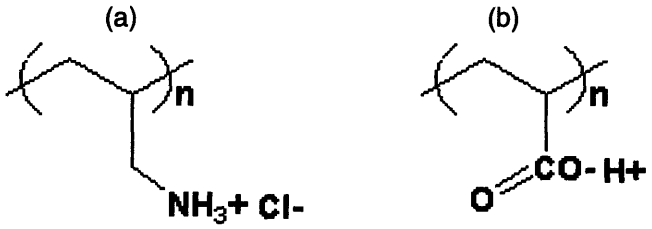

Figure 1-2. Chemical structures of the weak polyelectrolytes, (a) PAH and (b) PAA.

Films studied by Shiratori et al in the PAH/PAA pH matrix displayed a variety of morphologies. Three multilayer systems with very different properties in this matrix are the 6.5/6.5 PAH/PAA, 7.5/3.5 PAH/PAA, and 2.5/2.5 PAH/PAA films. This notation refers to the pH of the polyanion and polycation solutions during multilayer assembly. In the 6.5/6.5 PAH/PAA system, both polymers are considered fully charged and form thin layers (~3 Å)[25] that are tightly electrostatically stitched together with very few free acid or amine groups left in the film. In contrast, the 7.5/3.5 PAH/PAA films are very thick with a great deal of polymer loops and tails. This can be explained by the fact that at a pH of 3.5, the PAA is not fully charged and therefore, does not lay flat on the underlying PAH surface. However, due the high pH of the PAH solution, the PAA charges up in the next layering step and a large amount of PAH is attracted to the surface to compensate. The resulting films not only have a high thickness per layer, but have a surface rich in the polyelectrolyte last deposited. This is different from the 2.5/2.5 PAH/PAA multilayers where both solutions are kept at a low pH. This film still contains

a thick layer of PAA for the same reason as the 7.5/3.5 PAH/PAA system; however, a smaller amount PAH is attracted to the film surface during assembly since most of the acid groups in PAA are protonated at pH 2.5. The 2.5/2.5 PAH/PAA multilayers contain an abundance of free acid groups throughout the film for this reason. It should be noted that although we talk about layers of polyelectrolytes, the resulting films are very interpenetrated, and distinct layers are not present. Our group has used various PAH/PAA multilayers in this matrix to selectively adsorb block copolymers[29], create porous films[30, 31], plate nickel[32], deliver drugs[33], resist cell adhesion[34], pattern polymers[35], and make superhydrophobic surfaces[36].

1.2.3. Polyelectrolyte Multilayers as Biomaterials

Due to the types of materials that can be incorporated into polyelectrolyte multilayer films, the environmentally friendly assembly conditions, and their biocompatibility, these films make excellent candidates as biomaterials. Biologically relevant materials such as proteins[7], DNA[8], polysaccharides[37], hormones[38], and enzymes[39] have been incorporated into multilayers. In addition, polyelectrolyte multilayers have been investigated in the areas of biosensors[40], drug delivery[39, 41-46], and surfaces for controlled cell interactions[34, 38, 47-49].

Many research groups have studied polyelectrolyte multilayers as biomaterials. The Schaaf and Voegel research groups have studied protein interactions with multilayers[50], the mechanism of polypeptide multilayer assembly[51], cell interactions with multilayer surfaces[38, 52], and bioactive coatings from protein functionalization[53]. Work from the groups of Mohwald and Caruso has moved away from flat substrates and focused on using polyelectrolyte multilayer capsules templated on colloids for drug delivery[41, 54] and encapsulation of enzymes[39]. Multilayers have been shown to possess antimicrobial properties when they contain silver

nanoparticles[55] or are capped with poly(ethylene glycol)[56]. Others have looked at multilayers as coatings for specific biomedical applications such as stents or other cardiovascular devices that prevent thrombosis[57, 58], materials to repair blood vessels[59], and long-term implantable devices in the central nervous system[60, 61]. For cardiovascular devices, polyelectrolyte multilayers can interact with blood cells to either reduce or increase coagulation[48, 62], or can actually be templated onto platelets[63]. Besides the use of only organic species, polyelectrolyte multilayer research has also utilized inorganic species that can be incorporated and used as biomaterials[64, 65].

This thesis research is different from previous multilayer biomaterial work, because it takes advantage of tunable weak polyelectrolytes. In the past few years, the Rubner group has explored the use of weak polyelectrolyte multilayers as cell resistant and cell adherent surfaces[34, 49]. Mendelsohn et al. found that assembling weak polyelectrolytes under certain conditions led to films that completely resisted cell adhesion[34]. Furthermore, these ultra-thin films could be engineered to either support or resist cell adhesion by simply changing the pH of assembly solutions. This phenomenon was found to relate to the swelling of the films in buffered media. The cell adhesion assay results did not correlate well with hydrophilicity, surface charge, or chemical functionality since all of the films were hydrophilic and contained the same polymers. In addition, the results were independent of which polyelectrolyte was left as the top layer. The 2.0/2.0 PAH/PAA multilayers, which resisted the attachment of fibroblasts, swelled nearly 300%. In contrast, the 6.5/6.5 PAH/PAA multilayers swelled approximately 25%, and fibroblasts grew on them in numbers similar to control samples of tissue culture polystyrene (TCPS). In addition to PAH/PAA films, Yang et al. found that polyelectrolyte multilayers composed of PAA and polyacrylamide (PAAm) that also swelled to a high degree in buffer were

inert to cell adhesion[49]. Typical results of cell adhesion experiments on the PAH/PAA multilayers, 3.0/3.0 PAA/PAAm multilayers, and a TCPS control are shown in Figure 1-3. As can be seen in the figure, cell growth was dramatically affected by multilayer assembly conditions.

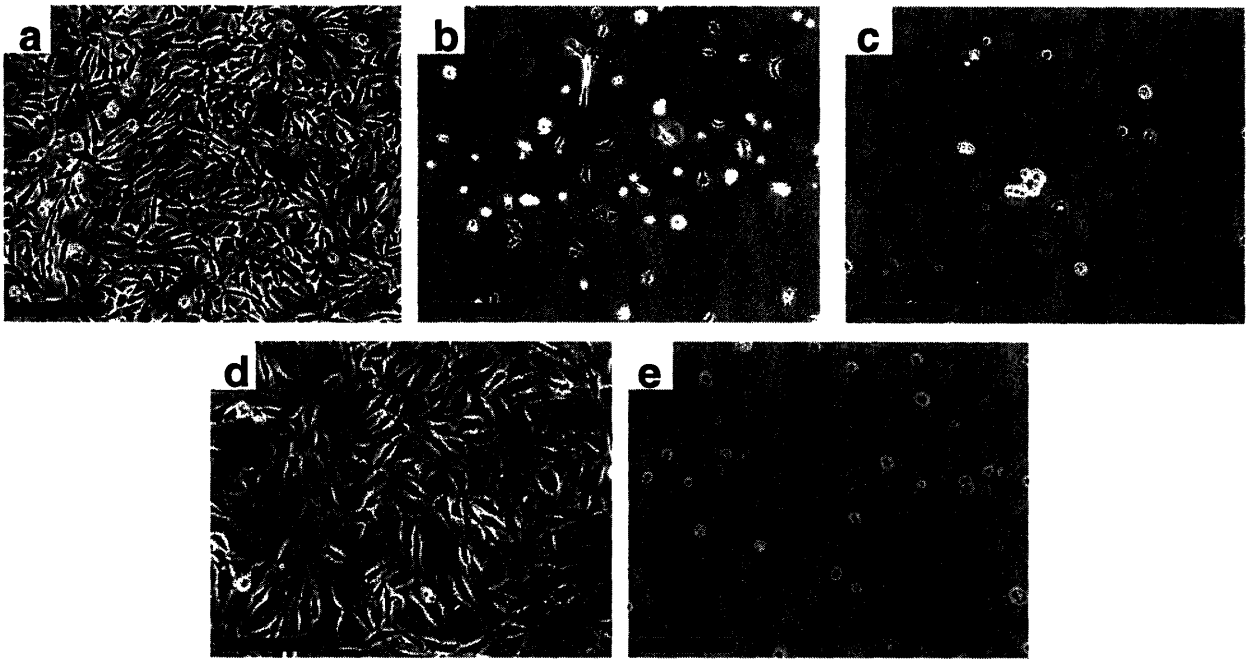

Figure 1-3. NR6WT fibroblasts after three days seeded at 10 000 cells/cm^2 onto (a) a 6.5/6.5 PAH/PAA multilayer, (b) a 4.0/4.0 PAH/PAA multilayer, (c) a 2.0/2.0 PAH/PAA multilayer, (d) a TCPS control and (e) a 3.0/3.0 PAA/PAAm multilayer (scale bar = 200 μm).

The Rubner and van Vliet groups recently studied various PAH/PAA films using a nanoindentation technique to better quantify the mechanical properties of PAH/PAA multilayers in buffer solution and understand their interactions with mammalian cells[66]. It was found that the modulus of the films increased by orders of magnitude as the assembly pH increased, and this correlated with growth of human microvascular endothelial cells as well as Mendelsohn's previous fibroblast results. Figure 1-4 shows that the stiffer films supported cell adhesion, whereas, the more compliant films did not. The fact that nanoscale polyelectrolyte multilayers

can change the chemical and mechanical nature of the surface enough to drastically influence cell behavior is the basis for later chapters of this thesis.

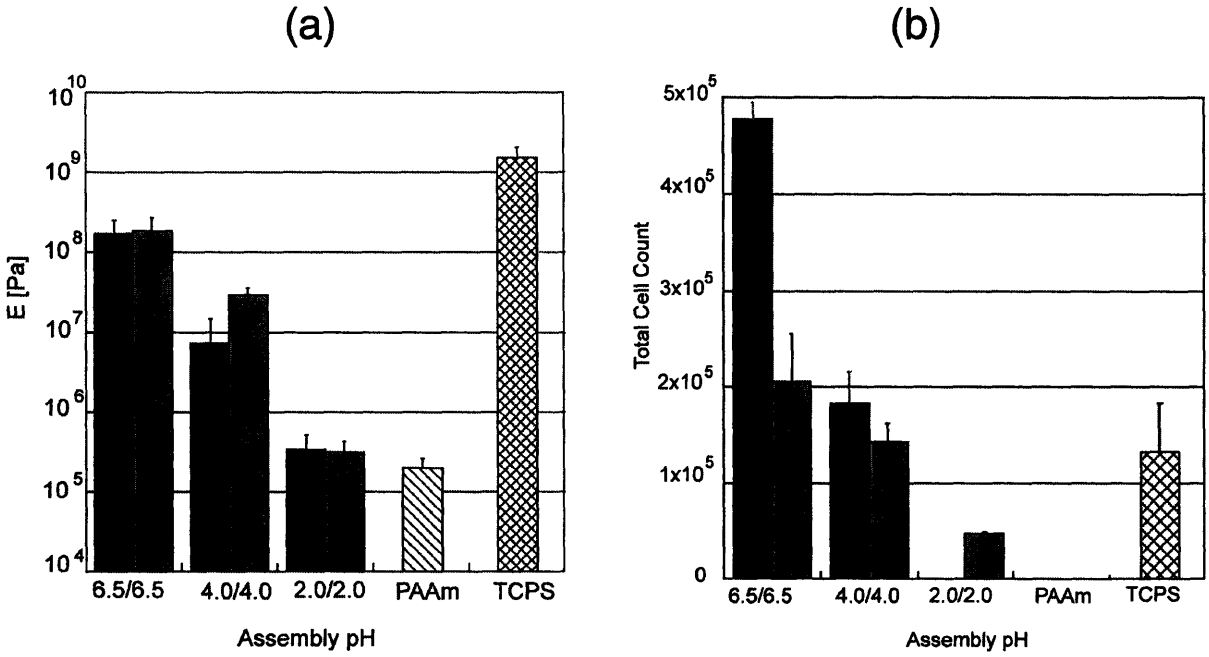

Figure 1-4. Graphs comparing (a) elastic modulus and (b) cell counts for human microvascular endothelial cells. The modulus was obtained using a nanoindentation technique, and cell counts were preformed seven days post-seeding. The black bars represent data from films with PAA as the outermost layer, and gray bars represent data from films with PAH as the outermost layer. Adapted from work of Thompson et al[66].

1.2.4. Patternability of Polyelectrolyte Multilayers

Many of the biological applications that will be discussed in later chapters utilize patterned multilayers. These thin films can be patterned using a variety of methods including polymer-on-polymer stamping (POPS) [67, 68], ink-jet printing[18], and photolithography[18]. For the 3.0/3.0 PAA/PAAm multilayers, many of these techniques are possible since upon assembly, the hydrogen-bonded films are soluble in neutral water. However, the films can be selectively crosslinked using heat or copolymers with a photo-initiator[18]. A different approach is presented

in this thesis. In chapter 3, the patterning of multilayers with areas to promote cell adhesion using POPS is studied. The POPS technique, developed by the Hammond group, is a more versatile approach to patterning than its predecessor, microcontact printing[69, 70] since it does not require a specific chemistry or substrate. Jiang et al. showed that POPS can act as a template for multilayer growth[67] or create a surface containing two different functional groups capable of selective functionality[68]. The work in this thesis builds on these concepts to study applications that would not be possible with homogenous multilayers.

1.3. Thesis Objectives and Outline

The major objective of this research is to explore applications for weak polyelectrolyte multilayers as biomaterials. The ability to tune these ultra-thin polymer films on the molecular level gives them interesting properties that could help address many important biomedical problems. The second chapter presents a method to pattern polyelectrolyte multilayers on the micron-scale utilizing polymer-on-polymer stamping (POPS). This versatile technique for surface patterning produces patterns with controlled thickness and functional group density. Chapter three provides an application for this surface patterning method; cell patterns and arrays when using a cell-inert polyelectrolyte multilayer film as the background. Using POPS, it was possible to control the ligand density and subsequent cell behavior on the patterned regions due to the tunability of the technique. A much different application, drug delivery, is discussed in the fourth chapter. We found that porous weak polyelectrolyte multilayers provided sustained drug release for days to weeks of both hydrophobic and hydrophilic model drugs. Finally, the fifth and sixth chapters present two different multilayer platforms for killing bacteria and preventing bacterial adhesion, respectively. In these chapters, a silver-loaded multilayer system for killing

bacteria and a superhydrophobic multilayer film that prevents fouling from proteins, cells, and bacteria are presented. In addition, the superhydrophobic multilayers can be patterned for high-throughput screening. Although at first glance these applications seem very different, they are tied together by the types of thin films used. The films were all composed of weak polyelectrolyte multilayers with varying degrees and types of post-treatment processing.

References for Chapter 1

(1) Decher, G.;Hong, J. D.;Schmitt, J. Buildup of Ultrathin Multilayer Films by a Self-Assembly Process: Iii. Consecutively Alternating Adsorption of Anionic and Cationic Polyelectrolytes on Charged Surfaces *Thin Solid Films* **1992**, *210*, 831-835.

(2) Decher, G. Fuzzy Nanoassemblies: Toward Layered Polymeric Multicomposites *Science* **1997**, *277*, 1232-1237.

(3) Schlenoff, J. B.;Dubas, S. T. Mechanism of Polyelectrolyte Multilayer Growth: Charge Overcompensation and Distribution *Macromolecules* **2001**, *34*, 592-598.

(4) Donath, E.;Sukhorukov, G. B.;Caruso, F.;Davis, S. A.;Mohwald, H. Novel Hollow Polymer Shells by Colloid-Templated Assembly of Polyelectrolytes *Angew. Chem. Int. Ed.* **1998**, *37*, 2202-2205.

(5) Chiarelli, P. A.;Johal, M. S.;Casson, J. L.;Roberts, J. B.;Robinson, J. M.;Wang, H.-L. Controlled Fabrication of Polyelectrolyte Multilayer Thin Films Using Spin-Assembly *Adv. Mater.* **2001**, *13*, 1167-1171.

(6) Chiarelli, P. A.;Johal, M. S.;Holmes, D. J.;Casson, J. L.;Robinson, J. M.;Wang, H.-L. Polyelectrolyte Spin-Assembly *Langmuir* **2002**, *18*, 168-173.

(7) Lvov, Y.;Ariga, K.;Kunitake, T. Assembly of Alternate Protein Polyion Ultrathin Films *Chem. Lett.* **1994**, 2323-2326.

(8) Lvov, Y.;Decher, G.;Sukhorukov, G. Assembly of Thin Films by Means of Successive Deposition of Alternate Layers of DNA and Poly(Allylamine) *Macromolecules* **1993**, *26*, 5396-5399.

(9) Yoo, D.;Wu, A.;Lee, J.;Rubner, M. F. New Electro-Active Self-Assembled Multilayer Thin Films Based on Alternately Adsorbed Layers of Polyelectrolytes and Functional Dye Molecules *Synth. Met.* **1997**, *85*, 1425-1426.

(10) Ariga, K.;Lvov, Y.;Kunitake, T. Assembling Alternate Dye-Polyion Molecular Films by Electrostatic Layer-by-Layer Adsorption *J. Am. Chem. Soc.* **1997**, *119*, 2224-2231.

(11) Wu, A.;Lee, J.;Rubner, M. F. Light Emitting Electrochemical Devices from Sequentially Adsorbed Multilayers of a Polymeric Ruthenium (II) Complex and Various Polyanions *Thin Solid Films* **1998**, *329*, 663-667.

(12) Clark, S. L.;Handy, E. S.;Rubner, M. F.;Hammond, P. T. Creating Microstructures of Luminescent Organic Thin Films Using Layer-by-Layer Assembly *Adv. Mater.* **1999**, *11*, 1031-1035.

(13) Ariga, K.;Lvov, Y.;Ichinose, I.;Kunitake, T. Ultrathin Films of Inorganic Materials (SiO2 Nanoparticle, Montmorillonite Microplate, and Molybdenum Oxide) Prepared by Alternate Layer-by-Layer Assembly with Organic Polyions. *Appl. Clay Sci.* **1999**, *15*, 137-152.

(14) Schaak, R. E.;Mallouk, T. E. Self-Assembly of Tiled Perovskite Monolayer and Multilayer Thin Films *Chem. Mater.* **2000**, *12*, 2513-2516.

(15) Stockton, W. B.;Rubner, M. F. Molecular-Level Processing of Conjugated Polymers. 4. Layer-by-Layer Manipulation of Polyaniline Via Hydrogen-Bonding Interactions *Macromolecules* **1997**, *30*, 2717-2725.

(16) Wang, L. Y.;Fu, Y.;Wang, Z.;Wang, Y.;Sun, C.;Fan, Y.;Zhang, X. Multilayer Assemblies of Poly(4-Vinylpyridine) Bearing an Osmium Complex and Poly(Acrylic Acid) Via Hydrogen Bonding *Macromol. Chem. Phys.* **1999**, *200*, 1523-1527.
(17) Sukhishvili, S. A.;Granick, S. Layered, Erasable, Ultrathin Polymer Films *J. Am. Chem. Soc.* **2000**, *122*, 9550-9551.
(18) Yang, S. Y.;Rubner, M. F. Micropatterning of Polymer Thin Films with pH-Sensitive and Cross-Linkable Hydrogen-Bonded Polyelectrolyte Multilayers *J. Am. Chem. Soc.* **2002**, *124*, 2100-2101.
(19) Kotov, N. A. Layer-by-Layer Self Assembly: The Contribution of Hydrophobic Interactions *Nanostruct. Mater.* **1999**, *12*, 789-796.
(20) Cui, X.;Pei, R.;Wang, Z.;Yang, F.;Ma, Y.;Dong, S.;Yang, X. Layer-by-Layer Assembly of Multilayer Films Composed of Avidin and Biotin-Labeled Antibody for Immunosensing *Biosens. Bioelectron.* **2003**, *18*, 59-67.
(21) Joly, S.;Kane, R.;Radzilowski, L.;Wang, T.;Wu, A.;Cohen, R. E.;Thomas, E. L.;Rubner, M. F. Multilayer Nanoreactors for Metallic and Semiconducting Particles *Langmuir* **2000**, *16*, 1354-1359.
(22) Wang, T. C.;Rubner, M. F.;Cohen, R. E. Polyelectrolyte Multilayer Nanoreactors for Preparing Silver Nanoparticle Composites: Controlling Metal Concentration and Nanoparticle Size *Langmuir* **2002**, *18*, 3370-3375.
(23) Mandel, M. *Polyelectrolytes,in Encyclopedia of Polymer Science and Engineering*, Kroschwitz, J. I., Editor. **1989**, John Wiley & Sons: New York. 739-829.
(24) Yoo, D.;Shiratori, S. S.;Rubner, M. F. Controlling Bilayer Composition and Surface Wettability of Sequentially Adsorbed Multilayers of Weak Polyelectrolytes *Macromolecules* **1998**, *31*, 4309-4318.
(25) Shiratori, S. S.;Rubner, M. F. Ph-Dependent Thickness Behavior of Sequentially Adsorbed Layers of Weak Polyelectrolytes *Macromolecules* **2000**, *33*, 4213-4219.
(26) Yoshikawa, Y.;Matsuoka, H.;Ise, N. Ordered Structure of Polyallylamine Hydrochloride in Dilute Solutions as Studied by Small-Angle X-Ray-Scattering *Br. Polym. J.* **1986**, *18*, 242-246.
(27) Choi, J.;Rubner, M. F. Influence of the Degree of Ionization on Weak Polyelectrolyte Multilayer Assembly *Macromolecules* **2005**, *38*, 116-124.
(28) Petrov, A. I.;Antipov, A. A.;Sukhorukov, G. B. Base-Acid Equilibria in Polyelectrolyte Systems: From Weak Polyelectrolytes to Interpolyelectrolyte Complexes and Multilayered Polyelectrolyte Shells *Macromolecules* **2003**, *36*, 10079-10086.
(29) Choi, J.;Rubner, M. F. Selective Adsorption of Amphiphilic Block Copolymers on Weak Polyelectrolyte Multilayers *J. Macromol. Sci. Pure Appl. Chem.* **2001**, *38*, 1191-1206.
(30) Mendelsohn, J. D.;Barrett, C. J.;Chan, V. V.;Pal, A. J.;Mayes, A. M.;Rubner, M. F. Fabrication of Microporous Thin Films from Polyelectrolyte Multilayers *Langmuir* **2000**, *16*, 5017-5023.
(31) Hiller, J.;Mendelsohn, J. D.;Rubner, M. F. Reversibly Erasable Nanoporous Anti-Reflection Coatings from Polyelectrolyte Multilayers *Nat. Mater.* **2002**, *1*, 59-63.
(32) Wang, T. C.;Chen, B.;Rubner, M. F.;Cohen, R. E. Selective Electroless Nickel Plating on Polyelectrolyte Multilayer Platforms *Langmuir* **2001**, *17*, 6610-6615.
(33) Berg, M. C.;Zhai, L.;Cohen, R. E.;Rubner, M. F. Controlled Release from Porous Polyelectrolyte Multilayers **In Preparation**.

(34) Mendelsohn, J. D.;Yang, S. Y.;Hiller, J.;Hochbaum, A. I.;Rubner, M. F. Rational Design of Cytophilic and Cytophobic Polyelectrolyte Multilayer Thin Films *Biomacromolecules* **2003**, *4*, 96-106.
(35) Berg, M. C.;Choi, J.;Hammond, P. T.;Rubner, M. F. Tailored Micropatterns through Weak Polyelectrolyte Stamping *Langmuir* **2003**, *19*, 2231-2237.
(36) Zhai, L.;Cebeci, F. C.;Cohen, R. E.;Rubner, M. F. Stable Superhydrophobic Coatings from Polyelectrolyte Multilayers *Nano Lett.* **2004**, *4*, 1349-1353.
(37) Richert, L.;Lavalle, P.;Payan, E.;Shu, X. Z.;Prestwich, G. D.;Stoltz, J. F.;Schaaf, P.;Voegel, J.-C.;Picart, C. Layer by Layer Buildup of Polysaccharide Films: Physical Chemistry and Cellular Adhesion Aspects *Langmuir* **2004**, *20*, 448-458.
(38) Chluba, J.;Voegel, J.-C.;Decher, G.;Erbacher, P.;Schaaf, P.;Ogier, J. Peptide Hormone Covalently Bound to Polyelectrolytes and Embedded into Multilayer Architectures Conserving Full Biological Activity *Biomacromolecules* **2001**, *2*, 800-805.
(39) Caruso, F.;Trau, D.;Mohwald, H.;Renneberg, R. Enzyme Encapsulation in Layer-by-Layer Engineered Polymer Multilayer Capsules *Langmuir* **2000**, *16*, 1485-1488.
(40) Decher, G.;Lehr, B.;Lowack, K.;Lvov, Y.;Schmitt, J. New Nanocomposite Films for Biosensors: Layer-by-Layer Adsorbed Films of Polyelectrolytes, Proteins or DNA *Biosens. Bioelectron.* **1994**, *9*, 677-684.
(41) Qiu, X.;Donath, E.;Mohwald, H. Permeability of Ibuprofen in Various Polyelectrolyte Multilayers *Macromol. Mater. Eng.* **2001**, *286*, 591-597.
(42) Vazquez, E.;Dewitt, D. M.;Hammond, P. T.;Lynn, D. M. Construction of Hydrolytically-Degradable Thin Films Via Layer-by-Layer Deposition of Degradable Polyelectrolytes *J. Am. Chem. Soc.* **2002**, *124*, 13992-13993.
(43) Quinn, J. F.;Caruso, F. Facile Tailoring of Film Morphology and Release Properties Using Layer-by-Layer Assembly of Thermoresponsive Materials *Langmuir* **2004**, *20*, 20-22.
(44) Burke, S. E.;Barrett, C. J. Ph-Dependent Loading and Release Behavior of Small Hydrophilic Molecules in Weak Polyelectrolyte Multilayer *Macromolecules* **2004**, *37*, 5375-5384.
(45) Nolan, C. M.;Serpe, M. J.;Lyon, L. A. Thermally Modulated Insulin Release from Microgel Thin Films *Biomacromolecules* **2004**, *5*, 1940-1946.
(46) Serpe, M. J.;Yarmey, K. A.;Nolan, C. M.;Lyon, L. A. Doxorubicin Uptake and Release from Microgel Thin Films *Biomacromolecules* **2005**, *6*, 408-413.
(47) Elbert, D. L.;Herbert, C. B.;Hubbell, J. A. Thin Polymer Layers Formed by Polyelectrolyte Multilayer Techniques on Biological Surfaces *Langmuir* **1999**, *15*, 5355-5362.
(48) Serizawa, T.;Yamaguchi, M.;Matsuyama, T.;Akashi, M. Alternating Bioactivity of Polymeric Layer-by-Layer Assemblies: Anti- Vs Procoagulation of Human Blood on Chitosan and Dextran Sulfate Layers *Biomacromolecules* **2000**, *1*, 306-309.
(49) Yang, S. Y.;Mendelsohn, J. D.;Rubner, M. F. New Class of Ultrathin, Higly Cell-Adhesion-Resistant Polyelectrolyte Multilayers with Micropatterning Capabilities *Biomacromolecules* **2003**, *4*, 987-994.
(50) Ladam, G.;Schaaf, P.;Cuisinier, F. J. G.;Decher, G.;Voegel, J.-C. Protein Adsorption onto Auto-Assembled Polyelectrolyte Films *Langmuir* **2001**, *17*, 878-882.

(51) Picart, C.;Lavalle, P.;Hubert, P.;Cuisinier, F. J. G.;Decher, G.;Schaaf, P.;Voegel, J. C. Buildup Mechanism for Poly(L-Lysine)/Hyaluronic Acid Films onto a Solid Surface *Langmuir* **2001**, *17*, 7414-7424.

(52) Richert, L.;Lavalle, P.;Vautier, D.;Senger, B.;Stoltz, J. F.;Schaaf, P.;Voegel, J.-C.;Picart, C. Cell Interactions with Polyelectrolyte Multilayer Films *Biomacromolecules* **2002**, *3*, 1170-1178.

(53) Jessel, N.;Atalar, F.;Lavalle, P.;Mutterer, J.;Decher, G.;Schaaf, P.;Voegel, J. C.;Ogier, J. Bioactive Coatings Based on a Polyelectrolyte Multilayer Architecture Functionalized by Embedded Proteins *Adv. Mater.* **2003**, *15*, 692-695.

(54) Qiu, X.;Leporatti, S.;Donath, E.;Mohwald, H. Studies on the Drug Release Properties of Polysaccharide Multilayers Encapsulated Ibuprofen Microparticles *Langmuir* **2001**, *17*, 5375-5380.

(55) Dai, J.;Bruening, M. L. Catalytic Nanoparticles Formed by Reduction of Metal Ions in Multilayered Polyelectrolyte Films *Nano Lett.* **2002**, *2*, 497-501.

(56) Boulmedais, F.;Frisch, B.;Etienne, O.;Lavalle, P.;Picart, C.;Ogier, J.;Voegel, J.-C.;Schaaf, P.;Egles, C. Polyelectrolyte Multilayer Films with Pegylated Polypeptides as a New Type of Anti-Microbial Protection for Biomaterials *Biomaterials* **2004**, *25*, 2003-2011.

(57) Thierry, B.;Winnik, F. M.;Merhi, Y.;Silver, J.;Tabrizian, M. Bioactive Coatings of Endovascular Stents Based on Polyelectrolyte Multilayers *Biomacromolecules* **2003**, *4*, 1564-1571.

(58) Tan, Q.;Ji, J.;Barbosa, M. A.;Fonseca, C.;Shen, J. Constructing Thromboresistant Surface on Biomedical Stainless Steel Via Alyer-by-Layer Deposition Anticoagulant *Biomaterials* **2003**, *24*, 4699-4705.

(59) Thierry, B.;Winnik, F. M.;Merhi, Y.;Tabrizian, M. Nanocoatings onto Arteries Via Layer-by-Layer Deposition: Toward the in Vivo Repair of Damaged Blood Vessels *J. Am. Chem. Soc.* **2003**, *125*, 7494-7495.

(60) Ai, H.;Meng, H.;Ichinose, I.;Jones, A. J.;Mills, D. K.;Lvov, Y. M.;Qiao, X. Biocompatibility of Layer-by-Layer Self-Assembled Nanofilm on Silicone Rubber for Neurons *J. Neurosci. Meth.* **2003**, *128*, 1-8.

(61) Ai, H.;Lvov, Y. M.;Mills, D. K.;Jennings, M.;Alexander, J. S.;Jones, S. A. Coating and Selective Deposition of Nanofilm on Silicone Rubber for Cell Adhesion and Growth *Cell Biochemistry and Biophysics* **2003**, *38*, 103-114.

(62) Serizawa, T.;Yamaguchi, M.;Akashi, M. Alternating Bioactivity of Polymeric Layer-by-Layer Assemblies: Anticoagulation Vs Procoagulation of Human Blood *Biomacromolecules* **2002**, *3*, 724-731.

(63) Ai, H.;Fang, M.;Jones, S. A.;Lvov, Y. M. Electrostatic Layer-by-Layer Nanoassembly on Biological Microtemplates: Platelets *Biomacromolecules* **2002**, *3*, 560-564.

(64) Koktysh, D. S.;Liang, X.;Yun, B. G.;PastorizaSantos, I.;Matts, R. L.;Giersig, M.;SerraRodriguez, C.;LizMarzan, L. M.;Kotov, N. A. Biomaterials by Design: Layer-by-Layer Assembled Ion-Selective and Biocompatible Films of Tio2 Nanoshells for Neurochemical Monitoring *Adv. Funct. Mater.* **2002**, *12*, 255-265.

(65) Sinani, V. A.;Koktysh, D. S.;Yun, B. G.;Matts, R. L.;Pappas, T. C.;Motamedi, M.;Thomas, S. N.;Kotov, N. A. Collagen Coating Promotes Biocompatibility of Semiconductor Nanoparticles in Stratified Lbl Films *Nano Lett.* **2003**, *3*, 1177-1182.

(66) Thompson, M. T.;Berg, M. C.;Tobias, I. S.;Rubner, M. F.;van Vliet, K. J. Quantifying the Role of Compliance in Cell Adhesion and Proliferation: Polyelectrolyte Multilayers as Mechanically Tunable Cell Substrata **Submitted to Biomaterials**.
(67) Jiang, X.;Hammond, P. T. Selective Deposition in Layer-by-Layer Assembly: Functional Graft Copolymers as Molecular Templates *Langmuir* **2000**, *16*, 8501-8509.
(68) Jiang, X.;Zheng, H.;Gourdin, S.;Hammond, P. T. Polymer-on-Polymer Stamping: Universal Approaches to Chemically Patterned Surfaces *Langmuir* **2002**, *18*, 2607-2615.
(69) Kumar, A.;Biebuyck, H. A.;Whitesides, G. M. Patterning Self-Assembled Monolayers: Applications in Materials Science *Langmuir* **1994**, *10*, 1498-1511.
(70) Kumar, A.;Whitesides, G. M. Patterned Condensation Figures as Optical Diffraction Gratings *Science* **1994**, *263*, 60-62.

Chapter 2 Polymer on Polymer Stamping of Weak Polyelectrolytes

2.1. Introduction

In recent years, a great deal of effort has been put forth to research thin films made from polyelectrolyte multilayers using the layer-by-layer assembly technique. Since this method for building layers of oppositely charged polyelectrolytes was first developed, many different materials have been employed to produce thin films using this approach[1-5]. Multilayer films produced in this layer-by-layer process offer many other desirable traits beyond the versatility in building materials. The film thickness and surface properties can be tailored with unequaled control since each layer is added sequentially. In addition, the process is relatively simple and typically utilizes aqueous solutions. Of specific interest to this paper is the behavior of multilayer films assembled with weak polyelectrolytes with pH-tunable charge densities. It has been shown that the thickness of adsorbed weak polyelectrolyte layers changes greatly according to the ionization degree of each polymer involved in the assembly process[4, 6]. Weak polyelectrolytes, such as poly(allylamine hydrochloride) (PAH) and poly(acrylic acid) (PAA), can deposit on a substrate to create very thick (up to 80 Å) layers when the films are fabricated under pH conditions where the polymers are not fully charged. Conversely, the two polymers can be used in their fully charged state to create thin layers similar to strong polyelectrolytes.

This means that films can be created with considerably different bulk and surface properties by using the same two polymers.

Patterning weak polyelectrolyte multilayer films on a micron-scale is highly desirable for various applications such as biosensors, tissue engineering implants, electronic devices, and photonic structures. Biological applications present some of the greatest opportunities particularly considering recent findings that specific PAA/PAH films are completely inert to mammalian cell attachment (specifically mouse fibroblasts), while others promote cell adhesion[7]. In addition, these multilayers are useful in directing the selective adsorption of block copolymers[8] or catalysts for further chemistry[9], which can play an important role in biological studies. Soft lithographic patterning techniques in which a chemically patterned surface acts as a template for the deposition of strong or weak polyelectrolyte multilayers have been developed[10-12] using microcontact printing methods to create chemical surface templates on gold and oxide surfaces[13-15]. This approach and other methods allow the formation of three-dimensional micron scale patterned multilayer films. The ability to pattern the topmost surface of a polyelectrolyte multilayer is particularly critical for a number of sensor and array applications; however, micro-contact printing techniques based upon thiol and silane chemistry on metal and metal oxide surfaces are not applicable to the surfaces of polymer multilayers. Recently, a technique, polymer-on-polymer stamping (POPS), has been developed, which involves the direct application of a polymer monolayer onto a surface[16, 17]. POPS, which has greatly widened the scope of suitable materials that can be transferred using a stamp, takes advantage of the multivalent nature of polymer chains to form a stable monolayer on the desired substrate. This method was originally developed to pattern a polyethylene oxide graft copolymer onto a polyelectrolyte multilayer surface[16]; more recent investigations have reported the use of block

copolymers containing a functional and an anchoring block segment to modify multilayer surfaces via electrostatic, secondary, and covalent interactions, and the ability to pattern strong polyelectrolytes onto oppositely charged polyelectrolyte multilayer surfaces[17] utilizing solely electrostatic interactions. This approach makes it possible to create micron scale features of differing chemical functionality over large areas on the underlying multilayer. Additional steps can be used to take advantage of the functionality on the patterned polymer or the unstamped region of the substrate, as demonstrated in the use of POPS on multilayer surfaces to template the deposition of additional multilayers[16], colloid deposition[18], and nickel plating[19]. Besides POPS, other soft lithographic methods have been developed to pattern polymer surfaces that take advantage of specific chemistry with the surface[20-23]. Soft lithographic techniques have many advantages over other patterning methods such as photolithography, including low cost, the ability to create large area patterns, and a wider variation in available surface chemistries. The stamping process does not require a clean room environment or the harsh chemicals necessary for most photolithography techniques, and can be used to obtain features down to one micron or less in size.

This chapter examines the extension of the POPS process to the transfer of weak polyelectrolytes onto weak polyelectrolyte multilayer platforms. The main advantage of working with weak polyelectrolytes is the ability to influence the charge density of the polymer by simple pH adjustments. In the stamping process, the pH of the polyelectrolyte ink can be adjusted to provide a polymer that is either fully charged in solution or completely uncharged. The pKa of PAH is approximately 9.0. Hence, at this pH, 50% of the functional groups are charged[24]. Therefore, adjustment of the ink solution pH to values well above and below pH 9.0 covers the range of ionization possibilities. The question still remains as to whether or not changing the

charge density of the polymer in the ink solution affects the thickness of the stamped features and the number of free functional groups in the transferred polymers. Because the stamping process is a dry one, it is unclear whether the thickness of the stamped layers can be tailored in manner similar to the adsorption of weak polyelectrolytes[6]. It has been shown that adsorption of weak polyelectrolytes at pH values that yield low charge can lead to a thicker adsorbed polymer layer. These experiments were designed to check the hypothesis that altering the ionization of the polyelectrolyte would change the thickness of the transferred polymer layer upon stamping as well as available functional groups.

This chapter also addresses issues such as the stability of the stamped pattern in a buffered solution as would be commonly used in biological experiments. We believe that these films are suitable for biological applications due to recent findings that weak polyelectrolyte multilayers can be created to resist cell adhesion. Patterning these particular films with different functional groups could allow directed chemistry to these regions on a micron scale. Such chemistry could present specific biological ligands for cell attachment, creating a template for controlling cell growth on virtually any surface. Also, multilayers offer the possibility of utilizing the functional groups within the film itself in addition to those on the surface.

2.2. Experimental Methods

1. Materials. Poly(acrylic acid) (PAA) (MW = 90,000) was purchased from Polysciences as a 25% aqueous solution. Poly(allylamine hydrochloride) (PAH) (MW = 70,000) and dansyl chloride were purchased from Aldrich. Poly(dimethylsiloxane) (PDMS) stamps were created by curing Sylguard 184 (a two ingredient elastomer kit purchased from Dow Chemical) on top of a silicon master with a striped photoresist pattern. All materials were used without any

further purification. Dulbecco's Phosphate Buffered Saline (PBS) solution was purchased from Gibco.

2. Substrate Preparation. As detailed in previous work[4], multilayer thin films of weak polyelectrolytes were made by a layer-by-layer dipping assembly technique, which utilized an HMS programmable slide stainer from Zeiss, Inc. to automate the process. For making the multilayer films, 10^{-2} M (based on repeat unit of the polymer) polyelectrolyte solutions were prepared with 18 MΩ Millipore water, and were pH-adjusted with either HCl or NaOH. Clean glass substrates were first submerged into the polyelectrolyte solution (PAH first) for 15 minutes, and then taken through a series of three rinse baths of water (pH unadjusted ~5.5) for 2, 1, and 1 minute, respectively. Afterwards, the slides were immersed in the oppositely charged polyelectrolyte solution for 15 minutes followed by the same rinse procedure. The process was then repeated until 20 layers were assembled to leave PAA as the outermost layer.

3. Stamping of weak polyelectrolytes. PDMS stamps were inked by immersion in 0.05 M (based on polymer repeat unit) polyelectrolyte solution (PAH) for 1 hour, similar to a previously described method[25]. The pH of the PAH ink was adjusted using HCl or NaOH. The stamps were then briefly rinsed with water and blown dry with air. The stamp was still wet when rinsed, and the pH of the rinse water was not adjusted. To ensure the degree of ionization of the PAH was not changed, the rinse step was kept less than 2 seconds. Finally, the stamp was brought into contact with a polyelectrolyte multilayer platform for 30 seconds. Some samples were then rinsed with water for 2 minutes to compare the stamped features before and after rinsing.

4. Dansyl Chloride Attachment. Samples stamped with PAH were reacted with dansyl chloride to check the uniformity of the pattern over large areas and show their ability to direct

chemistry. When dansyl chloride is bound to the primary amines of PAH in the stamped region of the films, the compound can be seen using fluorescence microscopy. For the treatment, a 10^{-2} M stock solution of dansyl chloride was prepared in N,N - dimethyl formamide (DMF). From this stock solution, 5 mL were added to 50 mL of 0.1 M sodium bicarbonate buffer solution at pH = 9.0 and stirred vigorously. Samples were then placed in this mixed solution and allowed to incubate for 2 minutes. The time was kept short to avoid having the dansyl chloride diffuse into the bulk of the film. Following the process, samples were rinsed for 2 minutes in water. The relative intensity of the fluorescent images was checked using the National Institute of Health's (NIH) ImageJ image analysis software. The reported values are not meant to be quantitative for the number of reacted amine groups, but are meant to compare the relative number of reacted groups for each stamping condition. The reported values were obtained by analyzing 6 spots from images taken of 3 different samples under the same lens and exposure time.

5. PBS Stability. The stability of the stamped patterns in a pH 7.4 buffered solution was checked using PBS. The samples were immersed in PBS for 3 days to check the stability of the patterns in biological applications.

6. Characterization. The thickness of the films was checked using a Tencor P-10 Surface Profiler (Tencor, Santa Clara, CA) to perform profilometry[4]. Reported values represent an average of at least 6 measurements for each sample. The Digital Instruments Dimension 3000 atomic force microscope (AFM) (Digital Instruments, Santa Barbara, CA) was used in tapping mode to obtain topographical information about the stamped area including heights of stamped features. Stamp height values were obtained by examining the sections of AFM data. Reported values represent an average of at least 10 data points taken from different areas of the samples. Four different samples were used for each stamping condition and multilayer platform. For

visualization of the PAH stamped regions labeled with dansyl chloride, a Zeiss Axioplan 2 fluorescence microscope (Carl Zeiss Inc., Thornwood, NY) was utilized. When using a DAPI filter, the stamped regions appear blue-green. The intensity of the fluorescence images was checked using the NIH ImageJ software.

7. Statistical Analysis. Analysis of variance (ANOVA) was employed to test the statistical significance of differences in stamped thickness values. ANOVA tests whether the variance between thickness values from different stamping conditions is greater than the variance within a reported thickness value for a given stamping condition. If this is the case, then the difference between two stamping conditions is statistically significant. The final result of the ANOVA is the p-value (or probability value). If the p-value is less than a significance level of 0.05 (based on a 5% level), than the groups are statistically different.

2.3. Results and Discussion

2.3.1. Characterization of Weak Polyelectrolyte Multilayer Films

In this study, we stamped PAH onto PAA/PAH multilayer films where PAA was the top layer. Figure 2-1 contains a schematic diagram of the POPS process; adhesion of the polymer to the multilayer surface can be based on electrostatic, hydrogen bonding, acid-base or covalent interactions. The process of submerging the entire PDMS stamp in the ink solution has been utilized in previous research[25]. As the diagram indicates, we believe that the polyelectrolyte uniformly coats the stamp during the inking process.

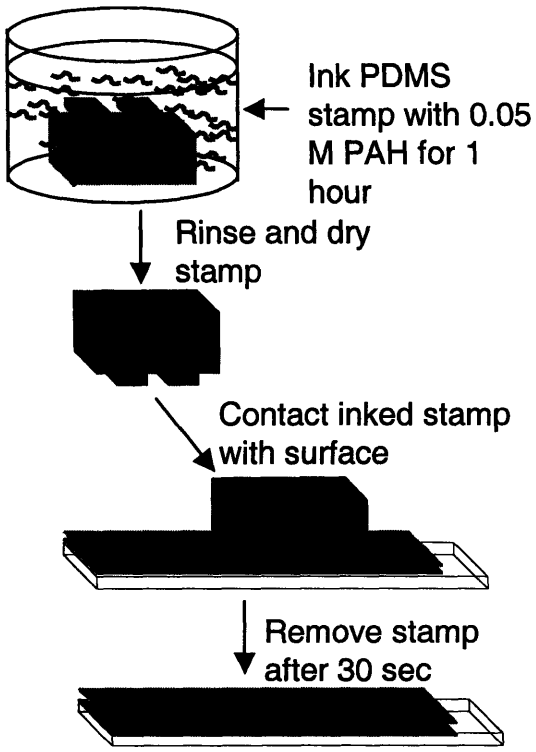

Figure 2-1. Diagram illustrating the polymer-on-polymer stamping process for PAH on a PAA/PAH multilayer platform.

We chose three different weak polyelectrolyte multilayer platforms to check the versatility of the POPS process when the surface roughness and chemical characteristics of the multilayer film are changed. Each of these three 10 bilayer PAA/PAH multilayer films was built using a different pH combination to create platforms that differ dramatically in architecture (a bilayer being one layer of PAH and PAA). Multilayer films of PAA/PAH assembled at pH 6.5/6.5, 3.5/7.5, and 2.5/2.5 (notation refers to the assembly pH of PAA and PAH) were prepared. The molecular architecture of the various PAA/PAH multilayer films has previously been described in detail[6]. Briefly, both polyelectrolytes are fully charged when deposited at 6.5/6.5, resulting in extremely thin layers. In this case, most of the polyion charged groups are paired with oppositely charged groups from the complimentary polyelectrolyte. The 6.5/6.5 films are relatively smooth (4 Å RMS roughness), with highly interpenetrated layers. There are

few remaining free functional groups from either PAA or PAH left in the interior of the film or at the surface due to the high degree of ionic crosslinking. The 3.5/7.5 PAA/PAH layers are very thick, loopy structures with a higher RMS roughness of 18 Å. The 2.5/2.5 films exhibit a bilayer thickness and RMS roughness that falls between those of the 6.5/6.5 and 3.5/7.5 PAA/PAH multilayers. The resulting films are rich in free acid groups both in the bulk and on the surface regardless of the top layer of the film. The 2.5/2.5 films are also of particular interest due to their ability to resist mammalian cell adhesion[7]. Table 2-1 compares the thickness and roughness values measured on dried films for each of the PAA/PAH multilayer films prepared for this study.

Table 2-1. Average incremental bilayer thickness (measured by profilometry) and RMS roughness (obtained from AFM) measurements for the three representative 10 bilayer PAA/PAH multilayer films used in stamping study.

PAA/PAH Film	Avg. Bilayer Thickness (Å)	Avg. RMS Roughness (Å)
6.5/6.5	6	4
2.5/2.5	42	10
3.5/7.5	106	18

2.3.2. Influence of Ink pH of PAH stamped onto Multilayers as Studied with Atomic Force Microscopy

PAH was stamped onto the three different PAA/PAH multilayer systems with PAA as the top layer. For all cases, the PDMS stamp was immersed in a 0.05 M PAH solution at room temperature for 1 hour. Three different ink solutions were used to present PAH with varying degrees of ionization, which were approximately 100% (pH = 3.5), 50% (pH = 9.0), and 0% (pH = 11.0). The pH values were chosen based on previous work that estimated the charge density of PAH in solution as a function of pH[24, 26]. After inking the stamp with PAH, the stamp was rinsed briefly in water to remove excess ink solution and blown dry with air. The dry stamps were then

brought into contact with the multilayer surface, which consisted of 10 bilayers of alternating PAH and PAA, for 30 seconds. This process was repeated for each ink pH and multilayer combination to yield a total of 9 different conditions. Following stamping, the patterned samples were characterized with AFM, rinsed for 2 minutes in water, and then re-characterized to explore the effects of the rinse step on the stamped regions. The pattern that was used for all of the stamping conditions contained lines of varying widths from 5 μm to 10 μm. In the resulting images, the thicker lines always indicate the stamped regions. The width of stamped PAH lines matched the PDMS stamp features, so no spreading was observed on the multilayer surface.

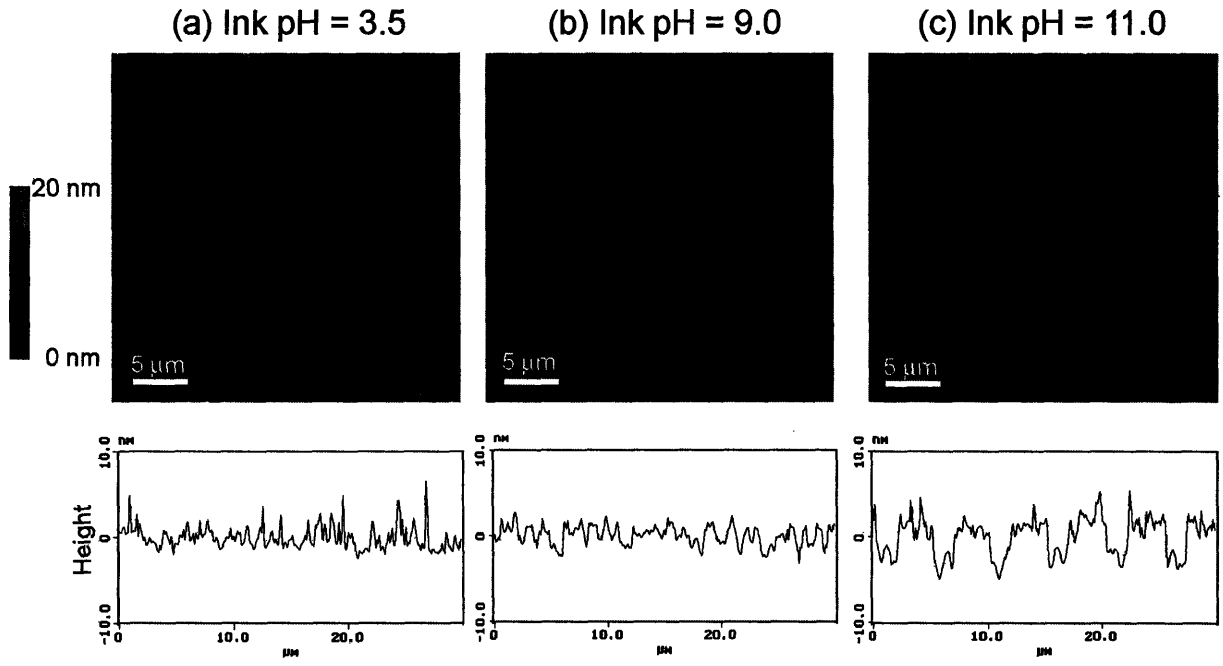

Figure 2-2. AFM height images and sectional analyses of 6.5/6.5 PAA/PAH multilayer platforms stamped with PAH at various ink pH's.

The 6.5/6.5 multilayer films were by far the smoothest platforms in this study, and consequently, the patterns were the easiest to visualize using AFM. Figure 2-2 shows AFM data for the 6.5/6.5 PAA/PAH multilayers at the three different stamping pH conditions after rinsing

the sample with water. Along with the pictures of the patterned regions, sectional analysis diagrams are presented to give a better idea about attributes of the stamped area. It should be noted that the same stamp design was used in all cases. However, different areas of the stamp surfaces were imaged, leading to different feature widths appearing in the AFM images. As can be seen directly from the sectional analysis in Figure 2-2, the thickness of the stamped regions increased from approximately 1.0 nm to 2.4 nm as the ink solution increased from pH = 3.5 to pH = 9.0, and reached 4.4 nm when the pH was raised to 11.0. Based on the ANOVA p-values (see experimental section), the increase in height with pH was statistically significant, as was the case for all of the multilayer platforms. These patterns are very distinct and show definite steps where the line pattern appears on the film, especially at the higher pH conditions. The same trend was observed for the 3.5/7.5 multilayer platforms; however, the high roughness of the underlying film caused the stamped layer to be rougher and obscured the pattern to some degree. The roughness of the films also accounts for the digitized look to the AFM images. For these samples, transferred PAH heights were 1.5 nm, 3.3 nm, and 5.7 nm for ink solution pH's of 3.5, 9.0, and 11.0, respectively. AFM pictures of these samples after rinsing in water can be seen in Figure 2-3. As can be seen by the sectional analysis, there is a fairly large range of error involved in determining stamped feature height due to the roughness of the film. However, the borders of the stamped lines and multilayer background become more defined as the pH of the PAH ink solution is increased. The patterned lines do not look as sharp as the 6.5/6.5 PAA/PAH samples due to the rougher topography. The 2.5/2.5 multilayers were also relatively rough films, and as a result, the patterned features were also harder to visualize using AFM compared to the 6.5/6.5 samples, as shown in Figure 4. However, the trend of increasing thickness with increasing pH was also found for the 2.5/2.5 multilayers. For this system, the PAH layer

stamped layer heights were 1.3 nm (ink pH = 3.5), 4.0 nm (ink pH = 9.0), and 6.5 nm (ink pH = 11.0). The trend of increasing stamped layer thickness with decreasing ionization can be attributed to the lower number of charged groups along the polymer backbone capable of ionic binding to the underlying multilayer film. As is the case with a weak polyelectrolyte chain adsorbed at a low degree of ionization, this should lead to a loopier and thicker structure for the stamped polymer. In addition, there is a conformational contribution to the trend in layer thickness. As the polyelectrolyte becomes less charged in a solution at a higher pH, the polymer chains collapse into a more random coil conformation, compared to the more extended chain shape of fully charged polyelectrolytes. Similar observations were made with previous work on the stamping of the strong polyelectrolytes SPS and PDAC; increased ionic strength, which causes shielding of charges on the polyion backbone, caused an increase in the amount of material transferred in the stamping process[27].

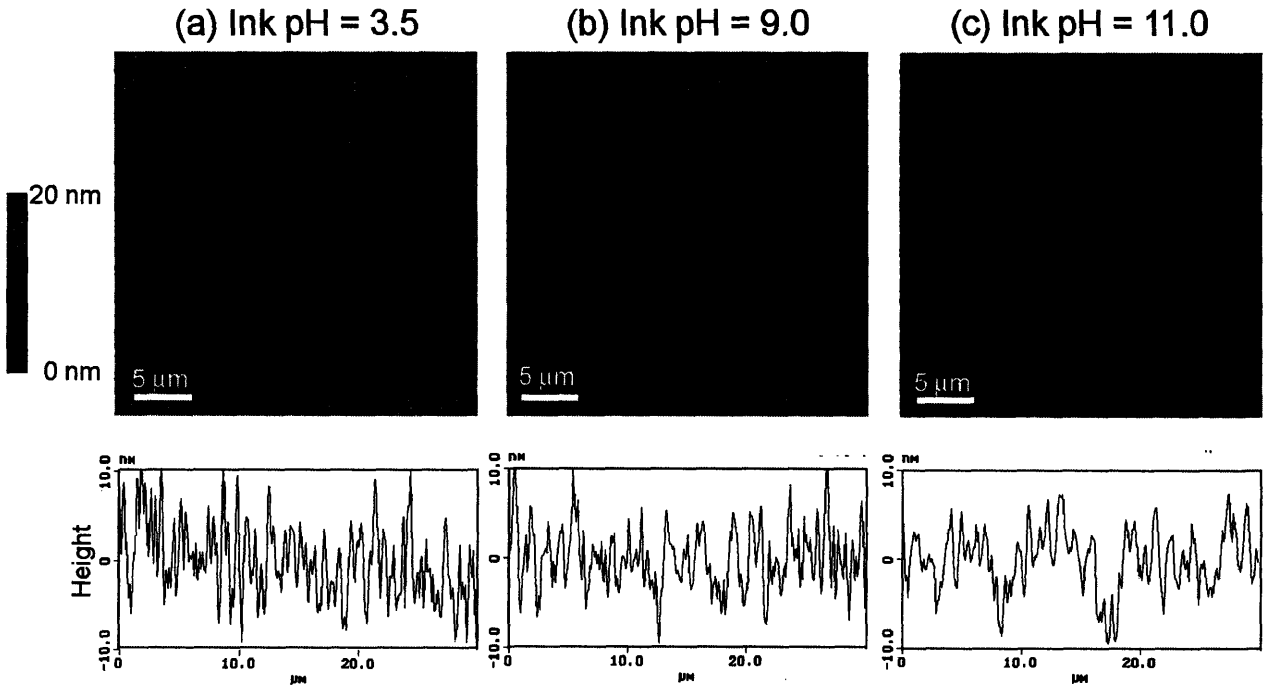

Figure 2-3. AFM height images and sectional analyses of 3.5/7.5 PAA/PAH multilayer platforms stamped with PAH at various ink pH's.

As stated previously, we obtained AFM data before and after rinsing the stamped samples with water. This was done to determine if the stamped features decrease in height after the sample is rinsed. Figure 2-5 compares the stamped layer thickness before and after rinsing for all three weak polyelectrolyte multilayer platforms and all three pH conditions. In most cases, the thickness of the transferred layer remained essentially the same after rinsing. The only case where the decrease in height was statistically significant was PAH stamped at pH 9.0 onto a 6.5/6.5 PAA/PAH film according to the ANOVA test.

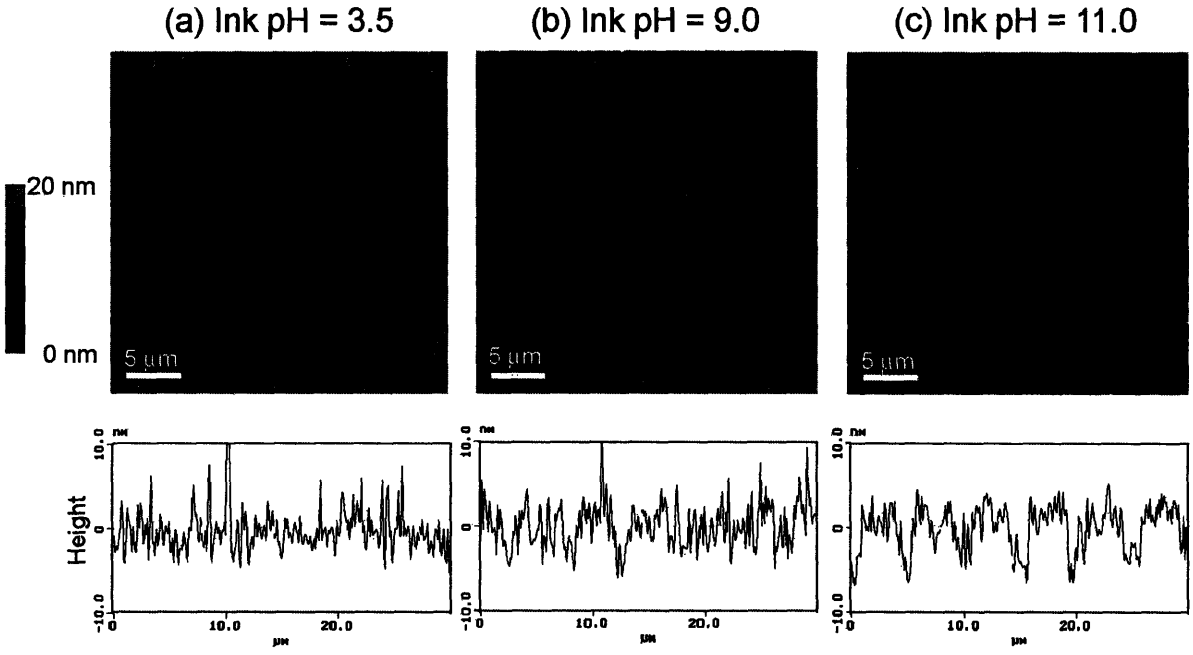

Figure 2-4. AFM height images and sectional analyses of 2.5/2.5 PAA/PAH multilayer platforms stamped with PAH at various ink pH's.

In previous work with the strong polyelectrolyte, PDAC[17], the rinse step removed a great deal of excess material initially transferred to the substrate by the stamp. The difference between the work presented in this paper and previous work may be the different PDMS stamp inking methods. In this work, the stamp is soaked in polymer solution and rinsed before contacting the substrate, while in the previous paper; the polyelectrolyte ink was brushed onto the stamp

without a rinse step for the PDMS stamp, resulting in a larger quantity of polyelectrolyte "ink" on the stamp. Figure 2-5 also helps to compare the stamped layer heights between the different multilayer films. From these graphs, it is apparent that the 2.5/2.5 and 3.5/7.5 platforms produce the thickest layers of transferred material, and the 6.5/6.5 platforms the thinnest layers at a given ink pH. The reason for this behavior can be explained by the films' relative affinities for PAH. In the 6.5/6.5 system, most of the acid groups in the top layer of PAA are ionically stitched up with the PAH layer below it, so there are few acid groups available to interact with the amine groups from the stamped PAH chains. However, in the 2.5/2.5 and 3.5/7.5 multilayers, there are many free acid groups on the surface due to the low pH at which the final layer of PAA was deposited; these free acids are available to interact with the stamped polyamines. The roughness of the multilayer substrate could also play a role in determining transferred layer height since the two rougher films (3.5/7.5 and 2.5/2.5 PAA/PAH multilayers) lead to the thickest stamped layer.

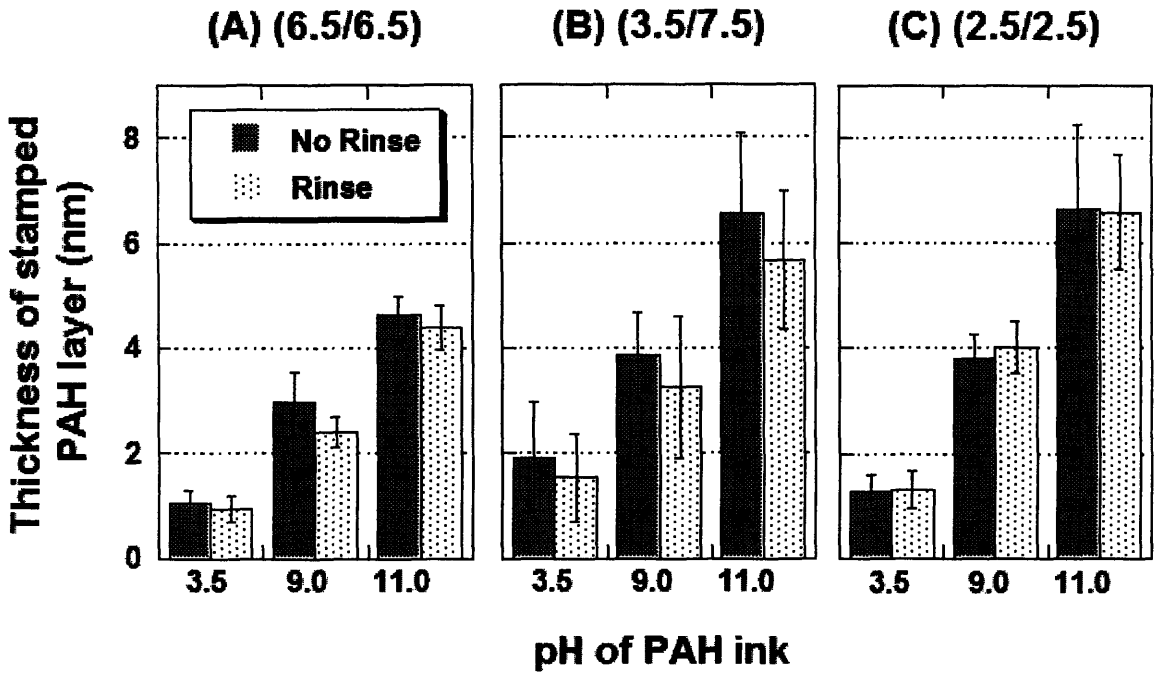

Figure 2-5. Thickness measurements from AFM of the stamped PAH layer inked at pH = 3.5, 9.0, and 11.0 before and after rinsing in water for 2 minutes on 6.5/6.5 PAA/PAH multilayers (a), 3.5/7.5 PAA/PAH multilayers (b), and 2.5/2.5 PAA/PAH multilayers (c).

2.3.3. Dansyl Chloride Attachment on Stamped PAH as a Function of Ink pH

To visualize the stamped layers over a larger area and to illustrate the point that the stamped polyelectrolyte's reactive groups can be taken advantage of through selective chemistry, dansyl chloride was attached to the stamped PAH regions. Dansyl chloride only fluoresces after it is bound to an amine, so a fluorescent image is a clear indication that a covalent bond is formed with the stamped PAH. The reaction proceeded by simply dipping the patterned substrate in a buffered dansyl chloride solution. We performed the reaction for each of the three multilayer substrates with PAH stamped at each ink pH. Dansyl chloride is a sulfonyl chloride that reacts with primary amines and emits a fluorescent color when excited with light in the near UV. A buffer solution of pH = 9.0 was chosen to ensure a supply of free amines. The resulting fluorescent patterns were visualized using a fluorescence microscope. The dansyl chloride

appeared to react with the PAH stamped regions over the entire area created by the stamp. Intensity values for each of the images were obtained by using image analysis software, and they are reported in Figure 2-6. For this analysis, testing conditions such as exposure time and magnification level were kept constant. The background was not subtracted from the reported intensity values.

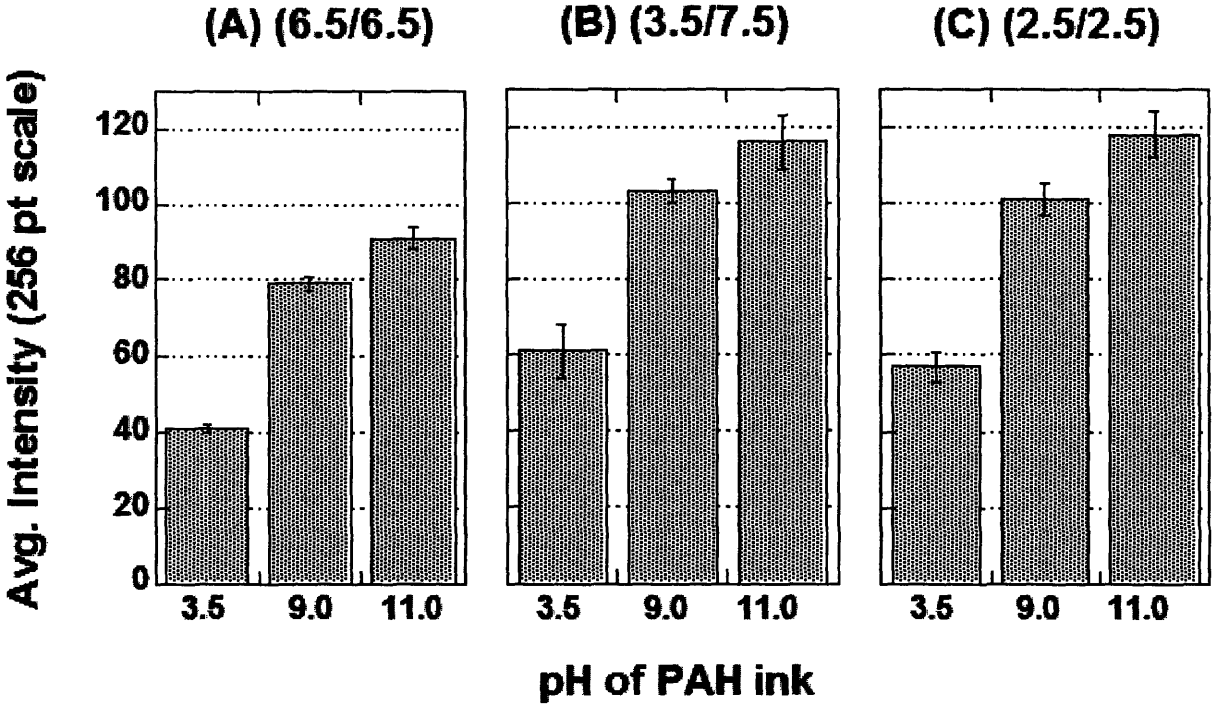

Figure 2-6. Fluorescent intensities of dansyl chloride labeled PAH stamped onto 6.5/6.5 PAA/PAH multilayers (a), 3.5/7.5 PAA/PAH multilayers (b), and 2.5/2.5 PAA/PAH multilayers (c).

The intensity measurements are not meant to be an exact number for the reactive amine groups in the transferred PAH layer; however, they do reflect the relative amount of amine groups that are marked by dansyl chloride for each ink condition and multilayer substrate. The reported values indicate that as the PAH stamped layer thickness increases, so does the number of available functional groups for additional chemistry. This trend can be seen by the increasing fluorescence intensity with increasing ink pH. In addition, the 6.5/6.5 PAA/PAH multilayers,

which were earlier shown to produce the thinnest PAH transferred layer, also lead to the lowest intensity values of the different multilayer substrates. Figure 2-7 shows a fluorescent image of the dansyl chloride labeled PAH for the 3.5/7.5 PAA/PAH sample stamped with PAH at a pH of 11.0 as an example of the fluorescent images obtained. The image also makes it clear that although AFM images may look rough for the 3.5/7.5 PAA/PAH films, a well-defined pattern is still formed. Performing specific chemistry on the stamped regions may be very useful in biosensor applications. By using a cell resistant multilayer system as a background, PAH could be stamped on top and reacted with specific biological ligands to create areas for cell adhesion. In Chapter 3, we will show how this idea can be applied to pattern mammalian cells using specific chemistry to attach RGD ligands to the stamped PAH surface. Any chemistry that reacts with a primary amine is possible, so this is an extremely versatile approach to create cell adhesive regions on a bio-inert background. Furthermore, since the conditions used to ink the stamp controls the amount of functional groups on the stamped surface, the density of attached ligands may also possibly be controlled. The attachment of dansyl chloride is just one example of the possibilities that are introduced by creating regions with two distinctive chemical groups on a surface.

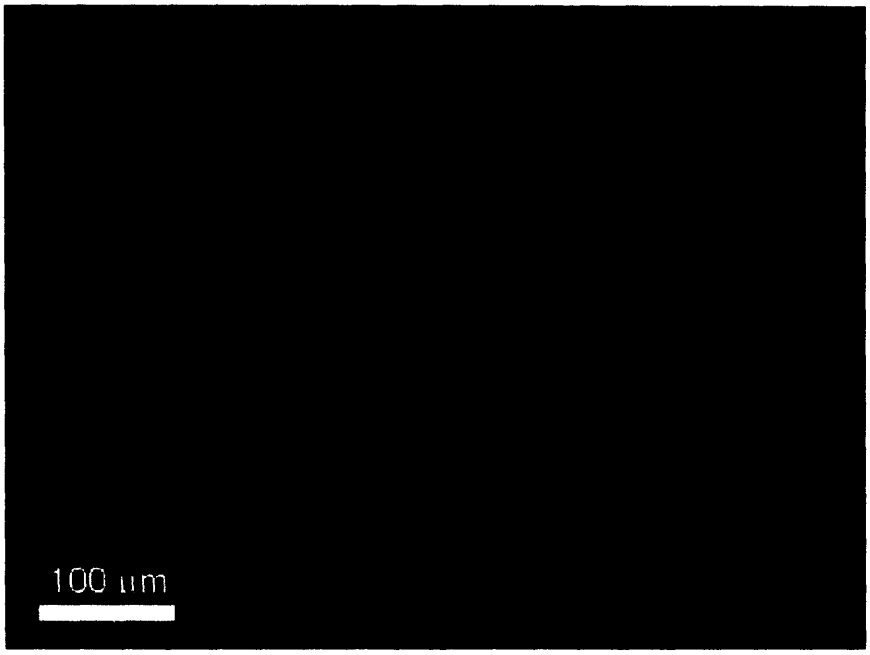

Figure 2-7. Fluorescent image of a 3.5/7.5 PAA/PAH multilayer platform stamped with PAH at pH 11 and subsequently reacted with dansyl chloride.

Finally, the stability of the stamped PAH layers was checked by an extensive rinse in a buffered solution. For this experiment, each of the three multilayer films was stamped with PAH (ink pH = 11.0) and then immersed in a phosphate buffer solution of pH = 7.4 for 3 days. After this treatment, the patterns were examined using AFM and dansyl chloride staining to confirm the stability of the stamped pattern. In all cases, the patterns were still present and very clear for each substrate with similar intensity values. Thus, it may be concluded that the created patterns on each of the polyelectrolyte multilayers are stable under buffered conditions. To check for PAH coming off the stamped films, the buffer solution used for treatment was used as an adsorption bath for a 2.5/2.5 PAA/PAH multilayer film (after dialysis to remove salts). Afterwards, this film was stained with dansyl chloride to mark any PAH that the film obtained from the bath. Upon fluorescence intensity comparison against 2.5/2.5 films dipped into known concentrations of PAH, it appears that there is less than 0.0001 M PAH in the buffer rinse solution. In fact, the intensity value is statistically the same as a film never dipped in a bath

containing PAH. Data for this comparison are presented in Table 2-2. The films were tested in buffered solution to check the appropriateness for use in biological applications. Since a great deal of biochemistry is done in buffered solutions, and any cell work must be done under physiological conditions; the stamped patterns must be able to withstand treatment in buffered conditions for long periods of time.

Table 2-2. Fluorescence intensity values of multilayer films dipped in the buffer rinse solution or standard PAH solutions.

PAH Concentration	Avg. Intensity (256 pt scale)
Buffer rinse	32 ± 3
0	34 ± 1
10^{-2} M	223 ± 1
10^{-3} M	225 ± 2
10^{-4} M	43 ± 1

2.4. Conclusions

We have extended the polymer-on-polymer stamping technique to the patterning of weak polyelectrolyte multilayer films with PAH when PAA is the top layer. As the pH of the PAH ink solution for the PDMS stamp is increased, the thickness of the transferred PAH layer increased as well as the number of amine groups available for further chemistry. The thickest layer of stamped PAH occurred when its degree of ionization was the lowest. The result was the same for each PAA/PAH multilayer system tested (6.5/6.5, 3.5/7.5, and 2.5/2.5). However, as the roughness of the underlying weak polyelectrolyte multilayer substrate increased, so did the roughness of the stamped pattern. In addition, PAH stamped on all three PAA/PAH multilayers directed selective chemistry of dansyl chloride. The amount of amine groups capable of reacting with dansyl chloride increased with increasing transferred layer thickness. Finally, the transferred PAH patterns were stable even after a three-day rinse in buffered solution. The

stability of the patterned films and their functionalities from the stamped material and underlying substrate make them excellent candidates for a range of applications. One of these applications, controlled ligand density on cell adhesive patterns, is explored in Chapter 3 of this thesis.

References for Chapter 2

(1) Decher, G. Fuzzy Nanoassemblies: Toward Layered Polymeric Multicomposites *Science* **1997**, *277*, 1232-1237.

(2) Lvov, Y.;Decher, G.;Sukhorukov, G. Assembly of Thin Films by Means of Successive Deposition of Alternate Layers of DNA and Poly(Allylamine) *Macromolecules* **1993**, *26*, 5396-5399.

(3) Lvov, Y.;Ariga, K.;Kunitake, T. Assembly of Alternate Protein Polyion Ultrathin Films *Chem. Lett.* **1994**, 2323-2326.

(4) Yoo, D.;Shiratori, S. S.;Rubner, M. F. Controlling Bilayer Composition and Surface Wettability of Sequentially Adsorbed Multilayers of Weak Polyelectrolytes *Macromolecules* **1998**, *31*, 4309-4318.

(5) Wu, A.;Yoo, D.;Lee, J. K.;Rubner, M. F. Solid-State Light Emitting Devices Based on the Tris-Chelated Ruthenium(II) Complex: 3. High Efficiency Devices Via a Layer-by-Layer Molecular-Level Blending Approach *J. Amer. Chem. Soc.* **1999**, *121*, 4883-4891.

(6) Shiratori, S. S.;Rubner, M. F. Ph-Dependent Thickness Behavior of Sequentially Adsorbed Layers of Weak Polyelectrolytes *Macromolecules* **2000**, *33*, 4213-4219.

(7) Mendelsohn, J. D.;Yang, S. Y.;Hiller, J.;Hochbaum, A. I.;Rubner, M. F. Rational Design of Cytophilic and Cytophobic Polyelectrolyte Multilayer Thin Films *Biomacromolecules* **2003**, *4*, 96-106.

(8) Choi, J.;Rubner, M. F. Selective Adsorption of Amphiphilic Block Copolymers on Weak Polyelectrolyte Multilayers *J. Macromol. Sci. Pure Appl. Chem.* **2001**, *38*, 1191-1206.

(9) Wang, T. C.;Chen, B.;Rubner, M. F.;Cohen, R. E. Selective Electroless Nickel Plating on Polyelectrolyte Multilayer Platforms *Langmuir* **2001**, *17*, 6610-6615.

(10) Hammond, P. T.;Whitesides, G. M. Formation of Polymer Microstructures by Selective Deposition of Polyion Multilayers Using Patterned Self-Assembled Monolayers as a Template *Macromolecules* **1995**, *28*, 7569-7571.

(11) Clark, S. L.;Montague, M.;Hammond, P. T. Selective Deposition in Multilayer Assembly: Sams as Molecular Templates *Supramol. Sci.* **1997**, *4*, 141-146.

(12) Clark, S. L.;Montague, M. F.;Hammond, P. T. Ionic Effects of Sodium Chloride on the Templated Deposition of Polyelectrolytes Using Layer-by-Layer Ionic Assembly *Macromolecules* **1997**, *30*, 7237-7244.

(13) Kumar, A.;Biebuyck, H. A.;Whitesides, G. M. Patterning Self-Assembled Monolayers: Applications in Materials Science *Langmuir* **1994**, *10*, 1498-1511.

(14) Kumar, A.;Whitesides, G. M. Patterned Condensation Figures as Optical Diffraction Gratings *Science* **1994**, *263*, 60-62.

(15) Xia, Y.;Mrksich, M.;Kim, E.;Whitesides, G. M. *J. Amer. Chem. Soc.* **1995**, *117*, 9576-9577.

(16) Jiang, X.;Hammond, P. T. Selective Deposition in Layer-by-Layer Assembly: Functional Graft Copolymers as Molecular Templates *Langmuir* **2000**, *16*, 8501-8509.

(17) Jiang, X.;Zheng, H.;Gourdin, S.;Hammond, P. T. Polymer-on-Polymer Stamping: Universal Approaches to Chemically Patterned Surfaces *Langmuir* **2002**, *18*, 2607-2615.

(18) Zheng, H.;Rubner, M. F.;Hammond, P. T. Particle Assembly on Patterned "Plus/Minus" Polyelectrolyte Surfaces Via Polymer-on-Polymer Stamping *Langmuir* **2002**, *18*, 4505-4510.

(19) Jiang, X.;Zheng, H.;Choi, J.;Rubner, M. F.;Hammond, P. T. **To Be Submitted.**
(20) Martin, B. D.;Brandow, S. L.;Dressick, W. J.;Schull, T. L. Fabrication and Application of Hydrogel Stampers for Physisorptive Microcontact Printing *Langmuir* **2000**, *16*, 9944-9946.
(21) Hyun, J.;Zhu, Y.;Liebmann-Vinson, A.;Beebe, T. P.;Chilkoti, A. Microstamping on an Activated Polymer Surface: Patterning Biotin and Streptavidin onto Common Polymeric Biomaterials *Langmuir* **2001**, *17*, 6358-6367.
(22) Hyun, J.;Ma, H.;Banerjee, P.;Cole, J.;Gonsalves, K.;Chilkoti, A. Micropatterns of a Cell-Adhesive Peptide on an Amphiphilic Comb Polymer Film *Langmuir* **2002**, *18*, 2975-2979.
(23) Lahann, J.;Balcells, M.;Rodon, T.;Lee, J.;Choi, I. S.;Jensen, K. F.;Langer, R. Reactive Polymer Coatings: A Platform for Patterning Proteins and Mammalian Cells onto a Broad Range of Materials *Langmuir* **2002**, *18*, 3632-3638.
(24) Choi, J.;Rubner, M. F. Influence of the Degree of Ionization on Weak Polyelectrolyte Multilayer Assembly *Macromolecules* **2005**, *38*, 116-124.
(25) Tan, J. L.;Tien, J.;Chen, C. S. Microcontact Printing of Proteins on Mixed Self-Assembled Monolayers *Langmuir* **2002**, *18*, 519-523.
(26) Yoshikawa, Y.;Matsuoka, H.;Ise, N. Ordered Structure of Polyallylamine Hydrochloride in Dilute Solutions as Studied by Small-Angle X-Ray-Scattering *Br. Polym. J.* **1986**, *18*, 242-246.
(27) Gourdin, S.;Hammond, P. T. **To Be Submitted.**

Chapter 3 Controlling Mammalian Cell Adhesion on Patterned Polyelectrolyte Multilayer Surfaces

3.1. Introduction

The ability to pattern mammalian cells in specific areas on a surface has become a very important topic of research due to its applications in tissue engineering, cell arrays, and biosensors. To control the spatial adhesion of cells, areas that promote cell attachment must be patterned on a cell-inert background. Early work to confine cells to micron-size areas was performed by Carter, where fibroblasts were patterned on islands of palladium[1]. Later, the Whitesides group utilized self-assembled monolayers (SAMs) to present microcontact printed adhesive islands against an inert ethylene glycol (EG) background to geometrically control cell adhesion[2]. Since this work, many other groups have used either EG or poly(ethylene glycol) (PEG) as a cell-inert background[3, 4] making it the standard for resisting cell attachment. However, other materials have been explored such as albumin[5], phospholipid bilayers[6], mannitol[7], and polyacrylamide (PAAm)-PEG interpenetrated networks[8]. Research with these materials has shown that mammalian cells can be geometrically confined on a surface by turning off their interactions with the surrounding area[9]. However, for some cell patterning applications, there are limitations to these systems including long-term cell resistance and substrate choice. Studies have shown, for example, that when using EG or PEG as the cell-resist material, the pattern breaks down after a few days and cells overrun the entire surface[7, 10]. The loss of pattern

integrity has been attributed to oxidation and degradation of the resist region by alcohol dehydrogenase and aldehyde dehydrogenase[11, 12]. Many of the alternative resist-materials have also had problems keeping cell patterns intact[12]. Mannitol and PAAm-PEG interpenetrated networks are exceptions, since they exhibit good long-term pattern fidelity. However, mannitol and other SAMs require that the substrate usually be gold or a metal oxide since they are often bound to the surface using thiol or silane chemistry. Consequently, many materials including plastics are not possible substrates with this chemistry. For these reasons, we have chosen to explore cell patterning using newly discovered cytophobic materials based on specifically engineered polyelectrolyte multilayers[13, 14].

Polyelectrolyte multilayers have become excellent candidates for biomaterial applications due to the high degree of molecular control over the architecture and thickness of the films, the ability to incorporate proteins or other biomolecules into the layers without losing their functionality, and the simple aqueous process used to make these thin films. Since the layer-by-layer assembly technique was first developed, a variety of materials have been used to construct multilayer thin films including biologically relevant ones such as DNA, proteins, and enzymes[15]. In the field of biomaterials, research efforts have focused on using polyelectrolyte multilayers in drug delivery devices[16-18], biosensors[19], and surfaces to study cell interactions[20-25]. Recently, polyelectrolyte multilayers have been explored as cell resistant materials. Mendelsohn et al. systematically studied how the processing of these thin films on a molecular level affects cell interactions[13]. Weak polyelectrolytes offer the advantage of being able to change the film's molecular architecture using the same two polymers by adjusting the assembly pH[26, 27]. Using this approach, it was found that highly swellable films (~300-400%) prohibit cell adhesion, and tight ionically stitched films support cell attachment. Therefore, proper choice in processing

conditions as well as materials is important to create cell resistant polymer coatings. In addition to the cytophobic polyelectrolyte multilayer systems formed through electrostatic interactions, it was also found that hydrogen bonded multilayers made from either polyacrylic acid (PAA) or polymethacrylic acid (PMA) and PAAm are cytophobic due to their high degree of swelling[14]. They also exhibit great reduction in adsorption of some proteins on their surfaces. Although after assembly, these films are soluble at or above neutral pH, they can be stabilized by heat or photochemistry to make them suitable for cell culture assays. Experiments with wild type (WT) NR6 fibroblasts have shown that these films resist cells for as long as 1 month and only a few layers of PAA and PAAm (1 of each) are required to render the surface inert to cell adhesion. The small number of required layers is very desirable from a commercial point of view. For these reasons, we have chosen PAA/PAAm multilayers for further modification to produce cell patterns. As previously demonstrated[14], PAA/PAAm multilayers can be selectively erased to create patterns suitable for cell attachment on the underlying tissue culture polystyrene (TCPS). In this work, a method to add patterned ligands for direction of cell adhesion through specific interactions on these highly swollen films is presented.

Polymer-on-polymer stamping (POPS)[28, 29] is a technique well suited to selectively attach cell adhesion molecules to a cytophobic multilayer surface in a defined geometry. It is a straightforward soft lithographic technique that can be used to change the chemical functionality of a surface on a micron-scale over a large area. By adding a second functional group to the surface, it is then possible to selectively react specific biological ligands instead of simply relying on non-specific interactions to promote cell adhesion. This is important for applications requiring a particular ligand-integrin interaction for sorting cells or for studying adhesion effects of specific integrins. POPS is a soft lithographic technique that takes advantage of electrostatic,

as well as other secondary bonding interactions, between polymers to pattern a polymer surface with another polymer. It is a variation on microcontact printing[30] that eliminates the need to use gold or metal oxide surfaces. In previous work, this method has been shown to produce high-resolution patterns of graft copolymers, block copolymers, and oppositely charged polyelectrolytes on polymer surfaces. Particularly relevant to this paper is work done previously to pattern poly(allylamine hydrochloride) (PAH), a weak polycation on a PAA surface[31]. This method can be directly applied to the PAA/PAAm multilayer films when PAA is the outermost layer. By stamping a weak polycation, it is possible to control the density of available functional groups on the surface by altering the charge density through pH adjustment of the ink solution.

The surface density of patterned functional groups is important since it directly relates to the density of cell-adhesive ligands in our process scheme. Specifically, we will show that the density of the adhesion molecule, RGD (arg-gly-asp) can be controlled by the stamping conditions. The tri-amino acid sequence, RGD, is a known adhesion molecule that exists in the extracellular matrix protein, fibronectin[32]. It was demonstrated that the proliferation, morphology, migration, cytoskeletal organization, and adhesion of WT NR6 fibroblasts depends on the density and spatial presentation of RGD on otherwise inert surfaces such as PEG hydrogels[33] and PEG comb copolymers[34-36]. Similar effects of varying RGD density have been reported for other cell types such as myoblasts[37], endothelial cells[38], and osteoblasts[39]. A variety of methods have been introduced to attach ligands to a surface including incorporation into hydrogels[40], addition to segments in comb copolymers[34], and reaction with surface functional groups[41]. For patterns of PAH, the amine groups can be utilized to covalently bond ligands.

A heterobifunctional protein crosslinker, Sulfosuccinimidyl 6-[3'-(2-pyridyldithio)-propionamido] hexanoate (Sulfo-LC-SPDP) is used to attach ligands to the PAH patterns. Since

this crosslinker acts to bridge an amine group to a thiol group, any peptide ending in cysteine (peptide with a thiol group) can be attached to the surface. To demonstrate the ability to control the adhesion of fibroblasts, the peptide, GRGDSPC, was investigated. This molecule contains the adhesion-promoting amino acid sequence, RGD, which has been shown to be a ligand for WT NR6 fibroblasts, which express the $\alpha_5\beta_1$ and $\alpha_V\beta_3$ integrins[33].

Combining the nano-scale architectural control of polyelectrolyte multilayers and the micropatterning technique of soft lithography, this work examines how RGD density can be controlled through processing conditions which, in turn, can be used to control and influence cell adhesion in predefined regions on an inert background. We will show that cell activities such as spreading, morphology, and cytoskeletal organization can be controlled within micron-scale patterns by simply altering the ligand surface density through changes in the stamp ink pH of a weak polycation, PAH. This approach offers several advantages over the often used method of varying RGD surface density by altering the concentration of ligand in a reaction solution since the upper limit on density is predetermined by the inking pH condition.

3.2. Experimental Methods

1. Materials. Poly(acrylic acid) (PAA) (MW = 90,000; 25% aqueous solution) and polyacrylamide (PAAm) (MW = 5,000,000; 1% aqueous solution) were purchased from Polysciences. Poly(allylamine hydrochloride) (PAH) (MW = 70,000) was purchased from Sigma-Aldrich. The peptides GRGDSPC, YGRGDSPC, GRGESPC, and dansyl chloride labeled GRGDSPC were supplied from the MIT Biopolymers Lab. The peptide, GRGDS, was purchased from American Peptide. The protein crosslinker, Sulfosuccinimidyl 6-[3'-(2-pyridyldithio)-propionamido] hexanoate (Sulfo-LC-SPDP), was purchased from Pierce

Biotechnology. Dulbecco's Phosphate Buffered Saline (PBS) solution was obtained from Gibco/Invitrogen. Poly(dimethylsiloxane) (PDMS) stamps for polymer-on-polymer stamping were created by curing Sylguard 184 (a two ingredient elastomer kit purchased from Dow Chemical) on top of silicon masters with various micron-scale photoresist patterns[31]. All materials were used without any further purification.

2. Substrate Preparation. As described previously[42], multilayer thin films of hydrogen bonding polymers were assembled using a layer-by-layer dipping technique. An HMS programmable slide stainer from Zeiss, Inc. was employed to automate the dipping process. Dilute polyelectrolyte solutions were prepared (10^{-2} M based on repeat unit of the polymer) with 18 MΩ Millipore water, and were pH-adjusted with HCl. For the PAA/PAAm films, a layer of PAH was first deposited on the substrate (either tissue culture polystyrene (TCPS) or glass) for 15 minutes, and then taken through a series of three rinse baths of 18 MΩ Millipore water for 2, 1, and 1 minute, respectively. All rinse baths were adjusted to a pH of 3.0 for the multilayer assembly to assure stability of the hydrogen-bonded system. Following the base layer of PAH, the substrates were immersed in alternating baths of PAA and PAAm solutions with the same rinse procedure in between polymer baths until 6 total layers were assembled leaving PAA as the outermost layer for the multilayer films.

3. Stamping of weak polyelectrolytes. PAH was stamped following a previously described procedure[31, 43]. Briefly, PDMS stamps were inked by immersion in a 0.05 M (based on polymer repeat unit) pH adjusted PAH solution for 1 hour. The stamps were then briefly rinsed with water (~2 sec) and blown dry with air. Finally, the patterned side of the stamp was brought into contact with a polyelectrolyte multilayer platform for 30 seconds. Samples were then rinsed for 2 minutes in a water bath (pH unadjusted).

4. Peptide Coupling. Stamped samples were first incubated at room temperature for 30 minutes in a solution of 0.5 mM Sulfo-LC-SPDP in PBS. Following addition of the crosslinker, the samples were rinsed twice in PBS for 5 minutes. The samples were then incubated at room temperature for 8 hours in a solution of 0.5 mM peptide (either GRGDSPC, dansyl chloride labeled GRGDSPC, YGRGDSPC or GRGESPC) in PBS. Samples were then soaked twice in PBS (first overnight and second for 5 minutes).

5. Cell Culture. Murine wild type (WT) NR6 fibroblasts were employed for the cell culture experiments. WT NR6 fibroblasts are a cell line derived from NIH 3T3 cells and were provided by Prof. Linda Griffith's laboratory at MIT. Unless stated otherwise, all materials used for cell culture were purchased from Gibco/Invitrogen. The multilayer substrates patterned with the desired ligand were sterilized by treatment with 70% (v/v) ethanol. As seen from previous work[13], the sterilization procedure does not change the properties of the multilayer films. The WT NR6 fibroblasts were cultured in pH=7.4 media composed of Modified Eagles Medium-α (MEM-α) with 7.5% (v/v) fetal bovine serum (FBS), 1% (v/v) sodium pyruvate (100 mM), 1% (v/v) nonessential amino acids (10 mM), 1% (v/v) Geneticin (G418) antibiotic (350 μg/ 10 mL PBS), 1% (v/v) L-glutamine (200 mM), 1% (v/v) penicillin (10,000 U/mL, from Sigma), and 1% streptomycin (10 mg/mL, from Sigma). Cells were kept in a humid incubator at 37.5 °C and 5% CO_2.

For cell attachment assays, WT NR6 fibroblasts were counted using a hemocytometer with trypan blue exclusion for cell viability, and seeded at ~10,000 cells/cm^2 onto the patterned substrates. The media was changed every 3 days over the course of the experiment. Pictures documenting cell growth, spreading, and morphology were taken using a Nikon Eclipse TE300 inverted phase contrast microscope with Openlab 3.0 software.

6. Radiolabeling and measurement. Radiolabeling the peptide, YGRGDSPC, with I-125 and measuring the surface radioactivity after coupling to Sulfo-LC-SPDP led to quantification of ligand surface density. The Griffith lab at MIT developed the iodination procedure used in this work. The tyrosine present in the sequence was iodinated using the Iodobead method. A solution of 1 mg/mL peptide in 2-[N-morpholinoethane sulfonic acid] buffer (Sigma) was mixed 1 to 4 with a solution of sodium iodide-125 (PerkinElmer) in PBS in the presence of an Iodo-Bead (Pierce Biotechnology). The reaction was quenched with sodium metabisulfate (12 mg/mL, Sigma) in PBS and then chased with potassium iodide (Sigma) in PBS. The radiolabeled peptide was separated from unreacted I-125 by fractionating the reaction mixture in a C18 Sep-Pak Reverse phase cartridge (Waters) with solutions of water, methanol, and trifluoroacetic acid. The fractions of radiolabeled peptides were diluted with unlabeled peptides (200:1) and coupled to PAH stamped surfaces activated with Sulfo-LC-SPDP. The activities of samples and standards of known peptide concentrations were measured with a Packard Cobra II Auto-Gamma counter. Reported values for each condition represent an average of 24 samples subtracted from the background.

7. Immunostaining. After the WT NR6 fibroblasts were on the GRGDSPC-patterned surfaces for 2 days, cytoskeletal organization was studied by staining for actin stress fibers and vinculin (present in focal adhesions). Unless otherwise stated, all products were purchased from Sigma-Aldrich, and dilutions were made in PBS. Cells were fixed with 3.7% formaldehyde solution and permeabilized with 0.1% Triton X-100. After blocking with 2% bovine serum albumin (BSA), the fibroblasts were labeled with monoclonal anti-vinculin antibody produced in a mouse (50:1 dilution). Afterwards, the WT NR6 fibroblasts were stained with Alexa Fluor® 488 goat anti-mouse IgG (H+L) (2 mg/mL, 50:1 dilution, Molecular Probes) and rhodamine

phalloidin (200 U/mL, 75:1 dilution, Molecular Probes). Finally, the ProLong® Antifade Kit solution was applied to all samples (Molecular Probes). A Zeiss Axioplan 2 fluorescence microscope (Carl Zeiss Inc., Thornwood, NY) with a high-resolution digital camera was used to take pictures of the stained samples.

8. Soluble RGD tests. To check the specificity of the RGD-integrin interaction, the peptide sequence GRGDS was added to the media (for a final concentration of 100 μM) after the WT NR6 fibroblasts had been on the RGD-patterned surfaces for 3 days. Cells using specific integrins for RGD to attach to the patterned areas should detach in the presence of this concentration of soluble RGD.

9. Atomic Force Microscopy. The Digital Instruments Dimension 3000 atomic force microscope (AFM) (Digital Instruments, Santa Barbara, CA) was used in tapping mode to obtain topographical information about the stamped area including heights of stamped features. Stamp height values were obtained by examining the cross sections of AFM data. Reported values represent an average of at least 10 data points taken from different areas of the samples. Four different samples were used for each stamping condition.

10. Statistical Analysis. Analysis of variance (ANOVA) was used to test the statistical significance of differences in stamped thickness, fluorescence intensity, and I-125 activity. ANOVA determines whether or not the variance between testing conditions is greater than the variance within testing conditions. The *p*-value (or probability value) is the result of the ANOVA test, and a value less than 0.05 means the conditions are statistically different (based on a 5% level).

3.3. Results and Discussion

3.3.1. Functionalization and Characterization of Patterned PAH with RGD Peptides

Hydrogen-bonded multilayers fabricated from PAA and PAAm were used to create a cell resistant background in this study. Details concerning bilayer thickness and the cytophobic behavior of these thin films have been reported in previous work[14]. A surface can be rendered inert to cell adhesion with as few as two layers of PAA and PAAm. For this study, five layers of alternating PAA and PAAm were assembled on either glass (for fluorescence studies) or TCPS (for cell culture assays) substrates with a previously deposited PAH base layer, leaving PAA as the outermost layer. Five layers (dry thickness of ~ 50 Å) were enough to render the TCPS surface completely inert to WT NR6 fibroblasts seeded at 10,000 cells/cm^2. Only floating cells were observed on the surface after cell seeding, and previous work found no attachment after as long as 1 month (seeding cells every 5 days). The WT NR6 cell line was chosen due to its strong propensity to attach to most synthetic and natural polymeric surfaces.

To pattern cells using specific integrin-ligand interactions on the PAA/PAAm multilayers, it is necessary to selectively attach ligands for the particular cell type in predefined areas that can interact with the cell's adhesion receptors. To achieve this, a different functionality was first introduced on the PAA surface. Polymer-on-Polymer Stamping (POPS) was used to introduce amine functional groups to the multilayer surface for subsequent reaction. PAH was stamped onto the PAA surface of the PAA/PAAm multilayers by inking a PDMS stamp with a 0.05 M PAH solution and then bringing the stamp into contact with the surface after drying. Our previous study[31] with PAA/PAH multilayers demonstrated that altering the pH

of the stamping ink served as a means to control the number of available functional groups on the patterned surface. In essence, the number of available functional groups increased with inking pH due to an increase in the thickness of the stamped material. We expected to see the same effect with the 3.0/3.0 PAA/PAAm films. This was confirmed through AFM by comparing patterns of PAH stamped on the PAA/PAAm films at ink pH's of 3.5, 7.0, 9.0, and 11.0. AFM results indicate that the patterned PAH follows a trend of increasing pattern height with increasing pH. This is due to the deprotonation of the weak polycation as the ink pH is increased; as a result, the polymer takes on a more random coil conformation. At pH 3.5, the polymer is essentially fully charged, and the stamped region has an average thickness of 1.6 nm. When the pH of the stamping ink is raised, amine groups along the PAH chain become unprotonated, and the resulting pattern increases in height due to the transfer of more material to the surface. The pattern height is 2.5 nm with an ink pH of 7.0, 3.6 nm for pH 9.0, and reaches 6.1 nm for pH 11.0. The differences in thickness are statistically significant as determined by ANOVA p-values less than 0.05 (see experimental section).

PAA/PAAm multilayers with patterned PAH were reacted with the heterobifunctional protein crosslinker, Sulfo-LC-SPDP in a pH 7.4 PBS solution for 30 min. Sulfo-LC-SPDP is commonly used to join two proteins containing an amine and a thiol group, respectively. We adopted the process recommended by the manufacturer (Pierce Biotechnology) and tuned the different process variables to functionalize our patterned multilayers. Sulfo-LC-SPDP attaches to the PAH patterns through a covalent bond formed by the reaction between the N-hydroxysuccinimide (NHS) group and a primary amine from the PAH. A high solution pH is desired for the reaction, where the amine groups of PAH are not protonated; however, too high of a solution pH would result in hydrolysis before reaction. After activation of the amine groups,

the other end of the Sulfo-LC-SPDP molecule was reacted with a peptide containing a thiol group in a pH 7.4 PBS solution. The thiol group reacts with the 2-pyridyl disulfide residue on Sulfo-LC-SPDP to form a disulfide. The sequence, GRGDSPC, was selected because it contains the RGD sequence known to promote cell adhesion in WT NR6 fibroblasts[33], and it ends in cysteine which contains a thiol group. A peptide labeled with dansyl chloride was used to check the specificity of the reaction and to insure no peptide adhesion to the cell-inert regions. Dansyl chloride is a molecule that fluoresces a blue-green color when attached to a primary amine. Figure 3-1 shows fluorescent micrographs of dansyl chloride labeled GRGDSPC attached to PAH stamped at pH 11.0 (a and b) on a 3.0/3.0 PAA/PAAm multilayer surface. The two different patterns used in this assay were 200 x 100 μm rectangles and lines of varying widths (25 μm lines are shown). Fluorescence is only seen in the stamped areas meaning the peptide sequence only reacted with Sulfo-LC-SPDP attached to the PAH regions.

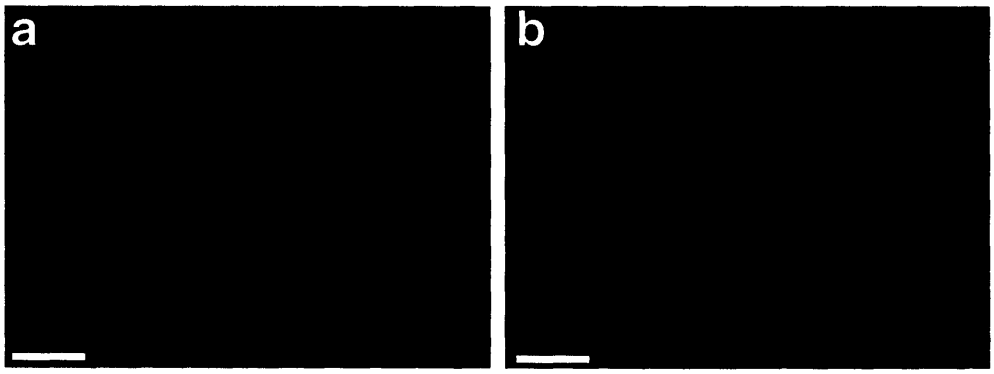

Figure 3-1. Fluorescence microscopy images of dansyl chloride labeled GRGDSPC sequences attached to PAH (a) line and (b) rectangle patterns stamped at pH = 11.0 (Scale bar, 100 μm).

Using Adobe Photoshop, the intensity of the dansyl chloride fluorescent regions can be analyzed to compare the relative number of peptides reacting on PAH regions created with different ink pHs. The fluorescent patterns become brighter as the PAH ink pH increases meaning a greater surface density of peptides. The average intensity for pH 3.5 is 0.21 compared

to 0.31 at pH 7.0 and 0.55 for pH 9.0 (normalized to pH 11.0 intensity). The differences are statistically significant and mean that ink pH offers a way to control the ligand surface density. It should be noted that in this study, ligand surface density refers to ligands bound throughout the thickness of the stamped material (up to 6.1 nm) since we assume cells can have access to all of these ligands in the swollen state. We believe our technique to control ligand density through simple pH adjustments in the stamping process is unique and offers process advantages compared to the alternative and more traditional method of varying ligand density by exposing a surface containing the same number of functional groups to solutions with different ligand concentrations. One advantage to our method is that multiple ligand densities can be easily introduced on the same surface by using multiple stamps inked at different pH. Figure 3-2 shows a fluorescent micrograph of such a surface presenting three different densities of fluorescein labeled GRGDSPC (intensities similar to dansyl chloride labeled peptides at given pH) attached to PAH stamped at pH 3.5 (vertical lines) and pH 11.0 (horizontal lines) on a 3.0/3.0 PAA/PAAm multilayer surface. This pattern was formed by first stamping the vertical 50 μm lines with a stamp inked at pH 3.5 (faint lines), and afterwards stamping a second set of lines with a stamp inked at pH 11.0 (brighter lines). Where the lines cross, a slightly higher density (1.07 normalized to pH 11.0 intensity) of ligand is observed. This type of pattern, which presents three different ligand densities on the same surface, would not be easily produced using the usual method of controlling ligand density.

Figure 3-2. Fluorescence microscopy image of fluorescein labeled GRGDSPC peptides attached to PAH stamped at pH 3.5 (vertical lines) and pH 11.0 (horizontal lines) using two separate stamps (Scale bar, 50 μm).

To quantitatively determine the ligand density of the stamped regions, peptides radiolabeled with I-125 were employed. The radioactivities of surfaces patterned with radiolabled ligands were compared to known peptide concentrations to calculate the ligand surface density. For samples stamped with PAH at pH 11.0, approximately 152,000 molecules/μm^2 of YGRGDSPC were attached to the patterned area. As expected, samples stamped with a lower pH ink had much lower peptide surface densities. When the PAH ink pH was lowered to 9.0, the ligand density dropped to 83,000 molecules/μm^2, and at ink pH 7.0, the density fell further to 53,000 molecules/μm^2. At the lowest ink pH tested, 3.5, the lowest peptide density, 25,000 molecules/μm^2, was obtained. Figure 3-3 displays a graph of these results. These ligand densities are similar to those studied previously in fibroblast experiments on highly compliant homogeneous surfaces[33].

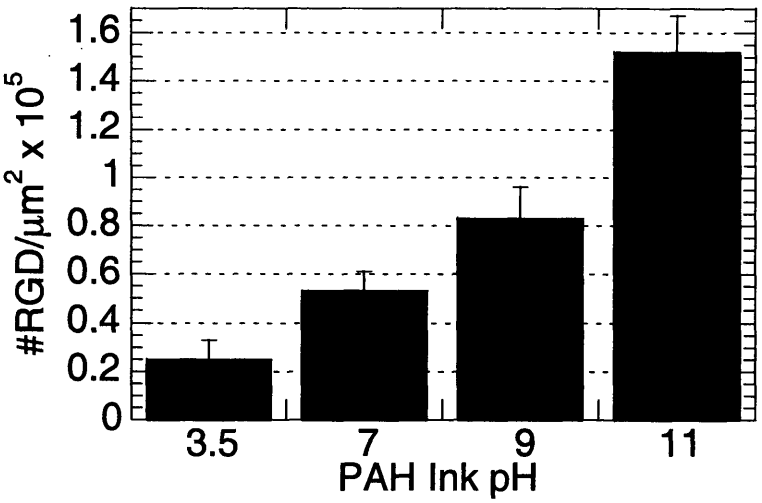

Figure 3-3. Ligand surface density as a function of PAH ink pH calculated from radiolabeling data.

3.3.2. Effect of Patterned RGD Density on WT NR6 Fibroblasts

After confirming the addition of GRGDSPC peptide sequences to the patterned PAH regions on the cytophobic multilayer background, we studied the effects of RGD density on WT NR6 fibroblast behavior. Cells were seeded at 10,000 cells/cm^2 and the attachment and spreading on the patterned surfaces was monitored for 5 days (except samples for long term cell resistance studies). Cells on samples stamped at pH 11.0 attached and spread to fill the patterned area a few hours after seeding. In contrast, fewer cells attached on patterned multilayers created with PAH inked at pH 3.5 and showed a rounded morphology. Even after 5 days, the patterns created with the lowest RGD density (PAH ink pH=3.5) did not become confluent with cells. Cells on surfaces patterned with intermediate RGD surface densities (pH 7.0 and pH 9.0) displayed behavior in between these two extremes. Figure 3-4 shows a comparison (2 days after seeding) of cell patterns. By visual inspection, more cells attach and pack closer together as the RGD density increases. It can be seen from the micrographs that the cells on the lowest RGD density patterns (pH 3.5) do not spread to nearly the same degree as on the higher density

surfaces. These results are consistent with what is seen on non-patterned surfaces of compliant polymers[33]. It can be concluded from this comparison that cell pattern density, as well as number of cells attached, increases with RGD density in the range investigated.

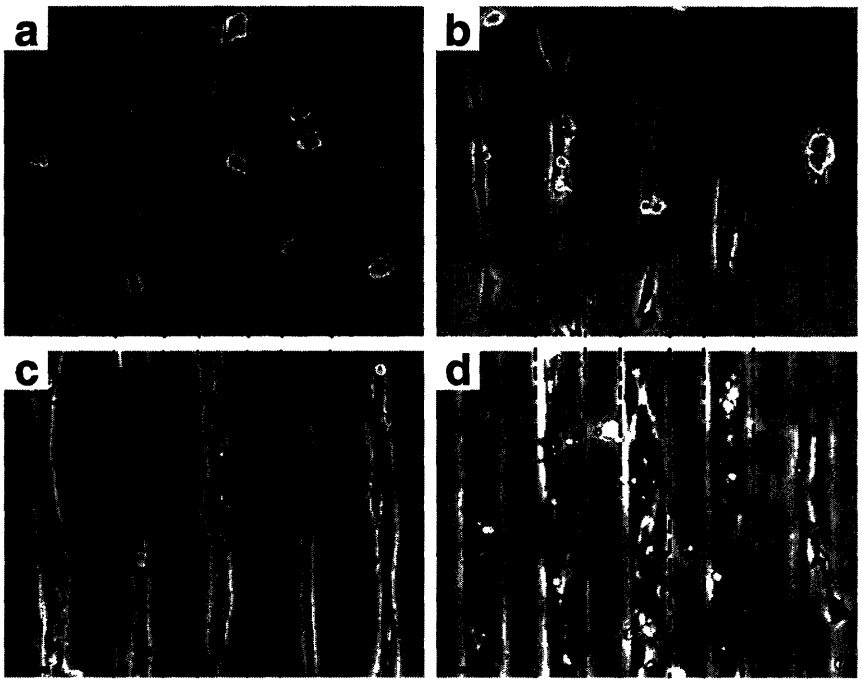

Figure 3-4. Phase contrast images of fibroblast adhesion on 50 μm patterned lines. Adhesion and spreading were compared for PAH stamped from ink solutions of pH (a) 3.5 (b) 7.0 (c) 9.0 (d) 11.0. Dotted lines were added to indicate a few of the patterned lines (Scale bar, 50 μm).

Patterns of different geometries were studied to determine the effect of line width or island size on cell adhesion and spreading. Lines varying from 10 to 100 μm were stamped along with rectangles ranging from 50 x 100 μm to 150 x 300μm. For all of the island sizes tested at pH 11.0, the cells spread and filled most of the adhesive rectangles. Due to the size of the rectangle patterns, multiple cells stuck to each island. For the line patterns tested, below a line width of 50 μm, lines of single cells were obtained. At higher widths, multiple cells filled the width of the adhesive lines. Figure 3-5 represents typical results from these cell assays. Cell patterns monitored for up to 1 month displayed no loss in fidelity during this time period. The

specificity of the ligand-integrin interaction was examined by two control experiments. First, soluble RGD ligand (GRGDS) was added to the culture medium at a concentration of 100 μM. In the presence of the soluble ligand, cells on the patterned area detached indicating a specific interaction. In a second set of experiments, the peptide, GRGESPC, was substituted in the surface fabrication procedure. The control sequence, RGE (arg-gly-glu) does not promote adhesion[44], and can be used to test the specificity of the ligand's interaction with the cell's adhesion receptor. Ensuing cell assays showed no cell attachment, indicating a necessity for an adhesion ligand on these patterned surfaces.

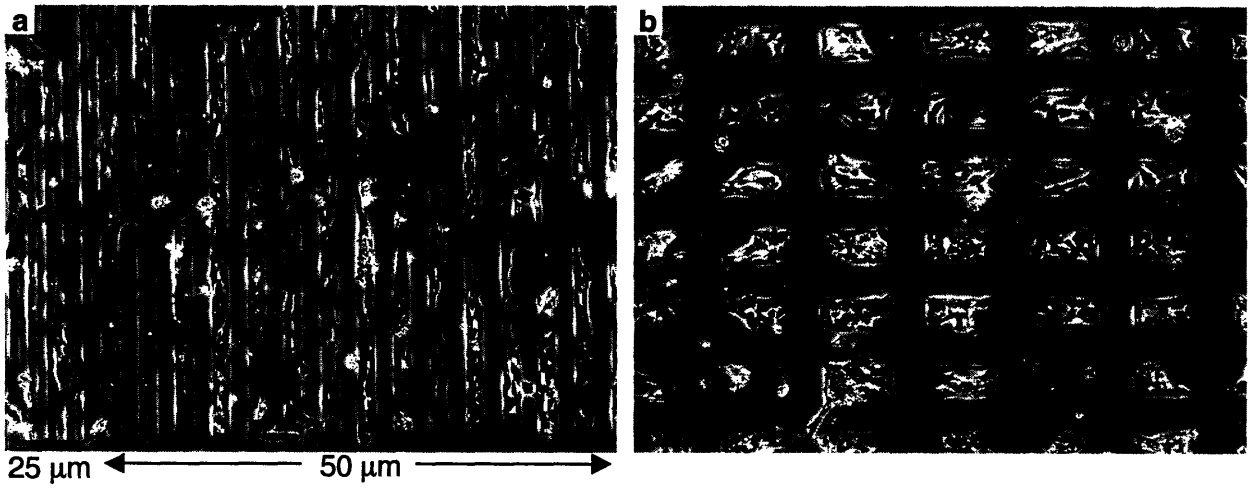

Figure 3-5. Phase contrast micrographs of WT NR6 fibroblasts adhering to patterns of high density GRGDSPC attached to PAH stamped at pH 11.0 on (a) lines with 25 μm to 50 μm widths and (b) 100 μm x 200 μm rectangles two days after seeding (Scale bar, 200 μm).

3.3.3. Effect of Patterned RGD Density on Cytoskeletal Protein Organization

To further study the differences RGD density invokes on patterned cells, we looked at the cytoskeletal protein organization. Cell cytoskeletal organization is an important aspect associated with variances in RGD density. The presence and arrangement of actin microfilaments and focal adhesion points help indicate the degree of adhesion strength and are central to adhesion signaling[45]. Focal adhesions are micron-sized structures usually located near

the periphery of the cell that form a strong adhesion to the substrate and secure bundles of actin microfilaments within the cell. They consist of a variety of proteins including vinculin, talin, and α-actinin, as well as signaling molecules such as focal adhesion kinase and paxillin[46]. Focal adhesion formation has important consequences on cell processes such as migration and helps determine adhesion strength. In this study, actin stress fibers were stained along with vinculin, a protein present in focal adhesions. Figure 3-6 illustrates the different results from the immunostaining corresponding to different GRGDSPC densities. Cells adhering to the patterns of low RGD density created by stamping PAH at pH 3.5 do not show focal adhesions or stress fibers spanning the cell's body. When the RGD density is increased to 53,000 RGD/μm^2 at stamp ink pH 7.0, stress fibers begin to become distinguishable but distinct focal adhesions are still not apparent. In contrast, cells on the higher RGD density patterns (83,000 RGD/μm^2 and 152,000 RGD/μm^2) form well-defined focal adhesions indicated by the bright green dashes located mostly at the periphery of the cell. In addition, actin microfilaments span the length of the cell. Clearly, the cytoskeletal proteins indicate a much stronger interaction with the patterned surface at a higher density of GRGDSPC.

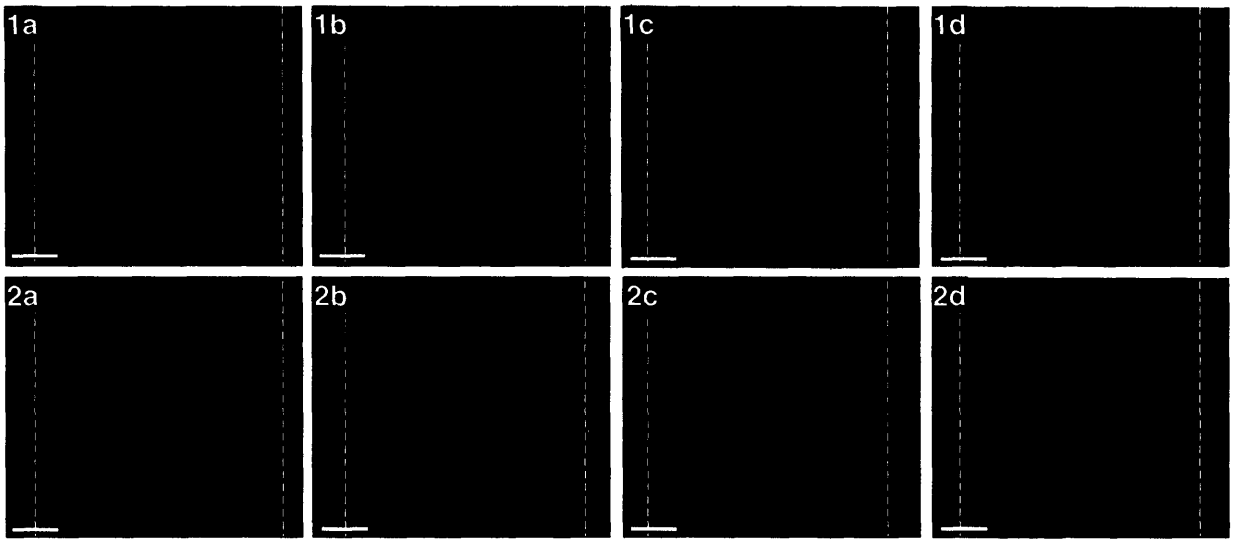

Figure 3-6. Immunostaining results for cytoskeletal proteins in WT NR6 fibroblasts. Actin stress fibers and vinculin stains were compared for PAH ink pH's of (1a and 2a) 3.5, (1b and 2b) 7.0, (1c and 2c) 9.0, and (1d and 2d) 11.0. The upper panel is composed of actin stains, and the lower panel is vinculin stains, and stamped areas are inside dotted lines (Scale bar, 20 μm).

On the highest RGD density patterns (83,000 and 152,000 RGD/μm^2), a majority of cells display well-formed stress fibers and focal adhesions. At similar RGD densities, Maheswari et al. reported this extent of cytoskeletal organization by clustering RGD on star polymers[33]. There are two possibilities why cells patterned on our very compliant multilayer films form well-defined focal adhesions and stress fibers, similar to the extent seen by Maheswari using clustered RGD. The first possibility is that our surfaces present clustered ligands. Ligand clustering could occur in our patterning scheme due to the change in conformation of PAH at high pH. The uncharged amine groups along the PAH backbone would tend to cluster together in the stamp ink solution, which could transfer to the surface as clusters of free amines for subsequent reaction with ligands. The other possibility is that our very swellable patterns by their nature present ligands in a manner that causes cells to cluster their integrins to form focal adhesions and stress fibers. Although more work needs to be done to determine which possibility is correct, this work clearly demonstrates the ability to pattern cells with a high degree of cytoskeletal protein

organization using a very simply stamping process. This eliminates the need to perform specific chemistry to cluster ligands or use fibronectin. It should be noted that on a much less compliant surface, silanized glass, Massia and Hubbell[47] found the critical density of RGD to produce focal adhesions in cells was 60 RGD/μm^2. Similar to our results, other groups working with more compliant polymer surfaces have found that significantly higher densities of RGD (ranging from 1,000 to well over 100,000 RGD/μm^2)[32, 33, 41, 48] are necessary to promote focal adhesion formation compared to the work by Hubbell and Massia. The rigidity of the surface along with the cytophobicity of the background both seem to be important in determining the minimum necessary RGD surface density to promote focal adhesion development.

We also looked at the role of geometry in stress fiber and focal adhesion formation. All of the rectangular patterns (50 x 100 μm and larger) were large enough for the cells to spread, and the cells formed focal adhesions primarily near the boundary of the pattern at the highest RGD density (data not shown). Figure 3-7 shows cells patterned on 10 (1a and 2a), 25 (1b and 2b), and 50 μm (1c and 2c) lines with the highest RGD density of 152,000 molecules/μm^2. On the very thin lines, the cells extended to great lengths, but well formed focal adhesions and stress fibers were not observed. However, the wider line widths allowed the cells to spread to a greater degree in two dimensions, and as a result, the fibroblasts spread and were able to interact more with the surface. In Figure 3-7, the bright green dashes near the periphery of the cells in 2b and 2c indicate the formation of focal adhesions, which are absent in 2a. These results are similar to a recent study by Chen et al. where pattern sizes that allow cell spreading were found to induce cell tension and focal adhesion formation[49]. In this case and in ours, cells must be allowed to adequately spread for formation of well-defined stress fibers and focal adhesions. The ability to

control integrin clustering through geometry could have applications in studying cell processes such as migration on a patterned surface since cytoskeletal proteins affect cell signaling.

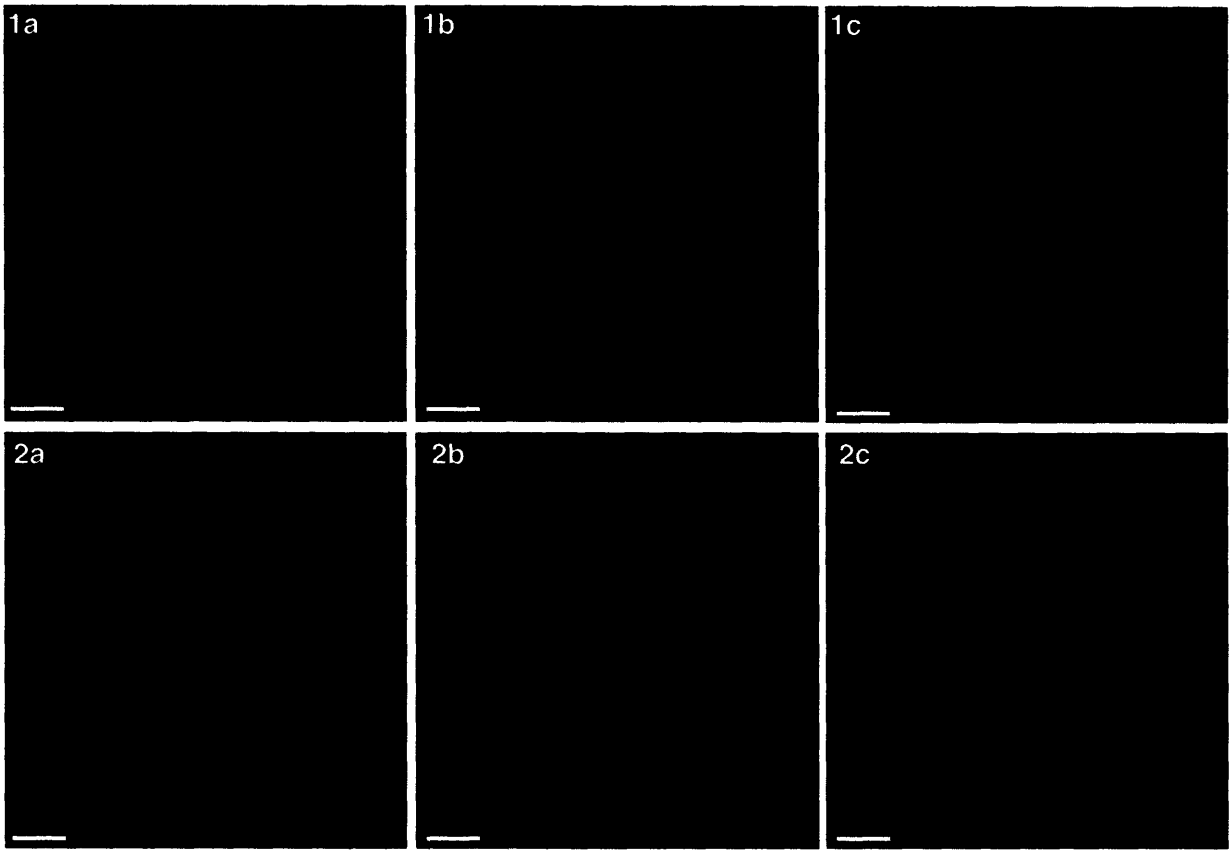

Figure 3-7. Geometric effects on cytoskeletal organization. Actin stress fiber and vinculin stains of WT NR6 fibroblasts attached to high density GRGDSPC, 152,000 molecules/μm^2, patterns of (1a and 2a) 10 μm, (1b and 2b) 25 μm, and (1c and 2c) 50 μm width lines. The upper panel is composed of actin stains, and the lower panel is vinculin stains (Scale bar, 10 μm).

3.4. Conclusions

We have demonstrated the ability to selectively attach WT NR6 fibroblasts to patterns composed of different RGD densities on a cell resistant polyelectrolyte multilayer surface. By stamping PAH, a weak polycation, we were able to control the RGD density simply through the stamping conditions to create patterns of varying amounts of functional groups for consequent reaction with the ligand, GRGDSPC. These patterns enabled us to study cell behavior at

differing ligand density under geometric constraints. We found that cell attachment, morphology, and cytoskeletal protein organization were affected by GRGDSPC density. This new methodology to create ligand patterns is a very versatile technique to control cell activity as well as cell alignment on these very compliant films. By using polyelectrolyte multilayers as the cytophobic background, we gain the advantages associated with these thin films including nanoscale control over thickness, ease of processing, and the ability to coat a wide variety of substrates and geometries. Our method to control ligand density has the advantage of being able to use the same reaction solution for many batches of samples without changing resulting ligand density. This means higher uniformity of ligand surface density across many samples. In addition, the patterns remain intact even after a month of cell culture making them superior to EG resist surfaces.

References for Chapter 3

(1) Carter, S. B. Haptotactic Islands: A Method of Confining Single Cells to Study Individual Cell Reactions and Clone Formation *Exp. Cell Res.* **1967**, *48*, 189.

(2) Chen, C. S.;Mrksich, M.;Huang, S.;Whitesides, G. M.;Ingber, D. E. Geometric Control of Cell Life and Death *Science* **1997**, *276*, 1425-1428.

(3) Hyun, J.;Ma, H.;Banerjee, P.;Cole, J.;Gonsalves, K.;Chilkoti, A. Micropatterns of a Cell-Adhesive Peptide on an Amphiphilic Comb Polymer Film *Langmuir* **2002**, *18*, 2975-2979.

(4) Lahann, J.;Balcells, M.;Rodon, T.;Lee, J.;Choi, I. S.;Jensen, K. F.;Langer, R. Reactive Polymer Coatings: A Platform for Patterning Proteins and Mammalian Cells onto a Broad Range of Materials *Langmuir* **2002**, *18*, 3632-3638.

(5) Ostuni, E.;Kane, R.;Chen, C. S.;Ingber, D. E.;Whitesides, G. M. Patterning Mammalian Cells Using Elastomeric Membranes *Langmuir* **2000**, *16*, 7811-7819.

(6) Groves, J. T.;Mahal, L. K.;Bertozzi, C. R. Control of Cell Adhesion and Growth with Micropatterned Supported Lipid Membranes *Langmuir* **2001**, *17*, 5129-5133.

(7) Luk, Y.-Y.;Kato, M.;Mrksich, M. Self-Assembled Monolayers of Alkanethiolates Presenting Mannitol Groups Are Inert to Protein Adsorption and Cell Attachment *Langmuir* **2000**, *16*, 9604-9608.

(8) Tourovskaia, A.;Barber, T.;Wickes, B. T.;Hirdes, D.;Grin, B.;Castner, D. G.;Healy, K. E.;Folch, A. Micropatterns of Chemisorbed Cell Adhesion-Repellent Films Using Oxygen Plasma Etching and Elastomeric Masks *Langmuir* **2003**, *19*, 4754-4764.

(9) Folch, A.;Toner, M. Microengineering of Cellular Interactions *Annu. Rev. Biomed. Eng.* **2000**, *2*, 227-256.

(10) Ostuni, E.;Chapman, R. G.;Liang, M. N.;Meluleni, G.;Pier, G.;Ingber, D. E.;Whitesides, G. M. Self-Assembled Monolayers That Resist the Adsorption of Proteins and the Adhesion of Bacterial and Mammalian Cells *Langmuir* **2001**, *17*, 6336-6343.

(11) Herold, D. A.;Keil, K.;Bruns, D. E. Oxidation of Polyethylene Glycols by Alcohol-Dehydrogenase *Biochem. Pharmacol.* **1989**, *38*, 73-76.

(12) Nelson, C. M.;Raghavan, S.;Tan, J. L.;Chen, C. S. Degradation of Micropatterned Surfaces by Cell-Dependent and -Independent Processes *Langmuir* **2003**, *19*, 1493-1499.

(13) Mendelsohn, J. D.;Yang, S. Y.;Hiller, J.;Hochbaum, A. I.;Rubner, M. F. Rational Design of Cytophilic and Cytophobic Polyelectrolyte Multilayer Thin Films *Biomacromolecules* **2003**, *4*, 96-106.

(14) Yang, S. Y.;Mendelsohn, J. D.;Rubner, M. F. New Class of Ultrathin, Higly Cell-Adhesion-Resistant Polyelectrolyte Multilayers with Micropatterning Capabilities *Biomacromolecules* **2003**, *4*, 987-994.

(15) Decher, G. Fuzzy Nanoassemblies: Toward Layered Polymeric Multicomposites *Science* **1997**, *277*, 1232-1237.

(16) Caruso, F.;Trau, D.;Mohwald, H.;Renneberg, R. Enzyme Encapsulation in Layer-by-Layer Engineered Polymer Multilayer Capsules *Langmuir* **2000**, *16*, 1485-1488.

(17) Chung, A. J.;Rubner, M. F. Methods of Loading and Releasing Low Molecular Weight Cationic Molecules in Weak Polyelectrolyte Multilayer Films *Langmuir* **2002**, *18*, 1176-1183.

(18) Vazquez, E.;Dewitt, D. M.;Hammond, P. T.;Lynn, D. M. Construction of Hydrolytically-Degradable Thin Films Via Layer-by-Layer Deposition of Degradable Polyelectrolytes *J. Am. Chem. Soc.* **2002**, *124*, 13992-13993.
(19) Decher, G.;Lehr, B.;Lowack, K.;Lvov, Y.;Schmitt, J. New Nanocomposite Films for Biosensors: Layer-by-Layer Adsorbed Films of Polyelectrolytes, Proteins or DNA *Biosens. Bioelectron.* **1994**, *9*, 677-684.
(20) Chluba, J.;Voegel, J.-C.;Decher, G.;Erbacher, P.;Schaaf, P.;Ogier, J. Peptide Hormone Covalently Bound to Polyelectrolytes and Embedded into Multilayer Architectures Conserving Full Biological Activity *Biomacromolecules* **2001**, *2*, 800-805.
(21) Grant, G. G. S.;Koktysh, D. S.;Yun, B.;Matts, R. L.;Kotov, N. A. Layer-by-Layer Assembly of Collagen Thin Films: Controlled Thickness and Biocompatibility *Biomed. Microdevices* **2001**, *3*, 301-306.
(22) Serizawa, T.;Yamaguchi, M.;Matsuyama, T.;Akashi, M. Alternating Bioactivity of Polymeric Layer-by-Layer Assemblies: Anti- Vs Procoagulation of Human Blood on Chitosan and Dextran Sulfate Layers *Biomacromolecules* **2000**, *1*, 306-309.
(23) Elbert, D. L.;Herbert, C. B.;Hubbell, J. A. Thin Polymer Layers Formed by Polyelectrolyte Multilayer Techniques on Biological Surfaces *Langmuir* **1999**, *15*, 5355-5362.
(24) Tryoen-Toth, P.;Vautier, D.;Haikel, Y.;Voegel, J.-C.;Schaaf, P.;Chluba, J.;Ogier, J. Viability, Adhesion, and Bone Phenotype of Osteoblast-Like Cells on Polyelectrolyte Multilayer Films *J. Biomed. Mater. Res.* **2002**, *60*, 657-667.
(25) Jessel, N.;Atalar, F.;Lavalle, P.;Mutterer, J.;Decher, G.;Schaaf, P.;Voegel, J. C.;Ogier, J. Bioactive Coatings Based on a Polyelectrolyte Multilayer Architecture Functionalized by Embedded Proteins *Adv. Mater.* **2003**, *15*, 692-695.
(26) Yoo, D.;Shiratori, S. S.;Rubner, M. F. Controlling Bilayer Composition and Surface Wettability of Sequentially Adsorbed Multilayers of Weak Polyelectrolytes *Macromolecules* **1998**, *31*, 4309-4318.
(27) Shiratori, S. S.;Rubner, M. F. Ph-Dependent Thickness Behavior of Sequentially Adsorbed Layers of Weak Polyelectrolytes *Macromolecules* **2000**, *33*, 4213-4219.
(28) Jiang, X.;Hammond, P. T. Selective Deposition in Layer-by-Layer Assembly: Functional Graft Copolymers as Molecular Templates *Langmuir* **2000**, *16*, 8501-8509.
(29) Jiang, X.;Zheng, H.;Gourdin, S.;Hammond, P. T. Polymer-on-Polymer Stamping: Universal Approaches to Chemically Patterned Surfaces *Langmuir* **2002**, *18*, 2607-2615.
(30) Kumar, A.;Whitesides, G. M. Patterned Condensation Figures as Optical Diffraction Gratings *Science* **1994**, *263*, 60-62.
(31) Berg, M. C.;Choi, J.;Hammond, P. T.;Rubner, M. F. Tailored Micropatterns through Weak Polyelectrolyte Stamping *Langmuir* **2003**, *19*, 2231-2237.
(32) Brandley, B. K.;Schnaar, R. L. Covalent Attachment of an Arg-Gly-Asp Sequence Peptide to Derivatizable Polyacrylamide Surfaces: Support of Fibroblast Adhesion and Long-Term Growth *Anal. Biochem.* **1988**, *172*, 270-278.
(33) Maheshwari, G.;Brown, G.;Lauffenburger, D. A.;Wells, A.;Griffith, L. G. Cell Adhesion and Motility Depend on Nanoscale Rgd Clustering *J. Cell Sci.* **2000**, *113*, 1677-1686.
(34) Irvine, D. J.;Mayes, A. M.;Griffith, L. G. Nanoscale Clustering of Rgd Peptides at Surfaces Using Comb Polymers. 1. Synthesis and Characterization of Comb Thin Films *Biomacromolecules* **2001**, *2*, 85-94.

(35) Irvine, D. J.;Ruzette, A.-V. G.;Mayes, A. M.;Griffith, L. G. Nanoscale Clustering of RGD Peptides at Surfaces Using Comb Polymers. 2. Surface Segregation of Comb Polymers in Polylactide *Biomacromolecules* **2001**, *2*, 545-556.
(36) Koo, L. Y.;Irvine, D. J.;Mayes, A. M.;Lauffenburger, D. A.;Griffith, L. G. Co-Regulation of Cell Adhesion by Nanoscale Rgd Organization and Mechanical Stimulus *J. Cell Sci.* **2002**, *115*, 1423-1434.
(37) Rowley, J. A.;Mooney, D. J. Alginate Type and RGD Density Control Myoblast Phenotype *J. Biomed. Mater. Res.* **2002**, *60*, 217-223.
(38) Mann, B. K.;West, J. L. Cell Adhesion Peptides Alter Smooth Muscle Cell Adhesion, Proliferation, Migration, and Matrix Protein Synthesis on Modified Surfaces and in Polymer Scaffolds *J. Biomed. Mater. Res.* **2002**, *60*, 86-93.
(39) Shin, H.;Jo, S.;Mikos, A. G. Modulation of Marrow Stromal Osteoblast Adhesion on Biomimetic Oligo Poly(Ethylene Glycol) Fumarate Hydrogels Modified with Arg-Gly-Asp Peptides and a Poly(Ethylene Glycol) Spacer *J. Biomed. Mater. Res.* **2002**, *61*, 169-179.
(40) Hern, D. L.;Hubbell, J. A. Incorporation of Adhesion Peptides into Nonadhesive Hydrogels Useful for Tissue Resurfacing *J. Biomed. Mater. Res.* **1998**, *39*, 266-276.
(41) Neff, J. A.;Tresco, P. A.;Caldwell, K. D. Surface Modification for Controlled Studies of Cell-Ligand Interactions *Biomaterials* **1999**, *20*, 2377-2393.
(42) Yang, S. Y.;Rubner, M. F. Micropatterning of Polymer Thin Films with pH-Sensitive and Cross-Linkable Hydrogen-Bonded Polyelectrolyte Multilayers *J. Am. Chem. Soc.* **2002**, *124*, 2100-2101.
(43) Tan, J. L.;Tien, J.;Chen, C. S. Microcontact Printing of Proteins on Mixed Self-Assembled Monolayers *Langmuir* **2002**, *18*, 519-523.
(44) Drumheller, P. D.;Hubbell, J. A. Polymer Networks with Grafted Cell Adhesion Peptides for Highly Biospecific Cell Adhesive Substrates *Anal. Biochem.* **1994**, *222*, 380-388.
(45) Sastry, S. K.;Burridge, K. Focal Adhesions: A Nexus for Intracellular Signaling and Cytoskeletal Dynamics *Exp. Cell Res.* **2000**, *261*, 25-36.
(46) Geiger, B.;Bershadsky, A.;Pankov, R.;Yamada, K. M. Transmembrane Crosstalk between the Extracellular Matrix and the Cytoskeleton *Nat. Rev. Mol. Cell Bio.* **2001**, *2*, 793-805.
(47) Massia, S. P.;Hubbell, J. A. An Rgd Spacing of 440 Nm Is Sufficient for Integrin Alpha V Beta 3- Mediated Fibroblast Spreading and 140 Nm for Focal Contact and Stress Fiber Formation *J. Cell Biol.* **1991**, *114*, 1089-1100.
(48) Hersel, U.;Dahmen, C.;Kessler, H. Rgd Modified Polymers: Biomaterials for Stimulated Cell Adhesion and Beyond *Biomaterials* **2003**, *24*, 4385-4415.
(49) Chen, C. S.;Alonso, J. L.;Ostuni, E.;Whitesides, G. M.;Ingber, D. E. Cell Shape Provides Global Control of Focal Adhesion Assembly *Biochem. Biophys. Res. Commun.* **2003**, *307*, 355-361.

Chapter 4 Controlled Release from Porous Polyelectrolyte Multilayers

4.1. Introduction

Controlled drug release materials have potential for utilization in biomedical implants, tissue engineering, and targeted drug delivery devices. The advantages of controlled release include greater drug effectiveness, better balanced drug concentrations in the body, and more convenience to the patient[1]. In addition, when the drug releasing agents are targeted for specific cell types or applied to an implant surface, they offer a means for local delivery, which reduces toxicity and increases the efficiency of the drug. One example of a drug releasing implant is a drug-eluting coronary stent for possible prevention of restenosis. Restenosis is a deleterious process that results in the narrowing or closing of an artery after some cardiac surgeries. In this application, coatings that elute a variety of drugs including anticoagulants, corticosteroids, and antimitotic agents have been employed[2, 3]. Porous materials offer a means to load such drugs and perhaps better control their release. The porous polyelectrolyte multilayers discussed in this paper can be designed to provide sustained release at a specified rate for a selected period of time, and therefore offer very promising properties as stent coatings as well as many other biomedical applications. In fact, one of the drugs studied, cytochalasin D, has been investigated for possible prevention of restenosis[4].

Over the last decade, polyelectrolyte multilayers have shown a great deal of promise due to the high degree of control over film properties, flexibility in choice of assembly components,

and ease of processing possible with these layer-by-layer assembled thin films. Polyelectrolyte multilayers are ultra-thin films, which are assembled one molecular layer at a time by taking advantage of attractive interactions between the constituents[5]. These films have shown potential in the area of biomaterials with particular applications in controlled cell-surface interactions[6-10], cell arrays[11], drug delivery[12-20], and biosensors[21]. In the area of drug delivery, polyelectrolyte multilayers coated onto drug microparticles have been shown to prolong the release time of the drug[13, 22]. The permeability of the drug through the multilayer coating could be controlled through changes in the number of layers and the polymers used during multilayer assembly. However, the maximum release time achieved was only on the order of hours when using the multilayer films as barriers. Longer release times have been achieved using thermoresponsive multilayers containing poly(N-isopropylacrylamide-co-acrylic acid) to deliver such drugs as insulin[18] and doxorubicin[19]. Another promising approach is degradable polyelectrolyte multilayers, which have been studied for releasing DNA[23] or charged polymer drugs such as heparin[24]. In this case, the films were built by alternating the selected drug with polyelectrolytes containing hydrolytically degradable ester bonds. A linear release profile was generated as the layers degraded and the drug could escape. Linear release means the rate of drug release remains constant over time, which is a very desirable attribute because it leads to a consistent drug concentration in a patient's body. Polyelectrolyte multilayers have also been examined as drug delivery coatings specifically engineered for stents[25]. In this case, sodium nitropusside was loaded into the multilayers during the polycation assembly steps.

Our approach with polyelectrolyte multilayers is very different. Instead of using the films as barriers to release or as degradable films, we utilized porous weak polyelectrolyte multilayers as micro- or nano-scale containers for holding and releasing the drug. A similar

strategy for controlled release has been used for porous silicon[26, 27], which is capable of sustained release of drug molecules over the course of hours to a few days. However, there are many distinct advantages to polyelectrolyte multilayers. Besides their ability to coat virtually any substrate, the key parameters of weak polyelectrolyte multilayers such as bilayer thickness and composition can be modified through simple pH adjustment during assembly[28]. Also, polymers provide a better means to mimic biological materials compared to silicon. Mendelsohn et al.[29] were the first to demonstrate a porosity transition in certain multilayers made from the weak polyelectrolytes, poly(allyl amine hydrochloride) (PAH) and polyacrylic acid (PAA). Since that time, these porous films have been suggested for use in many optical applications such as anti-reflection coatings[30], Bragg reflectors[31], and optical shutters[32]. In this work, we present data indicating that these pores can be loaded with small molecule drugs for controlled release in a buffer solution. Polyelectrolyte multilayers loaded with charged drugs have previously demonstrated controlled release into aqueous solutions[15, 17], but the films released small molecules very quickly in a buffer solution[15]. In contrast, porous PAH/PAA multilayers extend the total release time to many days in buffer. In addition, by changing the number of layers and pore size, the release duration and rate can be controlled. Finally, we show that multilayer heterostructures composed of alternating porous and non-porous regions act as dielectric mirrors that allow the drug loading process to be monitored optically. It should be noted that part of the work in this chapter has been done in collaboration with Dr. Lei Zhai at MIT.

4.2. Experimental Methods

Materials. Poly(acrylic acid) (PAA) (MW = 90,000; 25% aqueous solution) was purchased from Polysciences. Poly(allylamine hydrochloride) (PAH) (MW = 70,000),

poly(sodium 4-styrene-sulfonate) (SPS), Cytochalasin D, and ketoprofen were purchased from Sigma-Aldrich. Dulbecco's Phosphate Buffered Saline (PBS) solution was obtained from Gibco/Invitrogen. All materials were used without any further purification.

Substrate Preparation. As described previously[33], polyelectrolyte multilayer films were assembled using a layer-by-layer dipping technique. The dipping process was automated by an HMS programmable slide stainer from Zeiss, Inc. Dilute polyelectrolyte solutions were prepared (10^{-2} M based on repeat unit of the polymer) with 18 MΩ Millipore water, and were pH-adjusted with HCl or NaOH. PAH/PAA multilayers were built by alternately adsorbing PAH (pH=8.5) and PAA (pH=3.5) from 10^{-2} M aqueous solutions for 15 minutes onto a glass microscope slide or a PAH/SPS block. Between polymer solutions, the substrate was taken through a series of three rinse baths of 18 MΩ Millipore water for 2, 1, and 1 minute, respectively. This procedure was repeated until either 5, 8, 15, or 20 bilayers were built. A bilayer is defined as a layer of polycation and polyanion. PAH/SPS multilayers were assembled using 10^{-2} M aqueous solutions of PAH (pH=4.0) and SPS (pH=4.0) with 0.1 M NaCl added to the solutions. For these blocks, the substrate was immersed for 5 minutes in the polyelectrolyte solutions followed by the same rinsing procedure described above. The PAH/SPS blocks contained 50, 50.5, or 130 bilayers.

The multilayer films were assembled to contain either a single porous PAH/PAA region or an architecture composed of PAH/PAA and PAH/SPS alternating blocks. For films containing both types of blocks, a 50.5 bilayer block of PAH/SPS was assembled first, followed by alternating blocks of PAH/PAA and PAH/SPS with PAH/SPS left as the last block. The designations for all the films fabricated are presented in Table 4-1, where, for example $(PAH/PAA)_{15}$ corresponds to 15 bilayers of PAH/PAA.

Porosity Induction. The assembled polyelectrolyte multilayer films were immersed in pH 2.0, 2.2 or 2.3 water for 5 minutes followed by treatment in pH 5.5 (DI water) or pH 10.0 NaOH solution for 5 minutes. This sequential process creates either nanoporous or microporous films depending on the pH treatment as previously described[29, 31]. After the porosity transition, the films were then heated at 180 °C for 2 hours to crosslink the films and lock in the porous structure.

Drug Loading and Release. The model drugs, ketoprofen and cytochalasin D, were loaded into the porous multilayer films through either absorption or by wicking from a DMSO solution. For films loaded using absorption, the multilayers were immersed in the drug solution for 8 hours. The wicking experiments were carried out by placing the edge of the multilayer film into the drug solution and allowing the drug solution to wick up the film for 8 hours. Films were then rinsed in phosphate buffered saline (PBS) for 2 hours to displace the DMSO and eliminate any loosely bound drug. When DMSO filled the pores in the films, the reflectivity changed drastically, so, this phenomenon could be used to monitor the drug loading the pores and removal of DMSO during rinsing. After rinsing, samples were submerged in PBS, and the release of the drug was then monitored using a Cary 6000i UV-VIS NIR spectrophotometer from Varian. An aliquot was taken from the PBS solution (in which the sample was submerged), and the absorbance peak height of the aliquot was measured at 260 nm for ketoprofen or 280 nm for cytochalasin D. Finally the aliquot was returned to the sample container. The absorbance values were translated to concentration values by comparing to standard solutions for each drug. Standard solutions were prepared in PBS ranging in concentration from 10 ng/mL to 1000 ng/mL, and the applicability of Beers Law was confirmed for the absorbance values obtained in the drug release studies. After converting the absorbance peak heights to concentration values,

they were plotted versus time until a plateau was reached and persisted for at least 10 days. The total amount of drug released from the films was obtained from the value of drug concentration in the plateau region of the graph, and the time at which the plateau first developed was the total release time. For nanoporous films, in which the release curve was linear, the release flux could be obtained from the slope of a line fitted to the data.

Cell Culture. Murine wild type (WT) NR6 fibroblasts were provided by Prof. Linda Griffith's laboratory at MIT for the cell culture experiments. These fibroblasts are a cell line derived from NIH 3T3 cells. Unless noted otherwise, all materials used for cell culture were purchased from Gibco/Invitrogen. The substrates coated with cytochalasin D loaded multilayer films were sterilized by treatment with 70% (v/v) ethanol. As studied in previous work[9], the sterilization procedure does not change the properties of the multilayer films. The WT NR6 fibroblasts were cultured in pH=7.4 media comprised of Modified Eagles Medium-α (MEM-α) with 7.5% (v/v) fetal bovine serum (FBS), 1% (v/v) sodium pyruvate (100 mM), 1% (v/v) nonessential amino acids (10 mM), 1% (v/v) Geneticin (G418) antibiotic (350 μg/ 10 mL PBS), 1% (v/v) L-glutamine (200 mM), 1% (v/v) penicillin (10,000 U/mL, from Sigma), and 1% streptomycin (10 mg/mL, from Sigma). Cells were kept in a humid incubator at 37.5 °C and 5% CO_2.

For cell assays, WT NR6 fibroblasts were counted using a hemocytometer with trypan blue exclusion for cell viability, and seeded at ~10,000 cells/cm^2 onto the substrates. Micrographs documenting cell growth, spreading, and morphology were taken using a Nikon Eclipse TE300 inverted phase contrast microscope with Openlab 3.0 software.

DAPI staining. After the WT NR6 fibroblasts were on either the control or cytochalasin D releasing surfaces for 3 days, the nuclei were stained with 4',6-Diamidino-2-phenylindole

dihydrochloride (DAPI) to elucidate the effects of cytochalasin D. All products were purchased from Sigma-Aldrich, and dilutions were made in PBS. Cells were fixed with 3.7% formaldehyde solution and made permeable with 0.1% Triton X-100. The nuclei were then stained with 0.5 μg/mL DAPI solution for 15 minutes. A Zeiss Axioplan 2 fluorescence microscope (Carl Zeiss Inc., Thornwood, NY) with a high-resolution digital camera was used to take pictures of the stained samples.

Film Characterization. Dry film thicknesses were obtained using a Tencor P-10 Surface Profiler (Tencor, Santa Clara, CA). Each data point presented represents an average of at least three independent measurements. The error for profilometry was approximately 3%. The Digital Instruments Dimension 3000 atomic force microscope (AFM) (Digital Instruments, Santa Barbara, CA) was used in tapping mode to obtain topographical information about the film surface including average pore sizes and range in pore size.

Statistical Analysis. Analysis of variance (ANOVA) was used to test the statistical significance of release rate and amount released for the samples. ANOVA determines whether or not the variance in drug release between different multilayer architectures is greater than the variance within samples of the same multilayer architecture. A *p*-value (or probability value) of the ANOVA test that is less than 0.05 means the drug release properties are statistically different (based on a 5% confidence level).

4.3. Results and Discussion

4.3.1. Porous Film Characterization

In this study, two types of polyelectrolyte multilayer architectures were examined. These included multilayer films with only a single porous region, and heterostructure films containing

both porous and non-porous regions. Previous work demonstrated that structures with alternating porous and non-porous regions behave as dielectric mirrors due to the difference in the indices of refraction of the different regions and that these porous heterostructures could be loaded with small molecules such as liquid crystals[31]. Both types of multilayer films were loaded with either ketoprofen or cytochalasin D. In addition to these materials, we have successfully loaded and released progesterone, indomethacin, camptothecin, and beta-estradiol from nanoporous multilayers. Ketoprofen and cytochalasin D were selected from this group to study in detail: their chemical structures are shown in Figure 4-1. Cytochalasin D prevents cells from undergoing mitosis (discussed in detail in a later section) and therefore was used as a marker to prove that a drug released from a porous multilayer remains functional. Ketoprofen is an interesting drug because in neutral to high pH environments, the acid group loses its proton and becomes charged and relatively hydrophilic[34]. Ketoprofen and cytochalasin D were each dissolved in DMSO and loaded into the films using two methods: absorption and wicking. In the absorption process, the whole film was submerged in the drug solution, whereas only the edge of the film was brought into contact with the drug solution in the wicking method. By creating films that behave as dielectric mirrors, it was possible to monitor the wicking process through the change in reflectivity that occurs as the pores were filled with the DMSO solution during loading. This phenomenon will be discussed in detail later.

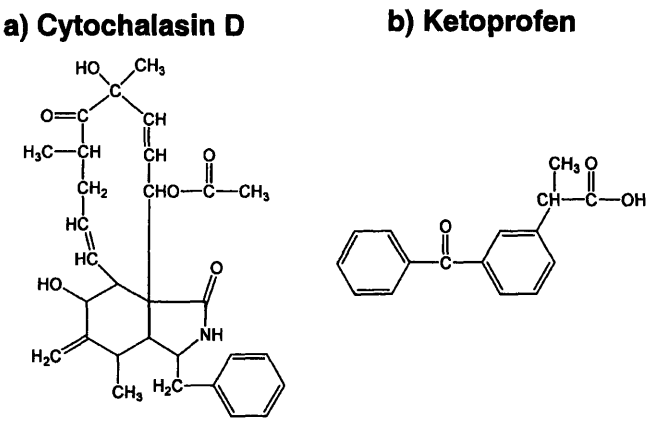

Figure 4-1. Chemical structures of (a) cytochalasin D and (b) ketoprofen.

Due to the molecular level control over assembly, many different parameters can be tuned in the multilayer heterostructures including the number of porous bilayers, number of non-porous bilayers, the arrangement of the porous bilayers (one region in the middle or several regions throughout the film), and the pore size (controlled post-assembly). Nine different architectures of polyelectrolyte multilayers were prepared to examine the effect that varying these parameters had on the drug release properties. Table 4-1 lists the different polyelectrolyte multilayers assembled, the dry film thicknesses before and after porosity induction, and the notation used for each film. There were three basic structures incorporated in this study. First, films were assembled that contained only porous PAH/PAA multilayers. These films are designated as 8NP, 15NP, 20NP, 15MP, and 20MP. In the notation, yNP or yMP, y refers to the number of porous PAH/PAA bilayers, and NP or MP is short for nanopores or micropores, respectively. The second basic structure examined was a sandwich structure (50-8NP-50, 50-5NP-50, 50-8NP-130) comprised of a porous region between non-porous regions. In the nomenclature, x-yNP-z, x is the number of non-porous PAH/SPS bilayers (nomenclature truncated to 50 from 50.5) nearest the substrate, y is the number of nanoporous PAH/PAA bilayers in the middle of the sandwich structure, and z is the number of non-porous PAH/SPS

bilayers in the outermost region of the film. Finally, one multilayer film was built in a multi-stack architecture (50-3(5NP-50)) containing 7 alternating non-porous and nanoporous regions. The region closest to the substrate contained 50.5 non-porous PAH/SPS bilayers. The other 6 regions were alternating nanoporous regions composed of 5 PAH/PAA bilayers and non-porous regions composed of 50 PAH/SPS bilayers. This configuration left PAH/SPS layers as the outermost region of the film.

Table 4-1. Thickness of multilayer films before and after porosity transition and thickness increase due to porosity induction. NP designates nanoporous films and MP designates microporous films.

	Notation	Thickness w/o pores (nm)	Thickness w/ pores (nm)	Thickness increase (nm)
$(PAH/PAA)_8$ NP	8NP	101	253	153
$(PAH/PAA)_{15}$ NP	15NP	202	373	171
$(PAH/PAA)_{20}$ NP	20NP	296	476	180
$(PAH/SPS)_{50.5}$ – $(PAA/PAH)_5$ – $(SPS/PAH)_{50}$ NP	50-5NP-50	251	327	77.5
$(PAH/SPS)_{50.5}$ – $(PAA/PAH)_8$ – $(SPS/PAH)_{50}$ NP	50-8NP-50	296	391	95.7
$(PAH/SPS)_{50.5}$ – $(PAA/PAH)_8$ – $(SPS/PAH)_{130}$ NP	50-8NP-130	494	577	83.4
$(PAH/SPS)_{50.5}$ – $[(PAA/PAH)_5$ – $(SPS/PAH)_{50}]_3$ NP	50-3(5NP-50)	551	688	137
$(PAH/PAA)_{15}$ MP	15MP	202	521	320
$(PAH/PAA)_{20}$ MP	20MP	296	625	329

The nanoporous films had an average pore diameter of 100 nm, and the pores ranged in diameter from approximately 10 nm to 150 nm (obtained through AFM and SEM, data not shown). The microporous films had pores ranging in diameter from approximately 300 nm to 2 microns with an average pore diameter of 1.0 micron. As shown in Table 4-1, the increase in film thickness due to the introduction of pores depended greatly on the architecture of the film.

In general, thicker multilayers showed a smaller percentage increase in thickness after the porosity induction. In addition, the introduction of non-porous regions further reduced the change in thickness resulting from pore formation. Details concerning the origin of this behavior have been previously reported[31]. Figure 4-2 shows AFM images of non-porous, nanoporous, and microporous 20 bilayer PAH/PAA films as examples of the surface morphology.

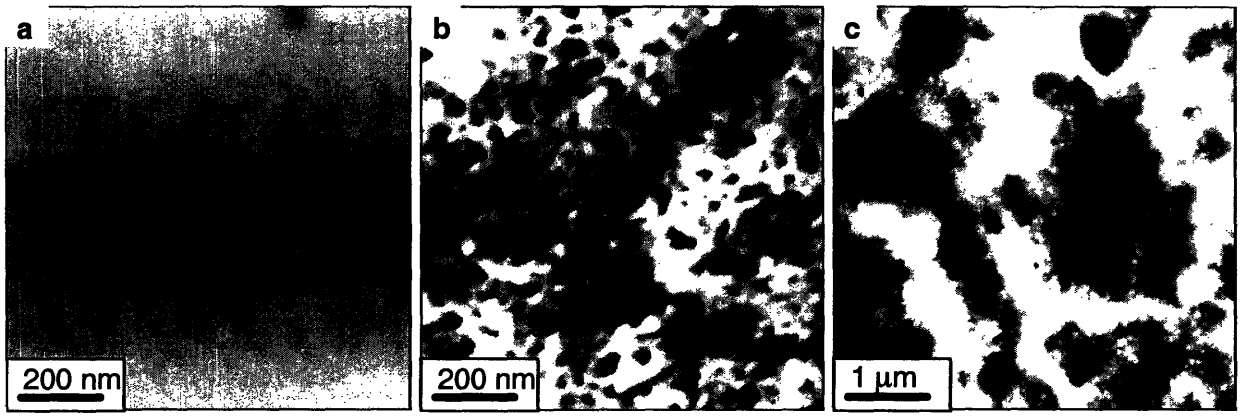

Figure 4-2. AFM images of (a) non-porous (image size = 1×1μm), (b) nanoporous (image size = 1×1μm), and (c) microporous (image size = 5×5μm) 20 bilayer PAH/PAA multilayer films.

4.3.2. Loading and Releasing Drugs

Both absorption and wicking from DMSO solutions provided efficient loading of ketoprofen and cytochalasin D. The wicking technique involved dipping one end of the film into the drug solution and allowing the liquid to wick up the film. Drug solutions only wicked into the porous regions when the films had a sandwich or stacked structure, which means the non-porous regions were necessary to provide sufficient capillary force for the wicking process. Thus, it was necessary to load the 8NP, 15NP, 20NP, 15MP, and 20MP films by the absorbance method. The wicking technique was developed in previous work, where it was shown that liquid crystals or ionic liquids could be successfully loaded into both nanoporous[31] and microporous[32] polyelectrolyte multilayers with outermost non-porous regions. As mentioned earlier, the

wicking front could be observed by the change in reflectivity of the polyelectrolyte multilayer films as the DMSO solution filled the pores. Figure 4-3 demonstrates this principle by showing a 50-3(5NP-50) multilayer film being loaded with 0.2 mg/mL cytochalasin D in DMSO. The change in color halfway up the film is due to the drug solution filling the pores and changing the film's reflectivity. The schematic next to the photograph depicts an edge on view of the porous regions filling with drug solution as the wicking proceeds. The wicking process took only a few minutes, but films were left for 8 hours in the drug solution. Films were also loaded with drugs by submerging the entire film into the drug solution and allowing it to absorb for 8 hours. This method allows the use of non-planar substrates and films without non-porous regions. Similar results were obtained from both loading techniques as long as the samples were thoroughly rinsed after the loading step. As a control, we attempted to load drugs into sandwich structured films with closed pores using both loading techniques. The wicking process was unsuccessful for these controls, and when drugs were absorbed into the films, the entire amount released in a few minutes during the rinse step. These control experiments indicate that open pores in the multilayers are essential for loading and controlled release of these particular drugs. To simplify matters, all data in the remainder of this paper were obtained from samples loaded via the absorption loading technique since it could be applied to all of the film architectures.

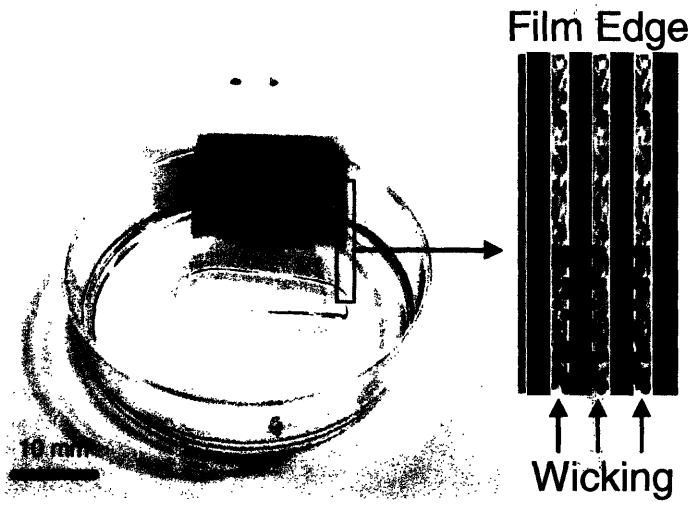

Figure 4-3. A DMSO solution containing 0.2 mg/mL cytochalasin D in the process of wicking into a 50-3(5NP-50) polyelectrolyte multilayer film and a schematic of the process. The change in reflectivity halfway up the film is due to the pores being filled with solution. The schematic next to the photograph is an edge on view of the wicking process.

Drug-loaded samples were rinsed for 2 hours in PBS to remove loosely bound drug and to displace DMSO. After rinsing and drying the porous multilayers, the reflectivity of the loaded (but DMSO-free) multilayers returned to essentially the same value observed before the loading process. The amount of drug loaded into the pores was therefore too small to affect the films' optical properties. This suggests that the drug does not fill the pores, but only coats the pore walls. Figure 4-4 displays the drug release results from 50-3(5NP-50) and 15MP films as examples of typical release profiles for a nanoporous and a microporous film, respectively. All nanoporous samples displayed zero-order release kinetics (constant slope on an amount released versus time plot) for nearly the entire time of the experiment. The deviation from zero-order kinetics in the last day or two results from the drug nearing total depletion. In contrast, the microporous films showed a release behavior that was far from linear, as shown in Figure 4-4. The differences between these two release behaviors will be discussed in detail in a later section.

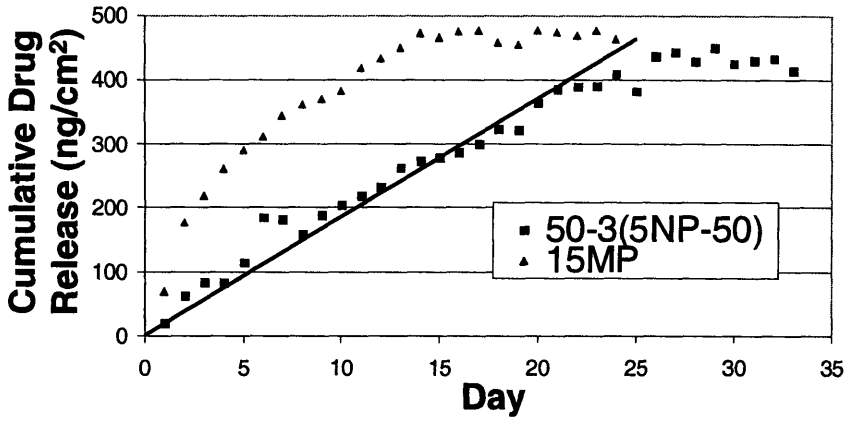

Figure 4-4. Plot of the cumulative amount of cytochalasin D released from 50-3(5NP-50) and 15MP films as a function of time (drug loaded from a 0.2 mg/mL DMSO solution in both cases).

For both nanoporous and microporous films, the samples were monitored for 10 days after the drug concentration in the PBS release solution reached a constant value. To determine if the build-up of drug concentration in the PBS release solution affected the total amount of drug released, each sample was placed in fresh PBS and monitored for 5 additional days following the above mentioned protocol. No more drug eluted, indicating that the drug concentration in solution did not influence the endpoint of release.

To study the effect of drug concentration in the DMSO loading solution, two different concentrations of each drug were used for a subset of nanoporous films. For ketoprofen, 0.2 mg/mL and 10.0 mg/mL concentrations were examined, and for cytochalasin D, 0.2 mg/mL and 1.0 mg/mL concentrations. Figure 4-5 shows that for all film architectures, the loading concentration had little effect on the total release time or release rate: these parameters increased slightly with an increased drug loading concentration, but most of the results were not statistically different. These results indicate that the amount of drug adsorbed to the pore walls is unaffected by the loading concentration. In other words, the ultra-thin coating of drug on the pore walls appears to be self-limiting.

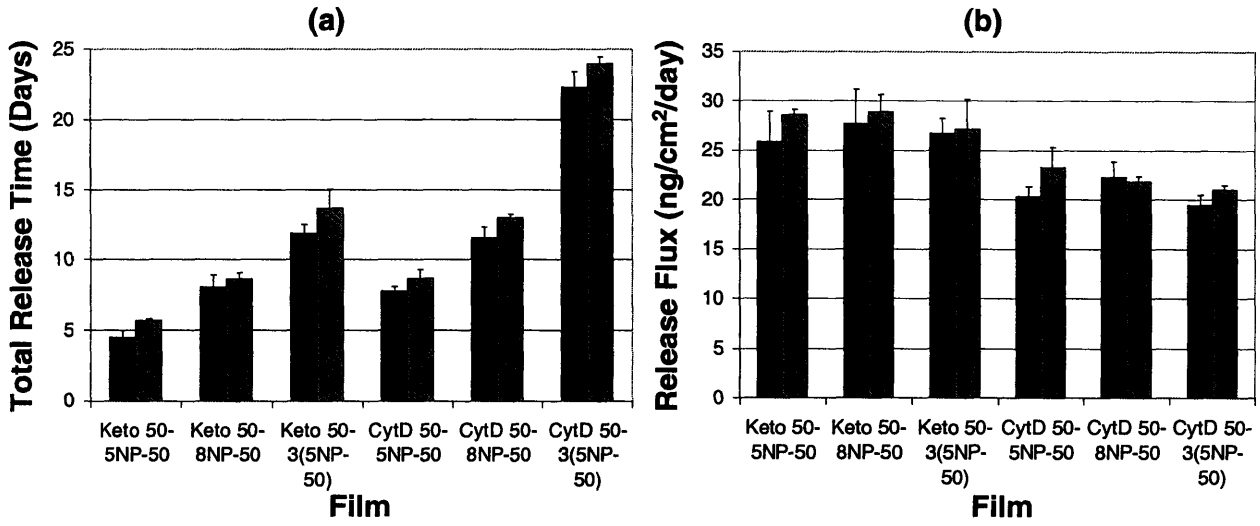

Figure 4-5. Graphs comparing the (a) total time to release and (b) release flux for ketoprofen and cytochalasin D at different loading concentrations. The solid bars are data from a film loaded with a 0.2 mg/mL DMSO loading solution, and the hatched bars are data from a film loaded with a 1.0 mg/mL solution for cytochalasin D and 10.0 mg/mL solution for ketoprofen.

Table 4-2 summarizes the release data for the multilayer films examined in this study with a loading concentration of 0.2 mg/mL for both ketoprofen and cytochalasin D. The multilayers in Table 4-2 were chosen to illustrate the effects of various key structural parameters on the drug release behavior of both homogeneous porous multilayers and multilayer heterostructures. These structural parameters included the number of porous bilayers, number of non-porous bilayers (in multilayer heterostructures), and the average pore size. Two important trends are observed in Table 4-2 and Figure 4-5. The first trend is that the total time to release increases as the number of porous bilayers increases. The second is that release flux stays relatively constant for a given drug but depends on whether the film is nanoporous or microporous. These trends will be discussed further in the next section.

Table 4-2. Release data for each film and drug tested at a drug loading concentration of 0.2mg/mL.

Film	Drug	Total Release Time (days)	Release Flux ($ng/cm^2/day$)	Total Amount Released (ng/cm^2)
8NP	ketoprofen	7.8	28.2[a]	219
	cytochalasin D	11.9	23.1	275
15NP	ketoprofen	15.6	22.8	356
	cytochalasin D	24.3	17.2	418
20NP	ketoprofen	18.4	22.0	405
	cytochalasin D	33.9	16.0	543
50-5NP-50	ketoprofen	4.5	25.8	116
	cytochalasin D	7.8	20.3	158
50-8NP-50	ketoprofen	8.0	27.8	223
	cytochalasin D	11.6	22.3	259
50-8NP-130	ketoprofen	7.5	27.7	209
	cytochalasin D	11.0	22.1	243
50-3(5NP-50)	ketoprofen	11.9	26.8	319
	cytochalasin D	22.3	19.5	435
15MP	Ketoprofen	6.0	50.7[b]	304
	cytochalasin D	14.0	33.6	471
20MP	ketoprofen	7.5	48.0	360
	Cytochalasin D	16.0	32.3	517

[a]For all NP films, the release flux was independent of time. [b]The reported values of release flux for MP films are effective mean values obtained by dividing the total amount of drug released by the total release time.

4.3.3. Effect of Film Architecture on Release

By examining the results from the 8NP, 50-8NP-50, and 50-8NP-130 films, it can be concluded that the PAH/SPS non-porous layers have no significant effect on the drug release properties. For these three films, the total release time, release flux, and total amount released are statistically the same. This result is not surprising since small molecule drugs have been shown to have high mobility in non-porous polyelectrolyte multilayers in a buffered environment[13, 15]. In previous reports, it was found that both PAH/PAA multilayers (non-porous) loaded with dye[15] and PAH/SPS multilayers built on drug particles[13] released the dye or drug molecules in a few minutes or less in a buffered environment. However, the non-porous film

regions do have important properties that influence drug loading and release. In our experiments, they allow the drug solution to wick into the porous regions during the loading process if this technique is desired. Second, these results show that the non-porous regions do not inhibit the drug release when stacked on top of the porous regions. This characteristic could be useful in applications where functionalizing the surface is required for controlling interactions with biopolymers or cells. In addition, non-porous regions can be incorporated to make the films into dielectric mirrors that could be utilized as optical sensors.

The release flux did not change significantly when the number of porous layers was increased in films with a given magnitude of pore size (nanoporous or microporous). Comparing the full set of nanoporous films: 8NP, 15NP, 20NP, 50-5NP-50, 50-8NP-50, 50-8NP-130, and 50-3(5NP-50), Table 4-2 and Figure 4-5 show that most exhibit a similar release flux, approximately 27 ± 2 ng/cm^2/day for ketoprofen and 21 ± 3 ng/cm^2/day for cytochalasin D . The films with 15 and 20 nanoporous bilayers show a slight reduction in flux, perhaps due to the lower thickness per bilayer of the porous region in these films which leads to a morphology change of the porous region. However, when the porous region is split by non-porous regions as in the case of the 50-3(5NP-50) films, the release flux is statistically the same as the 50-5NP-50 films.

For the nanoporous films, the total time to release the drug was directly proportional to the number of bilayers in the porous region(s). Figure 4-6 shows the total release time for each nanoporous system normalized by the number of bilayers in the porous region(s). Thus, the total release time is simply connected to the supply of drug in the nanoporous structure. Even if the porous region is split by a non-porous region, this proportionality holds, as apparent by the 50-3(5NP-50) film. For the nanoporous films, the average total release time is approximately 0.9

days/bilayer for ketoprofen and 1.5 days/bilayer for cytochalasin D. Because of this proportionality, longer release time periods than what is demonstrated in this study (approximately a month) are possible by increasing the number of porous bilayers in the film. However, this proportionality will be limited by the fact that uniform porosity transitions may not be possible for much thicker films.

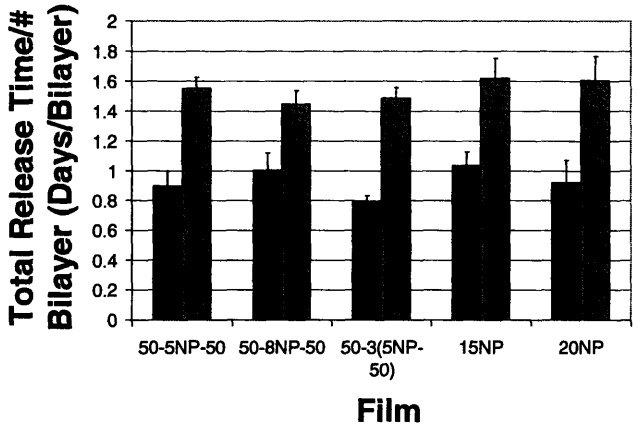

Figure 4-6. Total time of drug release normalized by the number of bilayers in the film. Drugs were loaded by absorption from a 0.2 mg/mL DMSO solution. Black bars represent total release time per bilayer for ketoprofen, and hatched bars represent total release time per bilayer for cytochalasin D.

As can be seen from these data, the total amount of released drug and the release flux are not drastically different for ketoprofen and cytochalasin D. Cytochalasin D does release somewhat slower and with a higher total amount released for all films in the study, but the difference is small considering the differences in structures and properties of the two drugs. Future work needs to be performed to elucidate the reasons for these subtle differences and determine the role that drug properties such as hydrophobicity and charge play in the release properties.

4.3.4. Release from nanoporous versus microporous films

In order to gain a better understanding of the observed zero-order release kinetics shown by the nanoporous films, drug release from microporous multilayers was also investigated. The 15MP and 20MP films contained micropores of approximately 0.3 to 2.0 μm in diameter. It was demonstrated earlier (see Figure 4-4) that these microporous films released drugs at a faster rate than the corresponding nanoporous structures. In addition, the constant release rate (zero-order kinetics) of nanoporous films was not observed for the microporous films. This important pore-size dependent difference in release mechanism is analyzed below.

The relative amount of drug released from both the microporous and nanoporous films can be described using a model developed by Peppas et al.[35],

$$\frac{M_t}{M_\infty} = kt^n \qquad (1)$$

where M_t is the total amount of drug released at time t, M_∞ is the total amount of drug released as time goes to infinity, k is a constant, and n is the exponent characteristic of the release mechanism. The value of n is equal to 1 for zero-order kinetics and is equal to 0.5 for Fickian diffusion. The drug release from the microporous films follows a Fickian diffusion mechanism. This is revealed in Figure 4-7a by how well the data fit to Equation 1 (using least squares) with n as 0.5. In contrast, the nanoporous films followed zero-order release kinetics as observed in Figure 4-7b. In this case, the data were described well by Equation 1 when n is set equal to 1. From this comparison, it is clear that the release mechanisms of microporous and nanoporous films are fundamentally different.

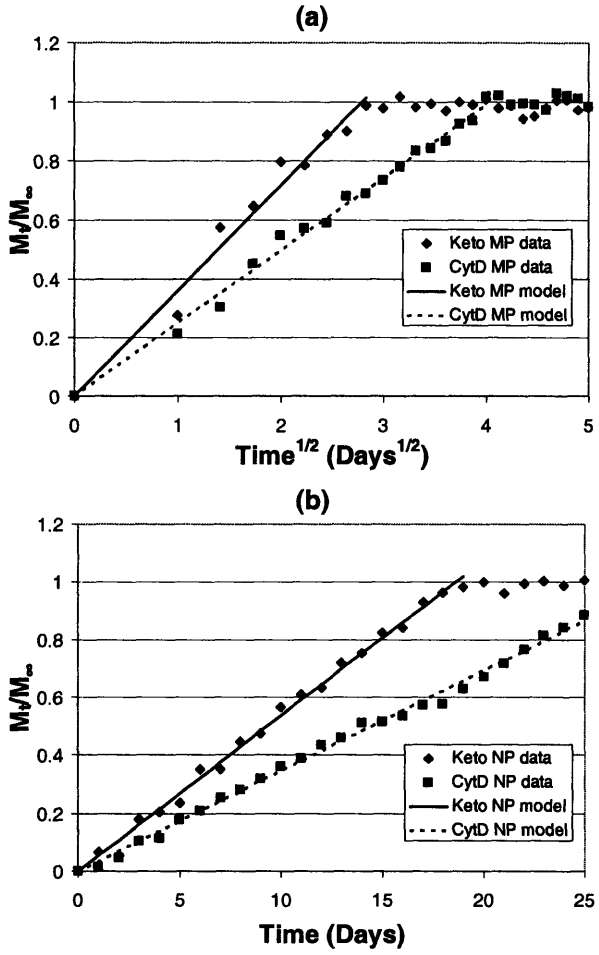

Figure 4-7. Comparison of ketoprofen and cytochalasin D release from (a) 20MP multilayers and (b) 20NP multilayers along with fitted curves from the model discussed in the text.

The reason for zero-order release kinetics from nanoporous films, but not from microporous films arises from differences in film morphology. The microporous and nanoporous film morphologies are represented schematically in Figure 4-8 to illustrate these differences. Micropores fill almost the entire thickness of the multilayer films and are very open to the surface. In contrast, only a small fraction of the pores are open to the surface in the nanoporous films. Since the micropores are open to the surface, the drug release follows Fickian behavior as it desorbs/dissolves from the pore wall. This phenomenon can be visualized as an open container where the molecules are free to diffuse into the continuous medium shown in

Figure 4-8a. The nanopores present a much different release mechanism where drug must release from a few openings on the surface. These "defects" are very infrequent in number relative to the total supply of drug molecules, a situation known to favor zero-order release kinetics[36, 37]. Inside the nanoporous films submerged in buffer solution, transport of the drug molecules is fast. When a molecule of drug is released from one of the defects (a nanopore at the surface), it is replaced by another on a timescale that is fast compared to the release mechanism. Thus the observed release is dominated by the slower, defect-controlled zero-order mechanism. Brooke and Washkuhn modeled this effect using a geometric gradient with a large supply of drug compared to a small opening for release[38]. This model, which captures the drug release behavior of nanoporous multilayers, is represented schematically in Figure 4-8b.

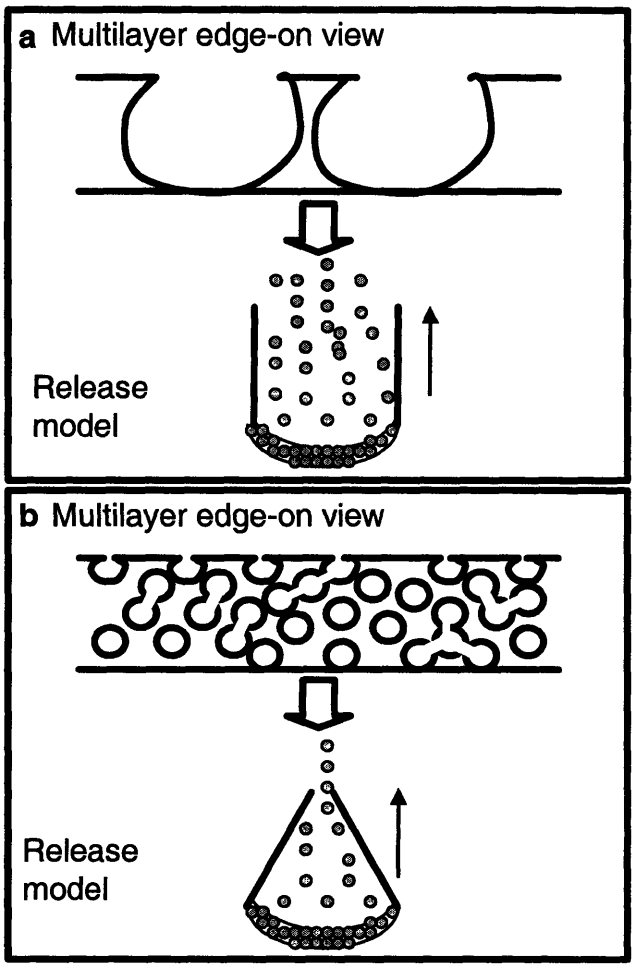

Figure 4-8. Schematic of porous multilayer films and implications on drug release for (a) microporous and (b) nanoporous films. The top drawing in each subsection represents an edge-on view of the multilayer, and the bottom drawing in each subsection compares conceptually the overall pore structure of a multilayer film to a single drug-containing vesicle.

4.3.5. Cytochalasin D Release to Mammalian Cells

To demonstrate that a drug released from a nanoporous multilayer platform maintained its functionality, cytochalasin D was released into a culture of fibroblasts. Cytochalasin D inhibits cytoplasmic cleavage by blocking formation of contractile microfilaments resulting in multinucleated cells[39]. WT NR6 fibroblasts were grown on the surface of 50-5NP-50, 50-8NP-50, and 50-3(5NP-50) films with and without cytochalasin D loaded into the pores. In all cases, the influence of the cytochalasin D release could be easily seen in the change in the morphology

of the fibroblasts. Figure 4-9 shows micrographs of fibroblasts on 50-3(5NP-50) films with DAPI stained nuclei. In the case of films loaded with cytochalasin D, the cells were multi-nucleated, and had a much different morphology compared to control samples. This effect arises from the cells' inability to form actin stress fibers in the presence of cytochalasin D. The effect of the cytochalasin D release first became apparent approximately two days after cell seeding. The change in morphology and number of multi-nucleated cells increased on the third and fourth days before finally killing the cells. Cytochalasin D was also added directly to the cell culture media of fibroblasts seeded on tissue culture polystyrene at concentrations ranging from 100 to 1000 ng/mL (concentrations typical in cell biology experiments[39]) for comparison. The resulting morphology of cells exposed to 200-400 ng/mL cytochalasin D was similar to that shown in Figure 4-9. These results demonstrate that cytochalasin D is still functional after release from the porous multilayer film.

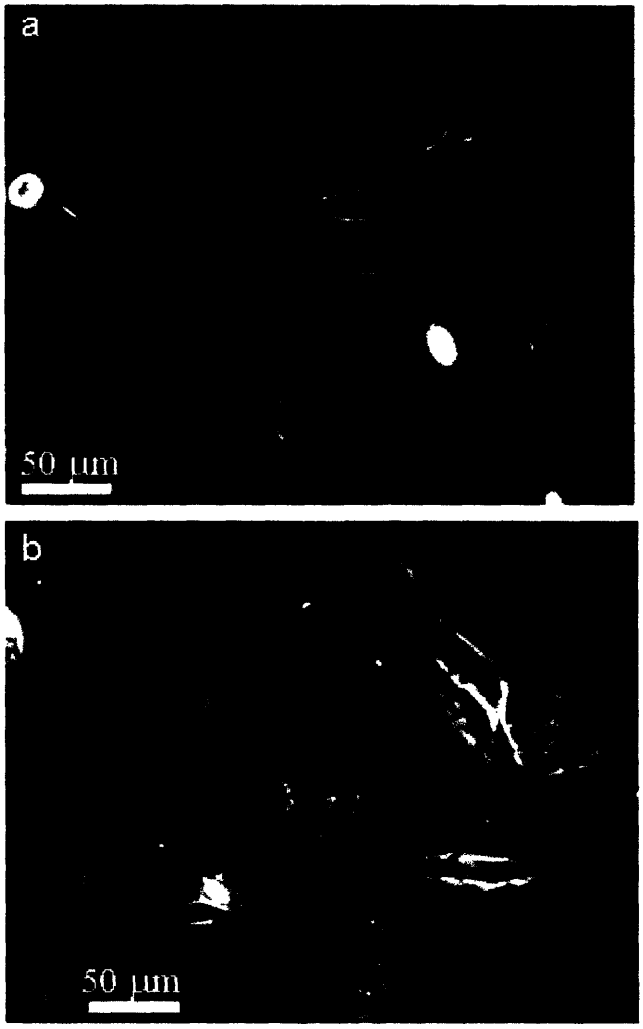

Figure 4-9. Microscope images of fibroblasts three days after seeding on 50-3(5NP-50) films with (a) no cytochalasin D and (b) cytochalasin D loaded from a 0.2 mg/mL DMSO solution. Nuclei were stained with DAPI.

4.4. Conclusions

We have developed porous polyelectrolyte multilayer ultra-thin drug delivery systems in which the amount of drug loaded into the film along with the rate at which it is released can be controlled by changing structural parameters of the film. Ketoprofen and cytochalasin D were studied to represent different types of drugs that can be loaded and released from these multilayer films. The amount loaded and released could be tuned by varying the number of

bilayers in the porous regions of films, and the release flux of a given drug could be controlled by varying the pore size. Microporous films released drug in accordance with Fickian diffusion, whereas the drugs loaded into nanoporous multilayers followed zero-order release kinetics. Incorporation of PAH/SPS non-porous layers in multilayer films had no distinguishable effect on the release behavior. However, the use of multilayer heterostructures that behaved as dielectric mirrors made it possible to monitor the drug loading.

References for Chapter 4

(1) Langer, R. New Methods of Drug Delivery *Science* **1990**, *249*, 1527-1533.

(2) Babapulle, M. N.;Eisenberg, M. J. Coated Stents for the Prevention of Restenosis: Part I *Circulation* **2002**, *106*, 2734-2740.

(3) Babapulle, M. N.;Eisenberg, M. J. Coated Stents for the Prevention of Restonosis: Part Ii *Circulation* **2002**, *106*, 2859-2865.

(4) Salu, K. J.;Huang, Y. M.;Bosmans, J. M.;Liu, X. S.;Li, S. Q.;Wang, L.;Verbeken, E.;Bult, H.;Vrints, C. J.;De Scheerder, I. K. Addition of Cytochalasin D to a Biocompatible Oil Stent Coating Inhibits Intimal Hyperplasia in a Porcine Coronary Model *Coronary Artery Disease* **2003**, *14*, 545-555.

(5) Decher, G. Fuzzy Nanoassemblies: Toward Layered Polymeric Multicomposites *Science* **1997**, *277*, 1232-1237.

(6) Elbert, D. L.;Herbert, C. B.;Hubbell, J. A. Thin Polymer Layers Formed by Polyelectrolyte Multilayer Techniques on Biological Surfaces *Langmuir* **1999**, *15*, 5355-5362.

(7) Serizawa, T.;Yamaguchi, M.;Matsuyama, T.;Akashi, M. Alternating Bioactivity of Polymeric Layer-by-Layer Assemblies: Anti- Vs Procoagulation of Human Blood on Chitosan and Dextran Sulfate Layers *Biomacromolecules* **2000**, *1*, 306-309.

(8) Chluba, J.;Voegel, J.-C.;Decher, G.;Erbacher, P.;Schaaf, P.;Ogier, J. Peptide Hormone Covalently Bound to Polyelectrolytes and Embedded into Multilayer Architectures Conserving Full Biological Activity *Biomacromolecules* **2001**, *2*, 800-805.

(9) Mendelsohn, J. D.;Yang, S. Y.;Hiller, J.;Hochbaum, A. I.;Rubner, M. F. Rational Design of Cytophilic and Cytophobic Polyelectrolyte Multilayer Thin Films *Biomacromolecules* **2003**, *4*, 96-106.

(10) Yang, S. Y.;Mendelsohn, J. D.;Rubner, M. F. New Class of Ultrathin, Higly Cell-Adhesion-Resistant Polyelectrolyte Multilayers with Micropatterning Capabilities *Biomacromolecules* **2003**, *4*, 987-994.

(11) Berg, M. C.;Yang, S. Y.;Hammond, P. T.;Rubner, M. F. Controlling Mammalian Cell Interactions on Patterned Polyelectrolyte Multilayer Surfaces *Langmuir* **2004**, *20*, 1362-1368.

(12) Caruso, F.;Trau, D.;Mohwald, H.;Renneberg, R. Enzyme Encapsulation in Layer-by-Layer Engineering Polymer Multilayer Capsules *Langmuir* **2000**, *16*, 1485-1488.

(13) Qiu, X.;Donath, E.;Mohwald, H. Permeability of Ibuprofen in Various Polyelectrolyte Multilayers *Macromol. Mater. Eng.* **2001**, *286*, 591-597.

(14) Vazquez, E.;Dewitt, D. M.;Hammond, P. T.;Lynn, D. M. Construction of Hydrolytically-Degradable Thin Films Via Layer-by-Layer Deposition of Degradable Polyelectrolytes *J. Am. Chem. Soc.* **2002**, *124*, 13992-13993.

(15) Chung, A. J.;Rubner, M. F. Methods of Loading and Releasing Low Molecular Weight Cationic Molecules in Weak Polyelectrolyte Multilayer Films *Langmuir* **2002**, *18*, 1176-1183.

(16) Quinn, J. F.;Caruso, F. Facile Tailoring of Film Morphology and Release Properties Using Layer-by-Layer Assembly of Thermoresponsive Materials *Langmuir* **2004**, *20*, 20-22.

(17) Burke, S. E.;Barrett, C. J. Ph-Dependent Loading and Release Behavior of Small Hydrophilic Molecules in Weak Polyelectrolyte Multilayer *Macromolecules* **2004**, *37*, 5375-5384.
(18) Nolan, C. M.;Serpe, M. J.;Lyon, L. A. Thermally Modulated Insulin Release from Microgel Thin Films *Biomacromolecules* **2004**, *5*, 1940-1946.
(19) Serpe, M. J.;Yarmey, K. A.;Nolan, C. M.;Lyon, L. A. Doxorubicin Uptake and Release from Microgel Thin Films *Biomacromolecules* **2005**, *6*, 408-413.
(20) Thierry, B.;Kujawa, P.;Tkaczyk, C.;Winnik, F. M.;Bilodeau, L.;Tabrizian, M. Delivery Platform for Hydrophobic Drugs: Prodrug Approach Combined with Self-Assembled Multilayers *J. Am. Chem. Soc.* **2005**, *127*, 1626-1627.
(21) Decher, G.;Lehr, B.;Lowack, K.;Lvov, Y.;Schmitt, J. New Nanocomposite Films for Biosensors: Layer-by-Layer Adsorbed Films of Polyelectrolytes, Proteins or DNA *Biosens. Bioelectron.* **1994**, *9*, 677-684.
(22) Qiu, X.;Leporatti, S.;Donath, E.;Mohwald, H. Studies on the Drug Release Properties of Polysaccharide Multilayers Encapsulated Ibuprofen Microparticles *Langmuir* **2001**, *17*, 5375-5380.
(23) Zhang, J.;Chua, L. S.;Lynn, D. M. Multilayered Thin Films That Sustain the Release of Functional DNA under Physiological Conditions *Langmuir* **2004**, *20*, 8015-8021.
(24) Wood, K. C.;Boedicker, J. Q.;Lynn, D. M.;Hammond, P. T. Tunable Drug Release from Hydrolytically Degradable Layer-by-Layer Thin Films *Langmuir* **2005**, *21*, 1603-1609.
(25) Thierry, B.;Winik, F. M.;Merhi, Y.;Silver, J.;Tabrizian, M. Bioactive Coatings of Endovascular Stents Based on Polyelectrolyte Multilayers *Biomacromolecules* **2003**, *4*, 1564-1571.
(26) Li, Y. Y.;Cunin, F.;Link, J. R.;Gao, T.;Betts, R. E.;Reiver, S. H.;Chin, V.;Bhatia, S. N.;Sailor, M. J. Polymer Replicas of Photonic Porous Silicon for Sensing and Drug Delivery Applications *Science* **2003**, *299*, 2045-2047.
(27) Anglin, E. J.;Schwartz, M. P.;Ng, V. P.;Perelman, L. A.;Sailor, M. J. Engineering the Chemistry and Nanostructure of Porous Silicon Fabry-Perot Films for Loading and Release of a Steroid *Langmuir* **2004**, *20*, 11264-11269.
(28) Shiratori, S. S.;Rubner, M. F. Ph-Dependent Thickness Behavior of Sequentially Adsorbed Layers of Weak Polyelectrolytes *Macromolecules* **2000**, *33*, 4213-4219.
(29) Mendelsohn, J. D.;Barrett, C. J.;Chan, V. V.;Pal, A. J.;Mayes, A. M.;Rubner, M. F. Fabrication of Microporous Thin Films from Polyelectrolyte Multilayers *Langmuir* **2000**, *16*, 5017-5023.
(30) Hiller, J.;Mendelsohn, J. D.;Rubner, M. F. Reversibly Erasable Nanoporous Anti-Reflection Coatings from Polyelectrolyte Multilayers *Nat. Mater.* **2002**, *1*, 59-63.
(31) Zhai, L.;Nolte, A. J.;Cohen, R. E.;Rubner, M. F. Ph-Gated Porosity Transitions of Polyelectrolyte Multilayers in Confined Geometries and Their Application as Tunable Bragg Reflectors *Macromolecules* **2004**, *37*, 6113-6123.
(32) Ahn, H.;Cohen, R. E.;Rubner, M. F. *Unpublished Work.*
(33) Yoo, D.;Shiratori, S. S.;Rubner, M. F. Controlling Bilayer Composition and Surface Wettability of Sequentially Adsorbed Multilayers of Weak Polyelectrolytes *Macromolecules* **1998**, *31*, 4309-4318.
(34) Rafols, C.;Roses, M.;Bosch, E. A Comparison between Different Approaches to Estimate the Aqueous Pka Values of Several Non-Steroidal Anti-Inflammatory Drugs *Analytica Chimica Acta* **1997**, *338*, 127-134.

(35) Ritger, P. L. A Simple Equation for Description of Solute Release 1. Fickian and Non-Fickian Release from Non-Swellable Devices in the Form of Slabs, Spheres, Cylinders or Discs *J. Controlled Release* **1987**, *5*, 23-36.
(36) Linsebigler, A. L.;Smentkowski, V. S.;Ellison, M. D.;Yates, J. T. Interaction of Cl2 with Fe(110) in the Temperature Range 90-1050 K *J. Am. Chem. Soc.* **1992**, *114*, 465-473.
(37) Kuznetsova, A.;Yates, J. T.;Liu, J.;Smalley, R. E. Physical Adsorption of Xenon in Open Single Walled Carbon Nanotubes: Observation of a Quasi-One-Dimensional Confined Xe Phase *J. Chem. Phys.* **2000**, *112*, 9590-9598.
(38) Brooke, D.;Wahkuhn, R. J. Zero-Order Drug Delivery System: Theory and Preliminary Testing *J. Pharm. Sci.* **1977**, *66*, 159-162.
(39) Cooper, J. A. Effects of Cytochalasin and Phalloidin on Actin *J. Cell Biol.* **1987**, *105*, 1473-1478.

Chapter 5 Bacteria Killing Properties of Silver-Loaded Polyelectrolyte Multilayers

5.1. Introduction

The adhesion of bacteria to surfaces can cause very severe problems including wound infection, corrosion of industrial systems, and public health issues. In addition, bacterial adhesion can also lead to biofilm formation, which is a complex formation of many different bacteria species, a polysaccharide matrix, and nutrient channels[1]. The bacteria in biofilms are less susceptible to antibiotics since they exist in a slow growing state and can protect themselves with the polysaccharide matrix[1]. In an attempt to prevent biofilm formation, many surface treatments have been developed to potentially kill bacteria on contact or leach an antimicrobial agent out into the environment. A great deal of the research efforts have focused on using either quaternary amines[2, 3], chitosan[4], furanones[5], or metals with intrinsic antibacterial properties such as silver[6-10] as antibacterial agents. Of the metal ions studied, silver is extremely promising due to both its effectiveness in killing bacteria and its biocompatibility.

Silver has been a well known antimicrobial agent for many centuries[11, 12]. In fact, the Romans used silver nitrate as a therapeutic agent 2000 years ago. The released silver ions are able to attach to biomolecules containing sulfur, nitrogen, or oxygen,[10] and can kill bacteria by interfering with its DNA replication and protein production[13]. Moreover, since it attacks a number of sites, very few bacteria strains are resistant to it[14]. It has also been demonstrated in numerous studies to be non-toxic to mammalian cells in culture[15, 16]. In recent reports, silver has been immobilized on surfaces using a variety of techniques including complexation of silver ions

with polymers[7], electroless deposition[6], dispersion of silver powder in a polymer matrix[10], and formation of silver nanoparticles[8, 9, 17-20]. The advantages of silver nanoparticles include their high surface to volume ratio and fine control over size possible in many synthesis routes. In situ synthesis of silver nanoparticles in solid matrices is especially appealing since it allows precise control over how and where the nanoparticles are incorporated. In previous work[17-19], it was found that one effective matrix for controlling metal nanoparticle synthesis is polyelectrolyte multilayers.

Polyelectrolyte multilayers are a relatively new class of materials that have received a great deal of attention in research laboratories since they were first introduced slightly over a decade ago[21, 22]. These ultra-thin polymer films offer unique control over thickness, molecular architecture, and properties due to their layer-by-layer assembly. In addition, their design is extremely flexible due to the variety of materials which can be included into the films and the simple, aqueous-based processing conditions. Their processing leads to conformal coatings over even complex geometries. As biomaterials, polyelectrolyte multilayers have been utilized as drug delivery devices[23-27], biosensors[28], cell mediated coatings[29-33], and cell arrays[34]. Of the different materials incorporated into multilayers, weak polyelectrolytes offer the unique ability to tune film properties such as incremental layer thickness, number of free functional groups, and mechanical properties[35] with simple pH adjustments during the assembly process[36, 37]. This tuning is possible since the charge density along the chain of a weak polyelectrolyte changes when the solution pH is adjusted. Wang et al. used the advantageous properties of weak polyelectrolytes to control the density of free carboxylic acid groups in multilayer films when polyacrylic acid (PAA) was chosen as the polyanion[18]. The free carboxylic acid groups in the multilayer were utilized as nanoreactors for in situ silver nanoparticle synthesis using an ion

exchange and subsequent reduction. The number of these free acid groups proved important in controlling the number and size of silver nanoparticles. In addition, the process allowed recovery of the carboxylic acid groups, so multiple silver loadings were possible. Bruening and coworkers also successfully incorporated silver nanoparticles into polyelectrolyte multilayers using films composed of polyethyleneimine – metal ion complexes and polyanions[19], and they demonstrated their efficacy as antibacterial coatings.

We use a very similar nanoparticle synthesis route to that developed by Wang et al. However, we utilize hydrogen-bonded polyelectrolyte multilayers composed of poly(acrylic acid) (PAA) and polyacrylamide (PAAm) instead of PAA/PAH multilayers. In addition, the silver reduction is performed in a solution of dimethylamine-borane (DMAB) instead of hydrogen gas. PAA/PAAm multilayers were previously found to show great resistance to mammalian cell adhesion for long periods of time with even a few layers[33]. Incorporation of silver nanoparticles into these films results in surfaces that not only kill bacteria, but render the surface inert to mammalian cell adhesion. The synthesis of silver nanoparticles in the multilayers, antibacterial properties, cytotoxicity effects, and long term release properties were researched in this work.

5.2. Experimental Methods

Materials. Poly(acrylic acid) (PAA) (MW = 90,000; 25% aqueous solution) and polyacrylamide (PAAm) (MW = 5,000,000; 1% aqueous solution) were purchased from Polysciences. Poly(allylamine hydrochloride) (PAH) (MW = 70,000) and silver acetate were bought from Sigma-Aldrich. Dimethylamine - borane (DMAB) was purchased from Alfa Aesar. Dulbecco's Phosphate Buffered Saline (PBS) solution was obtained from Gibco/Invitrogen.

Alamar Blue™ was procured from Biosource International. Sulfosuccinimidyl 6-[3'-(2-pyridyldithio)-propionamido] hexanoate (Sulfo-LC-SPDP) was purchased from Pierce Biotechnology. Peptides containing the amino acid sequence, GRGDSPC, were obtained from the MIT Biopolymers lab. All materials were used without any further purification.

Film Preparation. The layer-by-layer assembly process has been previously described in general[36], and for these hydrogen-bonded multilayers specifically[38]. Briefly, the polyelectrolyte multilayer films were assembled using a dipping process, which was automated by an HMS programmable slide stainer from Zeiss, Inc. Dilute polyelectrolyte solutions were prepared (10^{-2} M based on repeat unit of the polymer) with 18 MΩ Millipore water, and were pH-adjusted with HCl to pH 3.0. Multilayers were built by first adsorbing PAH onto glass substrates for 15 minutes followed by a series of rinse steps in 18 MΩ Millipore water for 2, 1, and 1 minutes, respectively. This process was then repeated with PAA and PAAm until either 3 or 9 PAA/PAAm bilayers were assembled. A bilayer is defined as one layer of PAA and one of PAAm. Films were then crosslinked at 95 °C for 8 hours to stabilize the films. This process was previously shown to form enough imide bonds to provide long term stability for the hydrogen-bonded multilayers[38]. Film thickness values were obtained using a Tencor P-10 Surface Profiler.

Silver nanoparticles were synthesized in the multilayer films similar to a previously described procedure[17, 18]. Briefly, polyelectrolyte multilayer films were submerged in a 5 mM aqueous silver acetate solution for 15 minutes, where the hydrogen ions associated with the free carboxylic acid underwent an ion exchange with the silver ions. Fifteen minutes was found to be enough time for these films to undergo this ion exchange process. After rinsing, the silver ions in the multilayers were reduced in a 5 mM DMAB aqueous solution for 30 seconds. Since the

free acid groups in the film were regenerated after reduction, the process could be repeated until the desired number of loadings was achieved (1 or 3 for this study).

Bacteria Culture and Assays. Airborne and waterborne bacteria assays were conducted using similar methods as described by Klibanov and coworkers[3]. Escherichia coli (E. coli, ATCC #14948) and Staphylococcus epidermidis (S. epidermidis, ATCC #14990) were obtained from American Type Culture Collection (ATCC). Bacteria were grown in LB Broth, Miller (manufactured by EMD chemicals and purchased from VWR) overnight. For waterborne experiments, bacteria were centrifuged at 2700 RPM for 10 minutes, and then resuspended in PBS after pouring off the supernatant. This process was repeated twice but with only 5 minute centrifugation. The cell density was then estimated by measuring the optical density at 540 nm (assuming 1.0 = 10^9/mL)[39] with a Cary 6000i UV-VIS NIR spectrophotometer. The bacteria solution was diluted with PBS to a final concentration of 10^6/mL for both strains. Samples were then submerged in the bacteria solution for two hours while shaken at 200 RPM in an incubator set to 37 °C. After incubation, the samples were rinsed three times for 5 minutes each in PBS. Following the rinsing steps, the samples were immediately covered with LB agar, Miller (purchased from EMD Chemicals through VWR). After waiting overnight, colony forming unites (CFU's) were counted in at least ten 2.7 mm x 2.1 mm area for each sample using a Zeiss Axioplan 2 optical microscope. At least 3 samples were run for each condition. For airborne experiments, the bacteria were centrifuged in a similar manner as described above, except deionized water was used instead of PBS. After dilution to 10^6/mL, the solution was sprayed onto samples using a chromatography sprayer. The spraying process was adjusted so that the CFU's were clearly distinguishable under a low magnification microscope objective but still provided a statistically significant number to determine percentage of bacteria killed.

Immediately after spraying the bacteria solution, the samples were covered with LB agar and left over night at 37 °C. CFU's were then counted in a similar manner as described above. At least 3 samples were run for each condition.

Cell Culture and Cytotoxicity Experiments. Murine wild type (WT) NR6 fibroblasts were kindly provided by Prof. Linda Griffith's laboratory at MIT for mammalian cell cytotoxicity experiments. These fibroblasts are a cell line derived from NIH 3T3 cells. Unless noted otherwise, all materials used for cell culture were purchased from Gibco/Invitrogen. The substrates coated with polyelectrolyte multilayers were sterilized by treatment with 70% (v/v) ethanol. As reported in previous work[32], the sterilization procedure did not alter the properties of the multilayer films. The WT NR6 fibroblasts were cultured in pH=7.4 media composed of Modified Eagles Medium-α (MEM-α) with 7.5% (v/v) fetal bovine serum (FBS), 1% (v/v) sodium pyruvate (100 mM), 1% (v/v) nonessential amino acids (10 mM), 1% (v/v) Geneticin (G418) antibiotic (350 μg/ 10 mL PBS), 1% (v/v) L-glutamine (200 mM), 1% (v/v) penicillin (10,000 U/mL, from Sigma), and 1% streptomycin (10 mg/mL, from Sigma). Cells were kept in a humid incubator at 37.5 °C and 5% CO_2.

For cell assays, WT NR6 fibroblasts were counted using a hemocytometer with trypan blue exclusion for cell viability. Two different cytotoxicity assays were performed. In the first one, fibroblasts floating above the cell resistant PAA/PAAm multilayers (with and without silver) for 24 hours were transferred to tissue culture polystyrene (TCPS), where attachment and proliferation were studied. In the second cytotoxicity assay, fibroblasts were studied on PAA/PAAm multilayer surfaces (with and without silver) functionalized with the adhesion peptide RGD to promote cell adhesion. For both studies WT NR6 fibroblasts were initially seeded at a density of approximately 5,000 cells/cm^2. Cell growth was quantified using an

Alamar Blue™ assay, which can be used as an indicator for cell proliferation. Alamar Blue™ was added to the cell culture either after initial seeding onto the RGD functionalized surfaces or transfer to TCPS, and the fluorescence due to reduction by the fibroblasts was monitored using a Molecular Devices Gemini fluorescence microplate reader after 24 and 48 hours.

Peptide Coupling. The peptide coupling has been previously described[34]. Briefly, a layer of PAH was adsorbed onto the PAA/PAAm multilayers by submerging the films into a 10^{-2}M aqueous PAH solution (pH=9.0). After three 2 minute rinses, the samples were incubated at room temperature for 30 minutes in a solution of 0.5 mM Sulfo-LC-SPDP in PBS to activate the amine groups in the PAH outermost layer. Following addition of the crosslinker, the samples were rinsed twice in PBS for 5 minutes. The samples were then incubated at room temperature for 8 hours in a solution of 0.5 mM peptide (GRGDSPC) in PBS where the thiol group on cysteine reacted with the 2-pyridyl disulfide residue on the crosslinker. Samples were then soaked twice in PBS (first overnight and second for 5 minutes).

Silver Depletion. The amount of silver in the polyelectrolyte multilayer films was tracked by examining the surface plasmon resonance (SPR) peak over time. The films were aged in PBS and studied using a Cary 6000i UV-VIS NIR spectrophotometer. The average of two samples is reported.

Statistical Analysis. Analysis of variance (ANOVA) was used to test the statistical significance of the number of CFU's for each sample. ANOVA determines whether or not the variance between different sample sets is greater than the variance within a set of samples made under the same conditions. The *p*-value (or probability value) is the result of the ANOVA test, and a value less than 0.05 means the samples are statistically different (based on a 5% level).

5.3. Results and Discussion

5.3.1. Antibacterial Efficacy

Four different sets of 3.0/3.0 PAA/PAAm multilayers were fabricated to study how film architecture and the number of silver loadings affected the antibacterial properties of the films as well as cytotoxicity to mammalian cells. A silver loading is defined as the entire silver nanoparticle synthesis cycle, which includes an ion exchange with silver acetate and later reduction in DMAB. Silver nanoparticle synthesis in multilayer films has been reported previously[17-19], but not with this particular multilayer system. Like silver nanoparticles loaded into PAH/PAA multilayers[17, 18], the PAA/PAAm films allow multiple loading steps due to the regeneration of the carboxylic acid groups. For this reason, it was possible to see how the number of silver loadings affected the amount of silver released into a buffer solution and its effect on both bacteria and mammalian cells. To study this effect, 3 bilayers of the PAA/PAAm system were assembled with PAAm as the outermost layer. Silver nanoparticles were then loaded into the multilayers either 0, 1, or 3 times. To study the effect of varying multilayer thickness, films were also created with 9 bilayers of PAA/PAAm and loaded with silver once. The nomenclature, (PAA/PAAm)x-y or MLx-y, will be used to identify the different samples, where x is the number of PAA/PAAm bilayers and y is the number of silver loadings. The (PAA/PAAm)3-1 and (PAA/PAAm)3-3 films had a dry thickness (before nanoparticle synthesis) of approximately 6.5 nm, whereas the (PAA/PAAm)9-1 and (PAA/PAAm)9-3 multilayers were approximately 90 nm as measured with profilometry. To obtain an estimate of the relative amount of silver nanoparticles in each system, the surface plasmon resonance (SPR) was analyzed. The results are shown in Figure 5-1 for the three multilayer systems with silver

nanoparticles. The SPR peak cannot be used to quantitatively determine the amount of silver. However, the peak height can be used to estimate silver content by comparing to previous results for silver-loaded PAH/PAA multilayer films[18] in which elemental analysis was also performed. Although in this work, we use a different polymer assembled with PAA and the silver reduction is performed using a different procedure, the comparison is useful to obtain a rough estimate of silver content. Using this comparison, the (PAA/PAAm)3-1 films contained approximately 35% ± 3% silver by weight and the (PAA/PAAm)3-3 and (PAA/PAAm)9-1 each contained approximately 55% ± 3% silver by weight. As can be seen in Figure 5-1, the amount of silver scales with both the number of silver loadings and the number of bilayers, although the relationship is not linear.

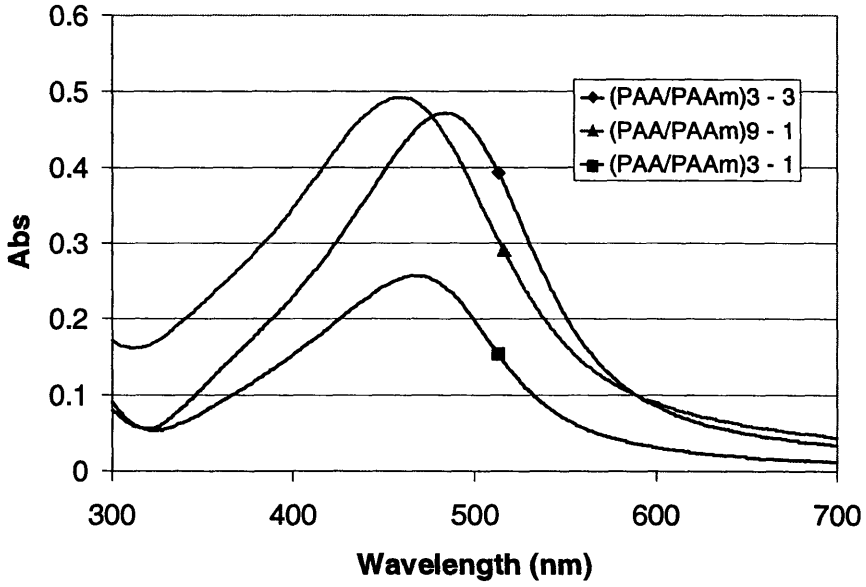

Figure 5-1. Surface plasmon resonance peaks of 3.0/3.0 PAA/PAAm polyelectrolyte multilayers with silver nanoparticles.

Airborne bacteria were modeled by spraying a bacteria solution containing either gram negative E. coli and gram positive S. epidermidis onto samples from a chromatography sprayer. It should be noted that in the airborne experiments, samples were not rinsed after being sprayed

with the bacteria solution. After spraying the samples, they were allowed to incubate at 37 °C overnight under LB agar, and the number of CFU's was counted. To account for variations in the spraying process, a multilayer sample was always sprayed simultaneously with a glass control. If the control varied significantly from others, the data for the multilayer samples was not counted in the average. CFU's were counted in at least 4 areas on at least 3 different samples for each species of bacteria and each multilayer film. Figure 5-2 contains micrographs showing the results for a glass control and a (PAA/PAAm)3-1 multilayer sample. On the glass control, CFU's appear as 50-100 μm diameter dark spots in the Figure 5-2a micrograph. The absence of these dark spots in Figure 5-2b indicates that the silver-loaded multilayer killed all the bacteria on the surface.

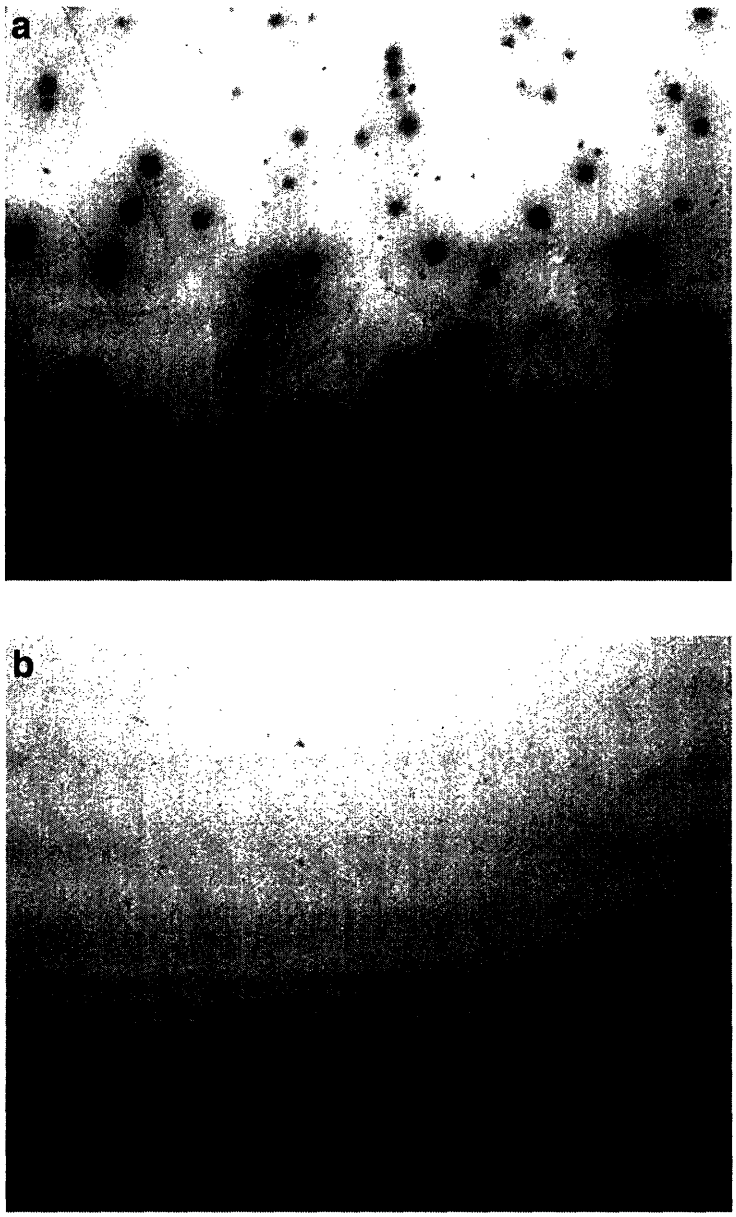

Figure 5-2. Micrograph of (a) glass control and (b) (PAA/PAAm)3-1 multilayer after being exposed to airborne bacteria and incubated overnight. Scale bar is 400 μm.

Figure 5-3 displays the CFU counting results for the airborne studies of E. coli and S. epidermidis. The density of CFUs was reported relative to the glass control. For both strains of bacteria, not one CFU was found on any of the multilayers containing silver nanoparticles. This was true even for the (PAA/PAAm)3-1 films, which contained the least amount of silver. These results show that polyelectrolyte multilayers deliver silver ions to the bacteria in a very efficient

manner since even the films with the lowest amount of silver killed all bacteria brought into contact. The multilayer films without silver showed a slight but statistically insignificant decrease in CFU's for both bacteria strains indicating that silver was necessary to successfully kill the bacteria.

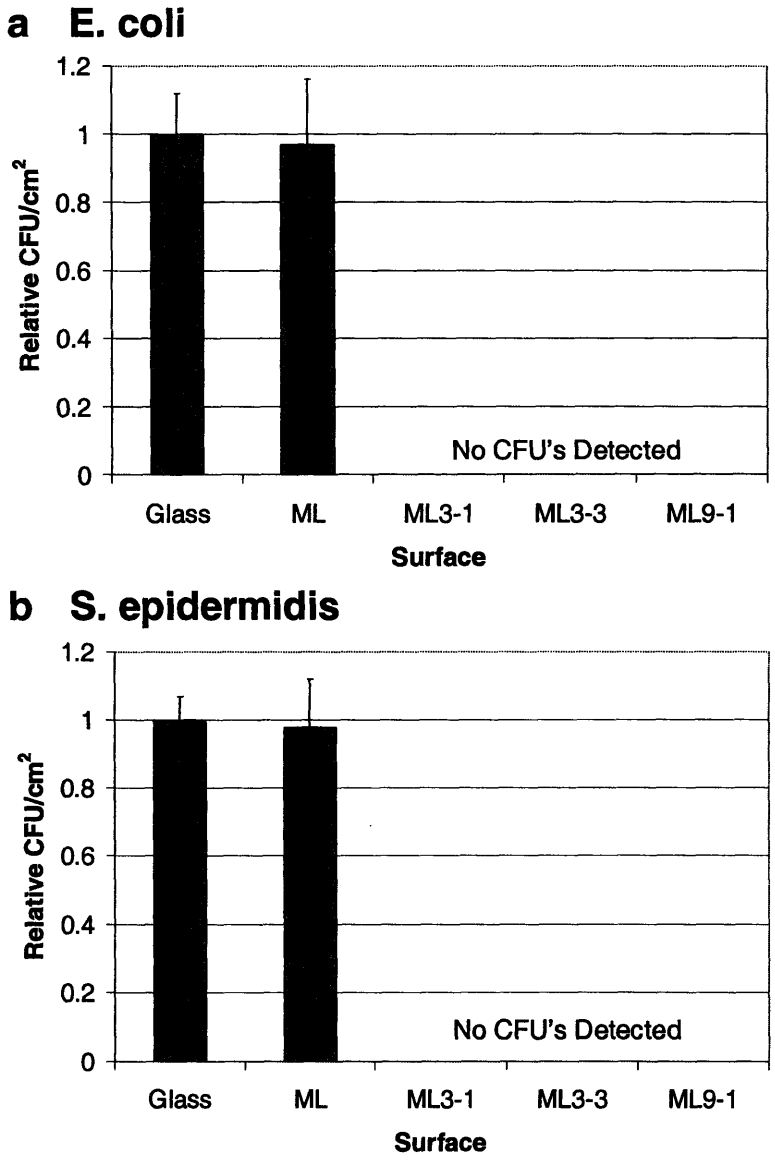

Figure 5-3. Graphs displaying airborne bacteria results for polyelectrolyte multilayers and glass controls of both (a) E. coli and (b) S. epidermidis. Samples were incubated overnight after spraying with bacteria. The CFU densities are reported relative to the glass controls.

The efficacy of killing waterborne bacteria was tested by shaking samples in flasks containing bacteria solution for two hours at 200 RPM and rinsed in PBS. Similar to the airborne model, CFU density was calculated after incubation overnight under LB agar at 37 °C. Figure 5-4 shows the results for E. coli and S. epidermidis. Like the airborne model, no CFU's were found on any samples containing silver, which once again points out the power of released silver ions to kill either gram negative or positive bacteria on contact. In contrast to the airborne model, PAA/PAAm multilayers with no silver significantly lowered the density of CFU's in the waterborne tests. This suggests that the multilayers decreased the adhesion of bacteria even if they could not kill the bacteria. For both the airborne and waterborne studies, the CFU counts for glass controls were between 700 and 1000 CFU/cm2 or approximately 3000-4000 CFU/sample. This means that since we did not see a single colony on any of the nine control samples, the polyelectrolyte multilayers with silver nanoparticles killed on contact greater than 99.99% of bacteria for each sample.

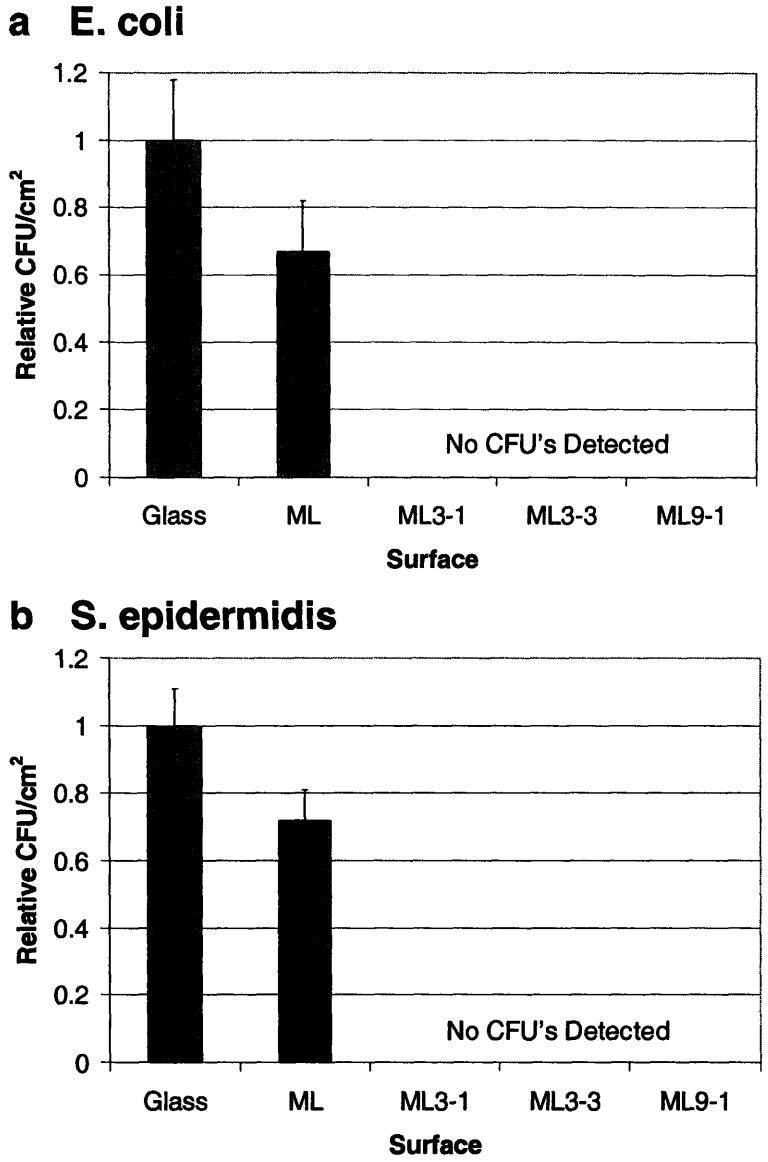

Figure 5-4. Results for waterborne antibacterial testing of (a) E. coli and (b) S. epidermidis on polyelectrolyte multilayers and glass controls. Samples were incubated overnight after 2 hours of exposure to waterborne bacteria. Results are shown relative to the glass controls.

5.3.2. Cytotoxicity of Silver Loaded Multilayers

Another important factor in considering an implant coating besides its antibacterial properties is its potential cytotoxicity to mammalian cells. If cytotoxic, the coatings could have deleterious effects on the patient. The effect of silver-loaded polyelectrolyte multilayers on WT

NR6 fibroblasts was studied using an Alamar Blue™ assay. Two different types of tests were run. Since 3.0/3.0 (PAA/PAAm) multilayers resist fibroblast adhesion[33], the cells floated above the surface, but did not die for a few days. The first cytotoxicity test involved transferring the cells, after they had floated for 1 day above the silver-loaded or non-loaded PAA/PAAm multilayers, to TCPS and monitoring cell proliferation for two days after reseeding using an Alamar Blue™ assay. To test the cytotoxicity to adherent cells, we functionalized the various multilayer surfaces with the adhesion peptide sequence, RGD (arg-gly-asp), using a previously described technique[34]. The tri-amino acid sequence, RGD, is a one of the most-studied adhesion ligands, and is contained in the protein, fibronectin[40]. The RGD chemistry was able to overcome the cell resistant multilayers, and the fibroblasts were able to attach to the surface so that their proliferation could be monitored for two days using Alamar Blue™. The results of both cytotoxicity studies are presented in Figure 5-5. The data are normalized to multilayer samples containing no silver. For both assays, the silver loading had no significant effect on cell growth. The PAA/PAAm3-3 and PAA/PAAm9-1, which contained the highest amount of silver, showed a slight decrease in cell proliferation, but the results were not statistically significant using an ANOVA test.

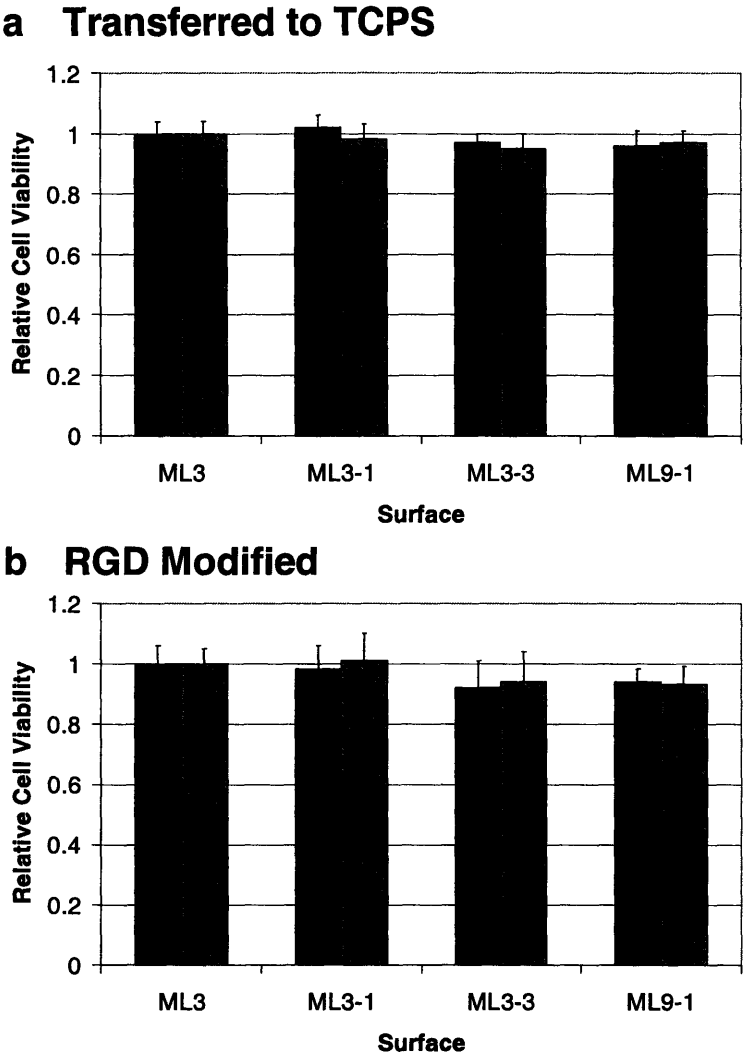

Figure 5-5. Cytotoxicity results comparing polyelectrolyte multilayers with and without silver nanoparticles. The data is normalized to the multilayers without silver for both the (a) floating cell assay and (b) RGD functionalization assay.

5.3.3. Rate of Silver Release

To evaluate the length of time that the polyelectrolyte multilayers could release antibacterial silver ions, the SPR peak from silver in the multilayer samples was monitored after submersion in PBS. The PBS was meant to simulate a buffered environment such as is found under physiological conditions. The release profiles are shown in Figure 5-6 for the three

different silver-loaded multilayers. The graphs were generated by plotting the peak height as a function of time in PBS. The absorbance of the PBS solution was also monitored to determine if silver nanoparticles leached out of the multilayer films. An SPR peak from silver developed and grew in the solution for the first 2 days, indicating that silver nanoparticles were leaching into the PBS. Therefore, the silver leaves the films by two different processes: leaching out of the film as nanoparticles and dissolution as ions. The effectiveness of the films in killing bacteria provides evidence that the second process takes place. All films were monitored for three weeks, and at the end of this time period, they still contained enough silver to be effective antibacterial coatings as confirmed through additional airborne and waterborne experiments. The films aged in PBS were taken through the same airborne and waterborne tests as freshly made films, and like the results discussed previously, no CFU's were detected on any of the silver-loaded multilayers. Besides aging silver-loaded films in PBS, similar experiments were also performed in WT NR6 fibroblast media (with serum). The silver release results were statistically the same in cell media as PBS.

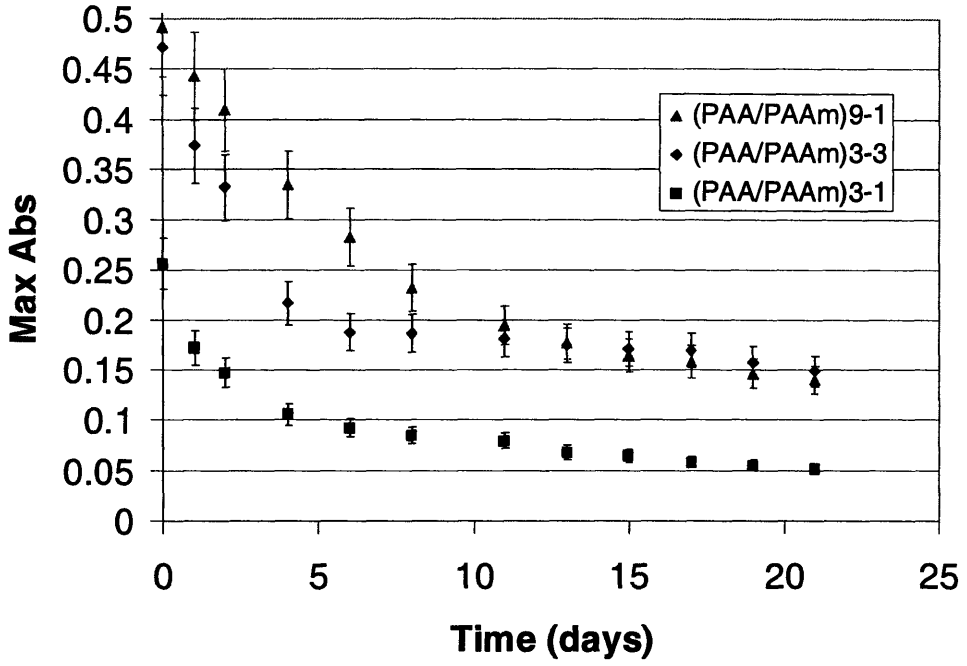

Figure 5-6. Change in silver content in the polyelectrolyte multilayer films as a function of time submerged in PBS.

5.4. Conclusions

In summary, we have demonstrated the antibacterial behavior of PAA/PAAm polyelectrolyte multilayers containing silver nanoparticles. The silver nanoparticles were synthesized in situ using free carboxylic acid groups in the multilayers as nanoreactors. The silver-loaded films killed greater than 99.99% of model gram negative and gram positive bacteria in both airborne and waterborne models compared to glass controls. In addition, the small of amount of silver ions released was non-toxic to fibroblasts grown on the surface after RGD functionalization and when cells floating above the surface of unfunctionalized multilayers were transferred to a TCPS surface. After 21 days in PBS, none of the samples were depleted of silver and all retained their ability to kill bacteria.

References for Chapter 5

(1) Costerton, J. W.;Stewart, P. S.;Greenberg, E. P. Bacterial Biofilms: A Common Cause of Persistant Infections *Science* **1999**, *284*, 1318-1322.

(2) Lewis, A. L. Phosphorylcholine-Based Polymers and Their Use in the Prevention of Biofouling *Colloids Surf., B* **2000**, *18*, 261-275.

(3) Tiller, J. C.;Lee, S. B.;Lewis, K.;Klibanov, A. M. Polymer Surfaces Derivatized with Poly(Vinyl-N-Hexylpyridinium) Kill Airborne and Waterborne Bacteria *Biotechnol. Bioeng.* **2002**, *79*, 465-471.

(4) Rabea, E. I.;Badawy, M. E.-T.;Stevens, C. V.;Smagghe, G.;Steurbaut, W. Chitosan as Antimicrobial Agent: Applications and Mode of Action *Biomacromolecules* **2003**, *4*, 1457-1465.

(5) Baveja, J. K.;Willcox, M. D. P.;Hume, E. B. H.;Kumar, N.;Odell, R.;Poole-Warren, L. A. Furanones as Potential Anti-Bacterial Coatings on Biomaterials *Biomaterials* **2004**, *25*, 5003-5012.

(6) Gray, J. E.;Norton, P. R.;Alnouno, R.;Marolda, C. L.;Valvano, M. A.;Griffiths, K. Biological Efficacy of Electroless-Deposited Silver on Plasma Activated Polyurethane *Biomaterials* **2003**, *24*, 2759-2765.

(7) Ignatova, M.;Labaye, D.;Lenoir, S.;Strivay, D.;Jerome, R.;Jerome, C. Immobilization of Silver in Polypyrrole/Polyanion Composite Coatings: Preparation, Characterization, and Antibacterial Activity *Langmuir* **2003**, *19*, 8971-8979.

(8) Zhang, L.;Yu, J. C.;Yip, H. Y.;Li, Q.;Kwong, K. W.;Xu, A.;Wong, P. K. Ambient Light Reduction Strategy to Synthesize Silver Nanoparticles and Silver-Coated TiO2 with Enhanced Photocatalytic and Bactericidal Activities *Langmuir* **2003**, *19*, 10372-10380.

(9) Shi, Z.;Neoh, K. G.;Kang, E. T. Surface-Grafted Viologen for Precipitation of Silver Nanoparticles and Their Combined Bactericidal Activities *Langmuir* **2004**, *20*, 6847-6852.

(10) Kumar, R.;Munstedt, H. Silver Ion Release from Antimicrobial Polyamide/Silver Composites *Biomaterials* **2005**, *26*, 2081-2088.

(11) Slawson, R. M.;Van Dyke, M. I.;Lee, H.;Trevors, J. T. Germanium and Silver Resistance, Accumulation, and Toxicity in Microorganisms *Plasmid* **1992**, *27*, 72-79.

(12) Silver, S. Bacterial Silver Resistance: Molecular Biology and Uses and Misuses of Silver Compounds *FEMS Microbiol. Rev.* **2003**, *27*, 341-353.

(13) Feng, Q. L.;Wu, J.;Chen, G. Q.;Cui, F. Z.;Kim, T. N.;Kim, J. O. A Mechanistic Study of the Antibacterial Effect of Silver Ions on Escherichia Coli and Staphylococcus Aureus *J. Biomed. Mater. Res.* **2000**, *52*, 662-668.

(14) Russell, A. D. Plasmids and Bacterial Resistance to Biocides *J. Appl. Microbiol.* **1997**, *82*, 155-165.

(15) Dowling, D. P.;Donnelly, K.;McConnell, M. L.;Eloy, R.;Arnaud, M. N. Deposition of Anti-Bacterial Silver Coatings on Polymeric Substrates *Thin Solid Films* **2001**, *398-399*, 602-606.

(16) Alt, V.;Bechert, T.;Steinrucke, P.;Wagener, M.;Seidel, P.;Dingeldein, E.;Domann, E.;Schnettler, R. An in Vitro Assessment of the Antibacterial Properties and Cytotoxicity of Nanoparticulate Silver Bone Cement *Biomaterials* **2004**, *25*, 4383-4391.

(17) Joly, S.;Kane, R.;Radzilowski, L.;Wang, T.;Wu, A.;Cohen, R. E.;Thomas, E. L.;Rubner, M. F. Multilayer Nanoreactors for Metallic and Semiconducting Particles *Langmuir* **2000**, *16*, 1354-1359.
(18) Wang, T. C.;Rubner, M. F.;Cohen, R. E. Polyelectrolyte Multilayer Nanoreactors for Preparing Silver Nanoparticle Composites: Controlling Metal Concentration and Nanoparticle Size *Langmuir* **2002**, *18*, 3370-3375.
(19) Dai, J.;Bruening, M. L. Catalytic Nanoparticles Formed by Reduction of Metal Ions in Multilayered Polyelectrolyte Films *Nano Lett.* **2002**, *2*, 497-501.
(20) Lin, X. Z.;Teng, X.;Yang, H. Direct Synthesis of Narrowly Dispersed Silver Nanoparticles Using a Single-Source Precursor *Langmuir* **2003**, *19*, 10081-10085.
(21) Decher, G.;Hong, J. D.;Schmitt, J. Buildup of Ultrathin Multilayer Films by a Self-Assembly Process: III. Consecutively Alternating Adsorption of Anionic and Cationic Polyelectrolytes on Charged Surfaces *Thin Solid Films* **1992**, *210*, 831-835.
(22) Decher, G. Fuzzy Nanoassemblies: Toward Layered Polymeric Multicomposites *Science* **1997**, *277*, 1232-1237.
(23) Caruso, F.;Trau, D.;Mohwald, H.;Renneberg, R. Enzyme Encapsulation in Layer-by-Layer Engineered Polymer Multilayer Capsules *Langmuir* **2000**, *16*, 1485-1488.
(24) Qiu, X.;Leporatti, S.;Donath, E.;Mohwald, H. Studies on the Drug Release Properties of Polysaccharide Multilayers Encapsulated Ibuprofen Microparticles *Langmuir* **2001**, *17*, 5375-5380.
(25) Vazquez, E.;Dewitt, D. M.;Hammond, P. T.;Lynn, D. M. Construction of Hydrolytically-Degradable Thin Films Via Layer-by-Layer Deposition of Degradable Polyelectrolytes *Journal- American Chemical Society* **2002**, *124*, 13992-13993.
(26) Wood, K. C.;Boedicker, J. Q.;Lynn, D. M.;Hammond, P. T. Tunable Drug Release from Hydrolytically Degradable Layer-by-Layer Thin Films *Langmuir, In Press*.
(27) Berg, M. C.;Zhai, L.;Cohen, R. E.;Rubner, M. F. Controlled Release from Porous Polyelectrolyte Multilayers **In Preparation**.
(28) Decher, G.;Lehr, B.;Lowack, K.;Lvov, Y.;Schmitt, J. New Nanocomposite Films for Biosensors - Layer-by-Layer Adsorbed Films of Polyelectrolytes, Proteins or DNA *Biosens. Bioelectron.* **1994**, *9*, 677-684.
(29) Elbert, D. L.;Herbert, C. B.;Hubbell, J. A. Thin Polymer Layers Formed by Polyelectrolyte Multilayer Techniques on Biological Surfaces *Langmuir* **1999**, *15*, 5355-5362.
(30) Serizawa, T.;Yamaguchi, M.;Matsuyama, T.;Akashi, M. Alternating Bioactivity of Polymeric Layer-by-Layer Assemblies: Anti- Vs Procoagulation of Human Blood on Chitosan and Dextran Sulfate Layers *Biomacromolecules* **2000**, *1*, 306-309.
(31) Chluba, J.;Voegel, J.-C.;Decher, G.;Erbacher, P.;Schaaf, P.;Ogier, J. Peptide Hormone Covalently Bound to Polyelectrolytes and Embedded into Multilayer Architectures Conserving Full Biological Activity *Biomacromolecules* **2001**, *2*, 800-805.
(32) Mendelsohn, J. D.;Yang, S. Y.;Hiller, J.;Hochbaum, A. I.;Rubner, M. F. Rational Design of Cytophilic and Cytophobic Polyelectrolyte Multilayer Thin Films *Biomacromolecules* **2003**, *4*, 96-106.
(33) Yang, S. Y.;Mendelsohn, J. D.;Rubner, M. F. New Class of Ultrathin, Higly Cell-Adhesion-Resistant Polyelectrolyte Multilayers with Micropatterning Capabilities *Biomacromolecules* **2003**, *4*, 987-994.

(34) Berg, M. C.;Yang, S. Y.;Hammond, P. T.;Rubner, M. F. Controlling Mammalian Cell Interactions on Patterned Polyelectrolyte Multilayer Surfaces *Langmuir* **2004**, *20*, 1362-1368.
(35) Thompson, M. T.;Berg, M. C.;Tobias, I. S.;Rubner, M. F.;van Vliet, K. J. Quantifying the Role of Compliance in Cell Adhesion and Proliferation:
Polyelectrolyte Multilayers as Mechanically Tunable Cell Substrata **In Preparation**.
(36) Yoo, D.;Shiratori, S. S.;Rubner, M. F. Controlling Bilayer Composition and Surface Wettability of Sequentially Adsorbed Multilayers of Weak Polyelectrolytes *Macromolecules* **1998**, *31*, 4309-4318.
(37) Shiratori, S. S.;Rubner, M. F. Ph-Dependent Thickness Behavior of Sequentially Adsorbed Layers of Weak Polyelectrolytes *Macromolecules* **2000**, *33*, 4213-4219.
(38) Yang, S. Y.;Rubner, M. F. Micropatterning of Polymer Thin Films with pH-Sensitive and Cross-Linkable Hydrogen-Bonded Polyelectrolyte Multilayers *J. Am. Chem. Soc.* **2002**, *124*, 2100-2101.
(39) Hogt, A. H.;Dankert, J.;Feijen, J. Adhesion of Coagulase-Negative Staphylococci to Methacrylate Polymers and Copolymers *J. Biomed. Mater. Res.* **1986**, *20*, 533-545.
(40) Brandley, B. K.;Schnaar, R. L. Covalent Attachment of an Arg-Gly-Asp Sequence Peptide to Derivatizable Polyacrylamide Surfaces: Support of Fibroblast Adhesion and Long-Term Growth *Anal. Biochem.* **1988**, *172*, 270-278.

Chapter 6 Anti-Fouling Properties of Superhydrophobic Polyelectrolyte Multilayers

6.1. Introduction

Surface coatings that resist fouling from biomolecules and micro-organisms have potential use in biomedical devices as well as industrial processes. The adhesion of bacteria, for example, can lead to biofilm formation which can cause hygienic problems and corrode pipes. Biofilms are complex structures containing many species of bacteria, channels for nutrient flow, and a protective protein matrix that can retard the actions of antibiotics or biocides[1]. Many different materials that elute antimicrobial agents or kill microbes on contact[2-11] have been developed in an attempt to prevent biofilm formation. A majority of these materials kill micro-organisms effectively, but do not sufficiently address prevention of fouling due to proteins or other biomolecules with some exceptions such as phosphoryl choline surfaces[2]. Prevention of non-specific adsorption of proteins and/or subsequent adhesion of mammalian cells is important since surfaces can be fouled by these processes[12, 13]. For this reason, another option is to use surfaces that resist non-specific adhesion or adsorption of microbes and proteins such as poly(elethylene glycol) PEG[12-17]. Surfaces coated with PEG have been found to eliminate cell adhesion and reduce bacterial adhesion as well as adsorption of proteins such as lysozyme and fibrinogen. However, this polymer is prone to oxidation and degradation by alcohol dehydrogenase and aldehyde dehydrogenase[18, 19] and loses its resistance in long term applications. In addition, many of the bactericidal and resist surfaces only reduce but do not eliminate bacterial contamination[13].

To try to address many of these problems, some research efforts have turned to superhydrophobic surfaces as potential anti-fouling coatings, although only limited work has been done in this area[20, 21]. Superhydrophobic surfaces exhibit an advancing water contact angle greater than 150° and a low contact angle hysteresis[22, 23]. Superhydrophobicity is not solely due to surface chemistry, but is instead a consequence of both surface chemistry and roughness. On suitably rough surfaces, two different states can exist. The Cassie state[24] exists when the roughness is such that water droplets do not enter the hollow spaces on the surface, and droplets can roll off. In contrast, the Wenzel state[25, 26] has a surface roughness in which water droplets fill the air pockets, and the droplets become pinned on the surface. Both states have high advancing water contact angles, but only the Cassie state has a receding contact angle close to the advancing one. The best anti-fouling surfaces are true superhydrophobic coatings that are self-cleaning. These surfaces prevent droplets of water from getting pinned to the surface, and therefore, are in the Cassie state. Superhydrophobic coatings have been formed using a variety of techniques such as roughening hydrophobic materials[27], forming well-ordered microstructures[28], or coating rough surfaces with hydrophobic molecules[29, 30]. Although, many of these superhydrophobic coatings have shown a great deal of promise, they often require expensive or tedious processing steps or show a lack in uniformity and stability. Recently, our group demonstrated layer-by-layer assembled superhydrophobic multilayers that exhibited long term stability and could be coated onto a broad range of substrates[31]. Other approaches with polyelectrolyte multilayer films have also generated superhydrophobic surfaces. Shiratori and coworkers used multilayers as sacrificial templates for forming superhydrophobic surfaces from SiO_2 nanoparticles[32], and the Schlenoff group made superhydrophobic multilayers using fluorinated polymers and clay particles[33].

Since layer-by-layer polyelectrolyte multilayers were first introduced[34, 35], a variety of functional materials have been incorporated into these ultra-thin films to address various biomaterial applications such as drug delivery[36-40], biosensors[40, 41], and cell resistant surfaces[42-44]. Of the different polyelectrolyte multilayers studied, films assembled from weak polyelectrolytes have promise due to the molecular tunability of layer thickness and properties with simple pH adjustments[45, 46]. Mendelsohn et al. found that weak polyelectrolytes assembled in layer-by-layer films under certain conditions underwent a reversible porosity transition when treated in an acidic environment[47]. These porous polyelectrolyte multilayers have potential applications in the areas of drug delivery[48], optical shutters[49], anti-reflection coatings[50] and Bragg reflectors[51]. Furthermore, by combining the micron scale roughness of the porous films with the nano-scale roughness introduced by adding SiO_2 nanoparticles, with subsequent fluorination, superhydrophobic multilayers could be produced[31]. The superhydrophobic multilayers exhibited an advancing and receding contact angle greater than 170°. Not only do the superhydrophobic multilayers show excellent long term stability, but very recent work has shown that the surfaces can be patterned with hydrophilic regions[52].

In this chapter, we tested the general anti-fouling properties of superhydrophobic polyelectrolyte multilayers by challenging the surface with proteins, mammalian cells, and bacteria. In addition, we used a simple polyelectrolyte patterning procedure to create hydrophilic spots on the surface. Surfaces with hydrophilic regions patterned against a hydrophobic background have potential applications in combinatorial chemistry and the screening of biological interactions[53, 54]. Many different methods[55-58] have been used to create patterns with contrasting wettability, but these techniques often include complex synthesis or do not lead to chemically functional patterns. We show the versatility of our patterning technique by

selectively depositing multilayers and promoting cell attachment on surfaces with various ligand densities. The various ligand densities were created by taking advantage of the ability to tune the number of functional groups present in polyelectrolyte patterns[40, 59]. Superhydrophobic patterned surfaces could be very useful as high-throughput screening assays. It should be noted that part of the work in this chapter has been done in collaboration with Dr. Lei Zhai at MIT.

6.2. Experimental Methods

Materials. Poly(acrylic acid) (PAA) (MW = 90,000; 25% aqueous solution) and polyacrylamide (PAAm) (MW = 5,000,000; 1% aqueous solution) were purchased from Polysciences. Poly(allylamine hydrochloride) (PAH) (MW = 70,000), poly(sodium 4-styrene-sulfonate) (SPS), fluorescein isothiocyanate (FITC) labeled bovine serum albumin (BSA), lysozyme, FITC, and SiO_2 nanoparticles were purchased from Sigma-Aldrich. (Tridecafluoro-1,1,2,2-terahydrooctyl)-1-trichlorosilane (semifluorinated silane) was purchased from United Chemical Technologies. Sulfosuccinimidyl 6-[3'-(2-pyridyldithio)-propionamido] hexanoate (Sulfo-LC-SPDP) was obtained from Pierce Biotechnology. The peptide, GRGDSPC, was synthesized by the Biopolymers lab at MIT. All materials were used without any further purification.

Film Preparation. The layer-by-layer assembly process of polyelectrolyte multilayers has been previously described[45], as has the assembly of superhydrophobic polyelectrolyte multilayers[31]. Briefly, the polyelectrolyte multilayers were assembled using an automated HMS programmable slide stainer from Zeiss, Inc. Polyelectrolyte solutions were prepared (10^{-2} M based on repeat unit of the polymer) with 18 MΩ Millipore water, and were pH-adjusted with HCl or NaOH. Multilayers were built by first building alternating layers of PAH and SPS (both

at pH = 4.0), with PAH being the first layer. In between each 15 minute polyelectrolyte adsorption step, the substrates were taken through a series of rinse steps in 18 MΩ Millipore water for 2, 1, and 1 minutes, respectively. This process was repeated until 8 layers were built of PAH and SPS, leaving SPS as the top layer. Next, the process was repeated with alternate layers of PAH (pH = 8.5) and PAA (pH = 3.5), beginning with PAH, until 201 total layers were assembled, leaving PAH as the top layer. The PAH/SPS layers improved adhesion between the substrate and the multilayer film.

After multilayer assembly, the films were taken through a two stage porosity induction process consisting of treatment in water adjusted to pH 2.7 for 2 hours and then water adjusted o pH 2.3 for 4 hours. The porous structure was locked in by crosslinking the films at 180 °C for 2 hours. After the crosslinking step, the films were alternately dipped in solutions of 1% SiO_2 nanoparticles and PAH (pH = 4.0) to make 5 SiO_2/PAH layers leaving the nanoparticles as the outermost layer. Finally, the multilayer films were treated with a semi-fluorinated silane using chemical vapor deposition (CVD) and heated at 180 °C for 2 hours.

Protein Adsorption Assay. Superhydrophobic multilayers and microporous multilayers were dipped into a 0.1 % phosphate buffered saline (PBS) solution of either FITC labeled bovine serum albumin (FITC-BSA) or FITC labeled lysozyme (FITC-lysozyme). FITC-lysozyme was created by reacting FITC with lysozyme in PBS and subsequent dialysis to separate unbound FITC. After 30 minutes, the samples were rinsed twice in PBS for 5 minutes and once in 18 MΩ Millipore water for 5 minutes. Fluorescence images were then captured using a Zeiss Axioplan 2 fluorescence microscope: the fluorescence intensity was compared using Adobe Photoshop 5.0 software.

Cell Culture. Murine wild type (WT) NR6 fibroblasts were kindly donated by Prof. Linda Griffith's laboratory at MIT. Unless noted otherwise, all materials used for mammalian cell culture were purchased from Gibco/Invitrogen. The superhydrophobic multilayers were sprayed with 70%(v/v) ethanol for sterilization. In previous work[43], it was found that this sterilization procedure did not alter a multilayer films' properties. The WT NR6 fibroblasts were grown under conditions previously described[40]. Briefly, the cells were grown in pH=7.4 media made from Modified Eagles Medium-α (MEM-α) with 7.5% (v/v) fetal bovine serum (FBS), 1% (v/v) sodium pyruvate (100 mM), 1% (v/v) nonessential amino acids (10 mM), 1% (v/v) Geneticin (G418) antibiotic (350 μg/ 10 mL PBS), 1% (v/v) L-glutamine (200 mM), 1% (v/v) penicillin (10,000 U/mL, from Sigma), and 1% streptomycin (10 mg/mL, from Sigma). Cells were kept in a humid incubator at 37 °C and 5% CO_2.

For cell adhesion assays, WT NR6 fibroblasts were counted using a hemocytometer, and trypan blue exclusion was used for cell viability. Cells were seeded on samples at ~10,000 cells/cm^2, and stained with LIVE/DEAD® fluorescent stain (from Molecular Probes). This stain stains dead cells red with ethidium homodimer-1 and live cells green with calcein AM. Fluorescent micrographs were taken of adherent cells using a Nikon Eclipse TE300 inverted phase contrast microscope with Openlab 3.0 software.

Bacteria Culture. Airborne and waterborne bacteria assays were performed using methods similar to those described by Klibanov and coworkers[3]. Escherichia coli (E. coli, ATCC #14948) and Staphylococcus epidermidis (S. epidermidis, ATCC #14990) were purchased from American Type Culture Collection (ATCC). The bacteria strains were grown in LB Broth, Miller (from EMD Chemicals through VWR), and the cell density was calculated by measuring the optical density at 540 nm (assuming an optical density of 1.0 is equal to

10^9/mL)[60]. Waterborne bacteria were introduced experimentally by first centrifuging the bacteria at 2700 RPM for 10 minutes, and then suspending the bacteria in PBS after pouring off the supernatant. This centrifugation process was repeated twice to remove any broth from the bacteria solution. The optical density was then measured again, and the bacteria solution was diluted with PBS to reach a final concentration of 10^6/mL. The superhydrophobic multilayers and controls were then shaken at 200 RPM in the diluted bacteria solution for two hours at 37 °C. After three 5 minute rinses in PBS, the samples were placed under a slab of Miller LB agar (purchased from EMD Chemicals through VWR). The samples were incubated overnight, and colony forming units (CFU's) were counted in at least 4 areas for each sample. At least 3 samples and glass controls were tested. For the superhydrophobic multilayers and microporous multilayers, the colonies were stained with 0.1% crystal violet (from Sigma) to increase contrast. For airborne experiments, a similar protocol for centrifugation was followed, except deionized water was used for resuspending bacteria and making dilutions. The 10^6/mL bacteria solution was loaded into a chromatography sprayer and misted onto the samples. At this point, half of the samples were rinsed three times in PBS, and half were not. Substrates were covered with LB agar immediately after the rinsing or spraying step, and left to incubate overnight at 37 °C. CFU's were then counted in at least 4 areas per sample, and at least 3 samples were run for each condition. Crystal violet was used to stain bacteria colonies on superhydrophobic and microporous surfaces.

Surface Patterning. As described in detail elsewhere[52], the superhydrophobic multilayers were patterned with a micropipettor filled with 0.01 M PAA solution composed of 40% isopropyl alcohol and 60% water. This solvent combination was found to be optimal for creating patterns of controlled size. The solution was spotted onto the surface in the desired

pattern and allowed to dry. Multilayers could then be selectively assembled on the patterned spots using the layer-by-layer technique for polyelectrolyte multilayer assembly described above. Multilayers were built with PAAm (pH = 3.0) and PAA (pH = 3.0). The PAAm/PAA multilayers were formed from hydrogen-bonding interactions and required post baking at 95 °C as previously described[61].

Peptide Coupling. Biological ligands were coupled onto the surface using a previously described method[40]. Briefly, patterned samples were first submerged for 30 minutes in a 0.5 mM solution of the crosslinker, Sulfo-LC-SPDP, in PBS. Samples were then rinsed twice in PBS for 5 minutes. Finally, the samples were incubated at room temperature for 8 hours in a solution of 0.5 mM peptide (GRGDSPC) in PBS and rinsed twice in PBS.

Statistical Analysis. Analysis of variance (ANOVA) was implemented to determine statistical differences between the density of CFU's on superhydrophobic multilayers, microporous multilayers, and glass controls. ANOVA determines whether or not the variance between testing conditions is greater than the variance within testing conditions. The *p*-value (or probability value) is the product of the ANOVA test, and a value less than 0.05 translates to a statistical difference (based on a 5% level).

6.3. Results and Discussion

6.3.1. Protein Adsorption Assays

A surface that is truly anti-fouling must resist a variety of different materials and biological organisms. Superhydrophobic coatings are possible candidates for anti-fouling applications since they allow only limited interactions of the surface with aqueous solutions. In

essence, a layer of air is created between the surface and water, so any material in the aqueous solution such as proteins, cells, or bacteria must cross this surface tension barrier before adhering to the surface. To test the hypothesis that superhydrophobic multilayers can act as anti-fouling coatings, their ability to resist protein adsorption was first studied. The properties of superhydrophobic multilayers have been described previously[31]. The superhydrophobic multilayers used in these studies had an advancing and receding contact angle greater than 170° as measured through a video contact angle analysis[31]. For these experiments, samples were exposed to solutions of FITC labeled BSA or FITC labeled lysozyme for 30 minutes. These proteins were chosen because of their charge difference (BSA is net negative and lysozyme is net positive).

In addition to superhydrophobic multilayers, we also tested microporous multilayers that were created by using the same processing conditions and porosity induction step as the superhydrophobic films. However, the microporous multilayers lacked the final nanoparticle deposition and fluorination steps used to create the superhydrophobic surfaces. These surfaces were chosen for comparison to the superhydrophobic multilayers because the have the same micron-scale roughness and are composed of the same polyelectrolytes. The microporous films have a high advancing contact angle of approximately 100°, but have a low receding contact angle of approximately 60°. For this reason, they were used to see if a micron-scale roughness was enough to obtain anti-fouling properties, or if it is necessary to have a superhydrophobic coating. Both microporous and superhydrophobic multilayers had significant background fluorescence (seen in samples not exposed to FITC-BSA), but this was subtracted from the fluorescence intensity after protein adsorption.

After exposure to either FITC-BSA or FITC-lysozyme, the superhydrophobic multilayers adsorbed no detectable amount of protein; the fluorescence intensity was not significantly different from the multilayer background fluorescence. In contrast, the microporous multilayers allowed significant amounts of both FITC-BSA and FITC-lysozyme to adsorb to the surface. The micrographs in Figure 1 show the FITC-BSA fluorescence intensity difference between superhydrophobic and microporous multilayers. In comparison to the fluorescence intensity of the superhydrophobic films (statistically the same as the background); FITC-BSA on microporous films had 2.4 times the fluorescence intensity. The FITC-lysozyme intensity on the microporous films was approximately 1.8 times higher than the multilayer background or superhydrophobic films. These results indicate that superhydrophobic coatings are capable of preventing proteins from fouling the surface.

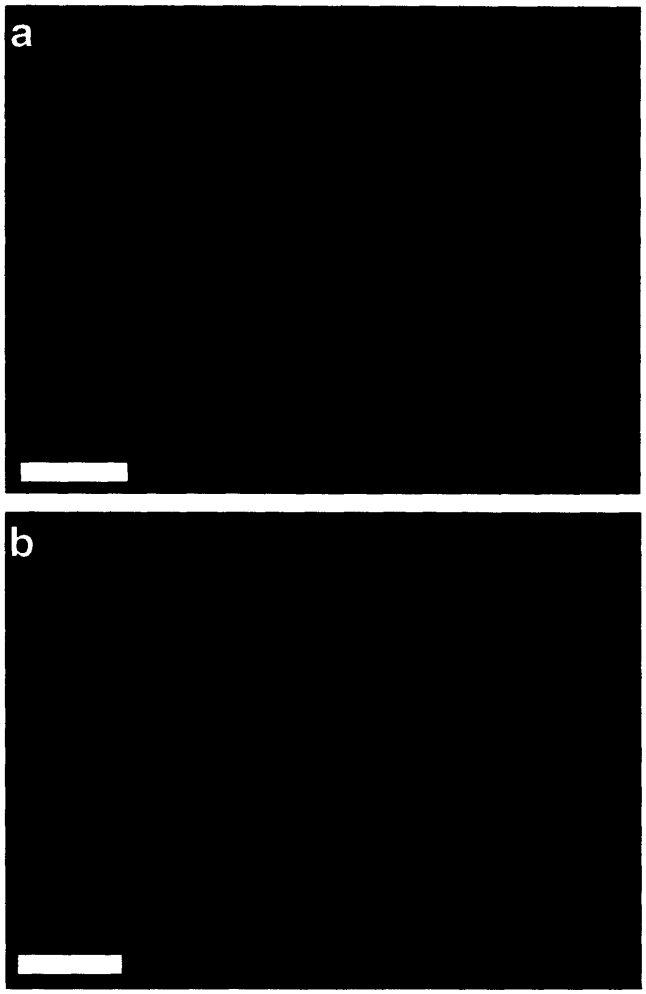

Figure 6-1. Fluorescence images of FITC labeled BSA adsorbed onto (a) a microporous multilayer and (b) a superhydrophobic multilayer. The films were exposed to a 1.0% FITC-BSA solution in PBS for 30 minutes. Scale bar is 100 μm.

The ability of superhydrophobic multilayers to prevent adsorption of both negatively and positively charged proteins is noteworthy because in previous work, proteins have been readily adsorbed to polyelectrolyte multilayer surfaces[43, 62-64], in some cases, regardless of the surface charge. In addition, various proteins have been incorporated into multilayer films through layer-by-layer assembly[65, 66]. In comparison to our results with superhydrophobic multilayers, other protein resistant surfaces such as PEG have been shown to reduce the adsorption of both positively and negatively charged proteins to 0.2% of a monolayer coverage for some proteins[12]. However, PEG coatings are known to lose their effectiveness over time due to degradation[18, 19].

To access the long-term stability of superhydrophobic multilayers, we repeated the protein adsorption assays and increased the exposure time from 30 minutes to one week. Even after one week, the multilayers maintained their superhydrophobic nature and did not allow a detectable amount of either FITC-BSA or FITC-lysozyme to adsorb to the surface. For these long-term experiments, the PAH/SPS layers assembled first on the glass substrate were critical. Superhydrophobic multilayers without these adhesion-promoting layers started to delaminate after the first two to three days of immersion in the protein solution. The ability to resist protein adsorption on a long term basis has important consequences since longer-term protein adsorption could lead to other biological interactions and fouling.

6.3.2. Mammalian Cell Resistance

To further explore the anti-fouling nature of superhydrophobic multilayers, these films along with microporous multilayers were tested for their ability to resist attachment of WT NR6 fibroblasts. We chose this line of fibroblasts because their ability to readily stick to a variety of surfaces would challenge the superhydrophobic surfaces. After seeding, the cells had to be stained with LIVE/DEAD® stain to image the adherent cells since we could not focus clearly through the translucent microporous structure using phase contrast microscopy. This dye stains live cells green with calcein AM and dead cells red with ethidium homodimer-1. As seen in Figure 2, the superhydrophobic multilayers completely resisted fibroblast adhesion for up to 3 days after seeding. The green spots in Figure 2b are live cells floating above the surface. In contrast, the fibroblasts grew and spread on the microporous multilayers. The number of cells was far less than what would be typical for tissue culture polystyrene, but a significant number attached. Similar to the case of protein adsorption, these results indicate that superhydrophobic multilayers completely repel the anchorage-dependent fibroblasts.

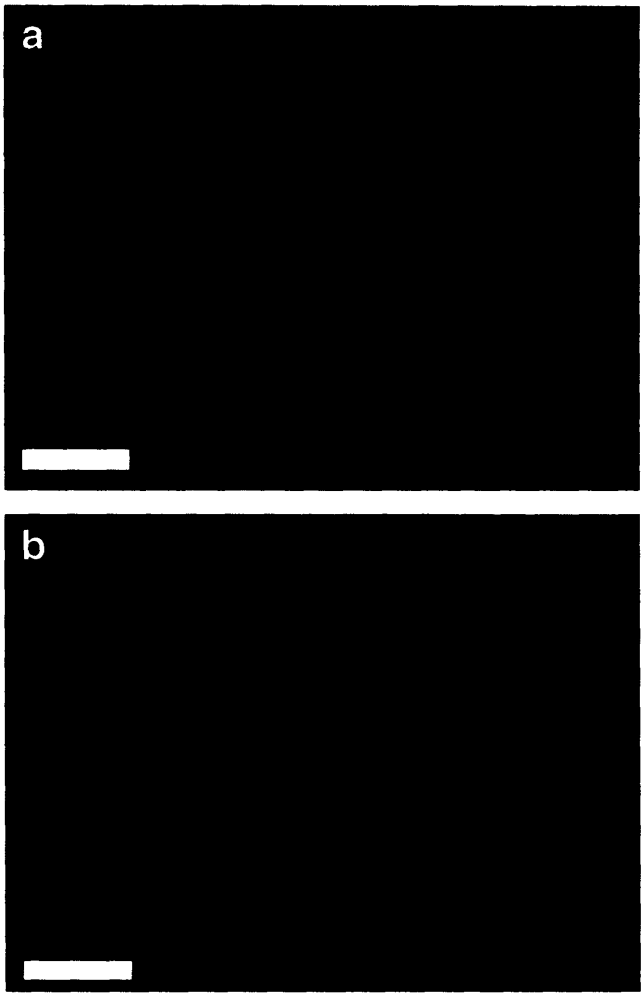

Figure 6-2. Fluorescent images of WT NR6 fibroblasts seeded on (a) microporous and (b) superhydrophobic multilayers at a density of 10,000 cells/cm^2. The cells were stained with LIVE/DEAD® stain three days after seeding to visualize the cells through the porous network of the multilayers films. Scale bar is 100 μm.

In previous work, it was found that multilayer systems assembled under specific conditions resist cell adhesion because of their highly swollen state in buffer and resulting low modulus[43, 67]. These physical attributes prevented fibroblasts from adhering to the surface. The mechanism underlying the ability of superhydrophobic multilayers to resist cell attachment is much different. As previously reported[31], the coatings do not allow water to interact with the surface and essentially exist with a thin layer of air at the interface. This phenomenon can be visualized by placing the superhydrophobic film in water and tilting the surface to a specific

angle at which a mirror-effect is observed. The mirror-effect is due to the total internal reflectance of light resulting from the contrast in the refraction indices of the water and thin layer of air at the interface. Assuming a refraction index of approximately 1.0-1.2 for the air gap with a small amount of porous material and a refraction index of 1.33 for water, a critical angle of approximately 49°- 64° for this effect can be calculated from Snell's Law. The mirror-effect would not be seen without the layer of air at the interface. Furthermore, the effective layer of air creates a surface tension that makes it impossible for a cell to break this barrier and adhere to the surface. The cells floating above the superhydrophobic multilayers were not dead, as verified by lack of red staining. Less than 1.0% of fibroblasts floating above either the superhydrophobic or microporous surface stained red. These particular fibroblasts were chosen for their ability to stick to a variety of surfaces; they are a challenge for any surface to repel[43].

To test the long term cell-inert properties of superhydrophobic multilayers, additional experiments were conducted in which new fibroblasts were reseeded on the surface every 3 days for a total of one week. At the end of this one week period, LIVE/DEAD® staining revealed that the surface had continued to completely resist cell adhesion for this extended period. In addition, the multilayers still had a contact angle greater than 170°. Similar to the long-term protein adsorption experiments, PAH/SPS buffer layers were critical for preventing delamination in the fibroblast experiments after 2 to 3 days.

6.3.3. Bacteria Adhesion Prevention

Bacterial contamination prevention is extremely important in a variety of applications. For this reason, the ability of superhydrophobic multilayers to repel both gram negative E. coli and gram positive S. epidermidis was examined. This study consisted of three different assays: airborne with no rinse step, airborne with a rinse step, and waterborne. The two different

airborne models were used to test whether or not rinsing was required to remove bacterial contamination after airborne bacteria were misted onto the surfaces. For these experiments, microporous multilayers and glass surfaces were used as controls. The results from the airborne studies are displayed in Figure 3. The data show that for both strains of bacteria, colony growth is only prevented on superhydrophobic surfaces that are rinsed after the bacteria were sprayed onto the surface. In fact, no CFU's were detected on the superhydrophobic multilayers after rinsing. In contrast, colonies of bacteria grew well on all of the control samples in the study even after the microporous films and glass were rinsed. This finding indicates the bacteria do not strongly attach to the superhydrophobic multilayers, but only sit on the surface because there is no means to remove them. As seen in these data, rinsing is necessary to remove bacteria from the superhydrophobic coatings. It is not surprising that the rinsing step is necessary in the airborne tests because without it, there is no means to remove the bacteria from the surface before the LB agar slab is placed on the sample. Hence, bacteria are free to multiply in the agar gel and have plenty of nutrients to grow. Unlike many antibacterial surfaces, the superhydrophobic multilayers have no mechanism to kill bacteria, only prevent their attachment. Therefore, a process such as rinsing must be performed to remove bacteria from the surface.

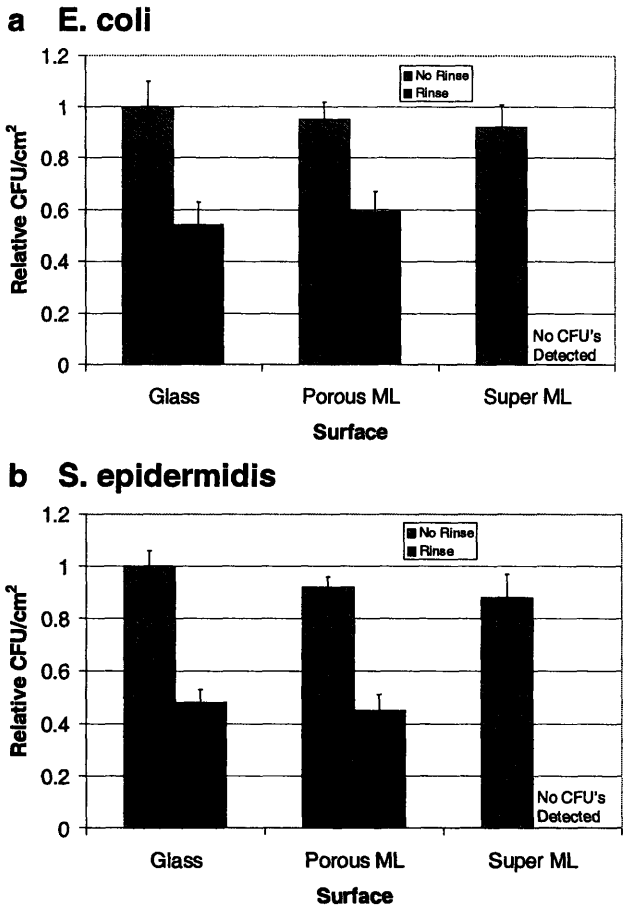

Figure 6-3. Results of bacterial growth microporous and superhydrophobic multilayers from an airborne model (relative to glass samples). The samples were sprayed with solutions of the bacteria strains (a) E. coli and (b) S. epidermidis and left overnight under a slab of agar . Hatched bars represent data from samples with no rinse, and black bars represent data from samples that were rinsed in PBS.

In the waterborne tests, the superhydrophobic multilayers completely repelled bacteria regardless of the strain being tested. These data are presented in Figure 4. As was the case for the airborne test, the microporous multilayers could not prevent bacteria of either strain from attaching to the surface. For the waterborne tests, rinsing was not necessary to remove bacteria from the superhydrophobic surface because the experiments were conducted in an aqueous environment. However, rinsing was performed to obtain more uniform colony growth on the microporous multilayers and glass substrates. The waterborne test is very useful because it

models bacteria coming into contact with surfaces in aqueous or buffered solutions. This situation is applicable to many industrial processes or biomedical applications.

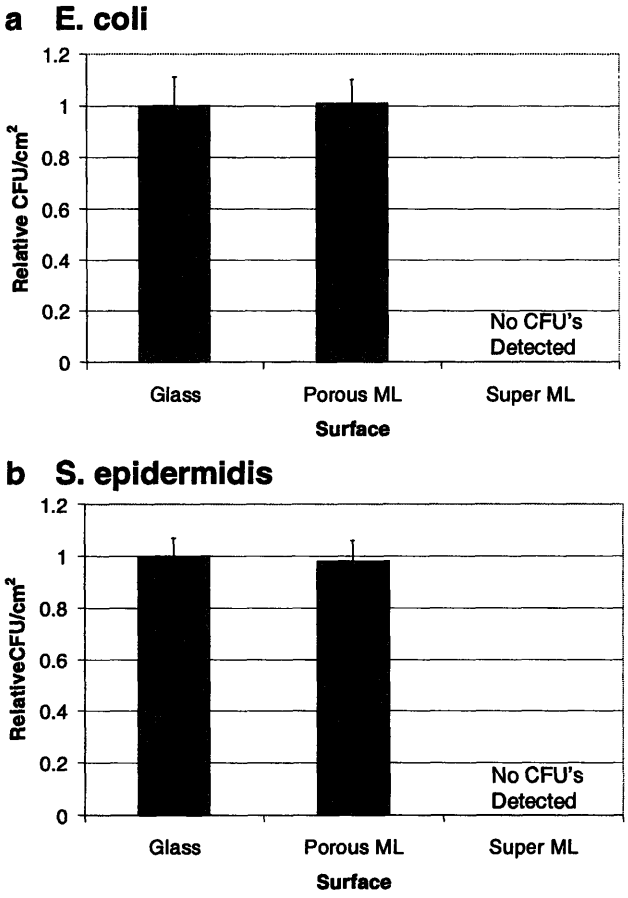

Figure 6-4. Waterborne test results for (a) E. coli and (b) S. epidermidis on microporous and superhydrophobic multilayers (results relative to glass controls). Samples were submerged in the bacteria solution for 2 hours and then placed under a slab of agar overnight.

The ability of superhydrophobic multilayers to prevent bacteria from fouling the surface suggests several possible applications, including prevention of industrial biofilm buildup and medical implant contamination. The major advantages of the superhydrophobic surfaces compared to other antibacterial coatings are that the superhydrophobic multilayers do not rely on the leaching of an antimicrobial agent into the environment and the surface does not get fouled

easily by proteins or other materials. Coatings that elute antimicrobials have a limited supply of the antimicrobial agent and hence, a limited lifetime of effectiveness. Alternatively, films that involve grafting antimicrobials to the surface could have a very limited lifetime if they do not resist adsorption of proteins or other fouling molecules. Superhydrophobic multilayers can potentially avoid both of these problems for long term use. This hypothesis was tested by aging the samples in LB broth for one week prior to performing the airborne and waterborne bacteria tests. After aging, the superhydrophobic multilayers did not show a decrease in contact angle or ability to resist bacterial adhesion. The multilayers maintained their superhydrophobicity and prevented attachment of both airborne (with rinsing) and waterborne bacteria. For further potency against bacteria, we are currently studying superhydrophobic films loaded with silver using a previously described technique[68].

6.3.4. Patterning by Selective Wetting

In addition to possible applications in bacterial adhesion and biofilm prevention, patterned superhydrophobic films could be utilized in laboratory experiments for directing bacterial or other aqueous solutions to specific areas. Orner et al. found that when spotting arrays of aqueous solutions, backgrounds with higher contact angles led to increased beading, which allowed a higher density of spots[54]. For this reason, superhydrophobic films are excellent candidates for use as a background for patterning arrays for DNA chips, cell culture, or combinatorial chemistry.

One simple way to wet these superhydrophobic surfaces is to use non-aqueous solutions. We take advantage of this fact to selectively foul the surface with molecules that facilitate layer-by-layer assembly. This creates hydrophilic patterns on the surface that can be used to not only

build multilayers, but to selectively place biological molecules or cells. A PAA solution consisting of 40% isopropyl alcohol and 60% water was previously found to produce the most well controlled patterns[52]. An array of spots approximately 700 μm in diameter was patterned onto the surface using a micropipettor to deposit the PAA solution. The ability to direct aqueous solutions to these hydrophilic regions was tested by depositing fluorescent dyes on these spots. Figure 6-5 is a photograph of three different fluorescent dye solutions spotted onto a patterned superhydrophobic multilayer film as an example. The droplets were 2 μL, and the colors of the solutions could be visualized by exciting the dyes with a UV lamp. The green dye is 6-FAM, the red dye is Rhodamine Red™-X, and the blue dye is AMCA-X.

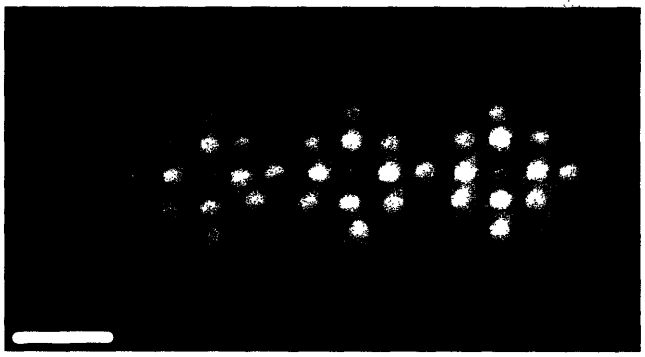

Figure 6-5. Photograph of droplets of fluorescent dyes in aqueous solutions on a patterned superhydrophobic multilayer surface. A UV lamp was held above the sample to excite the fluorophores. Scale bar is 10 mm.

The ability of the superhydrophobic surface to direct molecules to the patterned regions was also studied by selectively adsorbing proteins to the hydrophilic regions. Superhydrophobic films patterned with 700 μm spots of PAA using a micropipettor were submerged in a FITC-lysozyme solution for 30 minutes. As can be seen in Figure 6-6, the protein selectively adsorbed to the hydrophilic PAA patterns. The fluorescence intensity of the superhydrophobic background remained unchanged after submersion in the protein solution indicating that no

detectable amount of protein adsorbed to it. The patterning procedure could be automated using a robot to obtain smaller and more regular patterns.

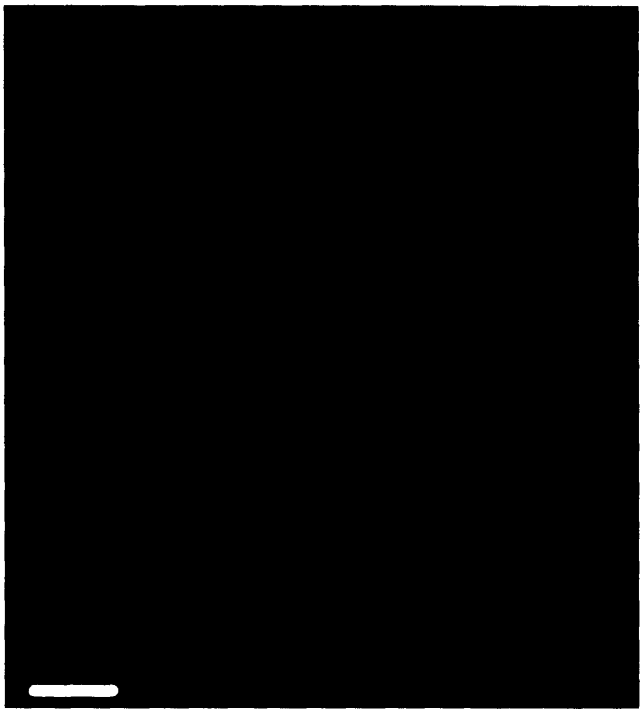

Figure 6-6. FITC labeled lysozyme selectively adsorbed to hydrophilic spots on a superhydrophobic polyelectrolyte multilayer background. Scale bar is 500 μm.

In addition to proteins, additional polyelectrolyte multilayers can be assembled on the PAA patterns. In this process, the patterned superhydrophobic films were completely submerged in both the polymer and rinse baths during the assembly process. The superhydrophobic background acted as a resist to multilayer buildup similar to PEG resists previously studied for multilayer templating[69, 70]. Multilayer assembly was therefore restricted to the patterned areas. The construction of 8.5/3.5 PAH/PAA multilayers was monitored by incorporating 1% FITC labeled PAH into the PAH solution. Figure 6-7 shows the increase in fluorescence intensity as more layers were built onto the patterned regions along with a micrograph of a patterned dot of fluorescently labeled multilayers. Besides directing growth of polyelectrolyte multilayers onto

predetermined regions, the superhydrophobic films also displayed a very high selectivity. The fluorescence intensity of the superhydrophobic surface outside the patterned multilayers was not significantly different than the background fluorescence observed prior to the assembly of the fluorescently labeled multilayers. This indicates that no detectable amount of FITC-PAH fouled the superhydrophobic background.

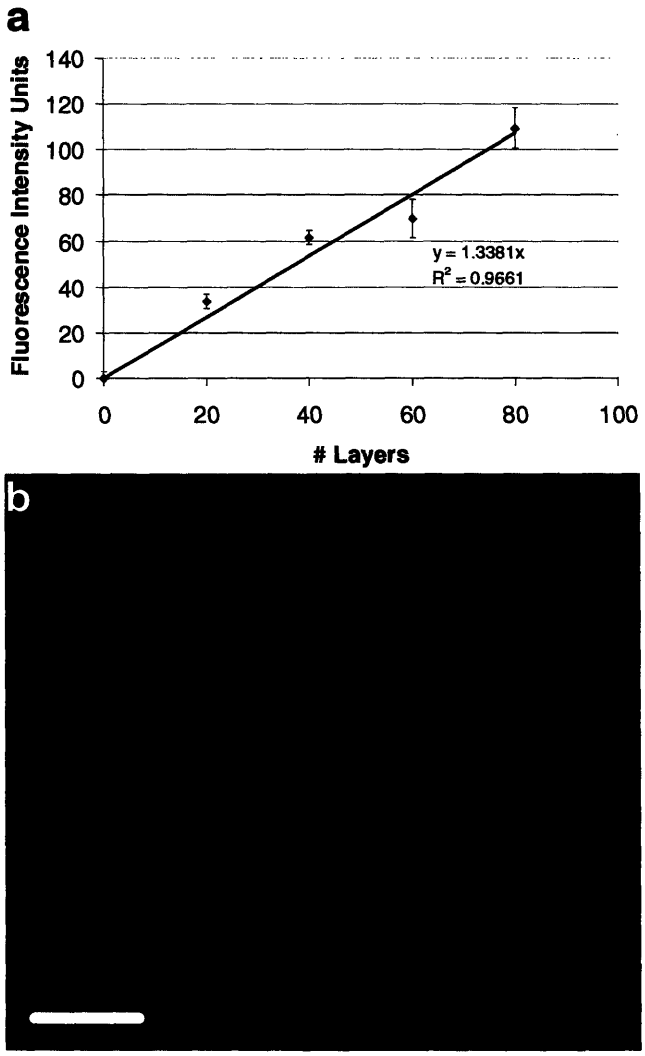

Figure 6-7. (a) Fluorescence intensity as a function of number of layers of 8.5/3.5 (FITC-PAH/PAA) along with a linear fitted trend line. (b) Fluorescence micrograph of 8.5/3.5 (FITC-PAH/PAA) multilayers assembled onto a patterned superhydrophobic multilayer film (10 layers). Scale bar is 200 μm.

After demonstrating that polyelectrolyte multilayers could be selectively assembled onto patterned superhydrophobic multilayer surfaces, 3.0/3.0 PAA/PAAm multilayers were assembled on PAA patterned spots to provide an example of how the films could be used in cell based arrays with different surface functionality. After the PAA/PAAm multilayers, which are known to resist cell adhesion[44], were constructed selectively on the patterned regions, peptides containing the adhesion promoting sequence, RGD (arg-gly-asp), were coupled onto the surface in various densities. The tri-amino acid sequence, RGD, is a well-studied cell adhesion molecule that is contained in the extracellular matrix protein, fibronectin[71]. As previously found with polymer-on-polymer stamped surfaces[40, 59], the RGD density can be tuned by adsorbing PAH at different pH conditions to alter the functional group density at the surface. Subsequent coupling of ligands to the amine groups resulted in different peptide densities. PAH was adsorbed to the patterned PAA/PAAm multilayers at pH 3.5, pH 7.0, and pH 9.0 by spotting the PAH onto the multilayer regions. This correlated to approximately 100%, 75%, and 50% charge density along the polymer chain in solution, respectively[72]. After peptide coupling, the RGD density was approximately 25,000 RGD/μm^2 for PAH adsorbed from a pH 3.5 solution, 53,000 RGD/μm^2 for pH 7.0, and 83,000 RGD/μm^2 for pH 9.0 (estimated from previous work[40]). When WT NR6 fibroblasts were seeded onto the patterned films by immersing the entire film in the cell culture media, cells only attached to the RGD patterns and more cells grew on the patterned areas with higher RGD densities. These patterns were several millimeters in size to provide a large sample area, and the cells' nuclei were stained with DAPI for better detection since the pores interfered with phase contrast microscopy. Figure 6-8 shows the edge of an RGD pattern to show the selectivity of the fibroblasts. The relative fibroblast coverage can be estimated by measuring the fluorescence intensity of the DAPI stain. The cell coverage on patterns with PAH adsorbed at

pH 3.5 and 7.0 were approximately 28% and 84%, respectively (when compared to patterns with PAH adsorbed at pH 9.0). These results show that the patterned superhydrophobic films can direct both specific chemistry and cell adhesion. Spotted patterns with different functionality can be easily assembled for screening their cell adhesion properties.

Figure 6-8. A fluorescence micrograph of WT NR6 fibroblasts with their nuclei DAPI stained on a pattern with created by adsorbing PAH at pH = 9.0 and attaching RGD. Scale bar is 100 μm.

The ability to direct aqueous solutions or cells to predetermined regions on the surface is very powerful. For instance, DNA or protein microarrays could be formed by simply dipping a patterned superhydrophobic film into a solution containing the molecule of choice. In addition, solutions with different molecules could be added to different regions by spotting the solutions or using a pattern consisting of intricate channels. The patterns could be reduced in size by using a more sophisticated patterning tool than a micropipettor.

6.4. Conclusions

We have successfully demonstrated the anti-fouling nature of superhydrophobic polyelectrolyte multilayers against many common biological entities such as proteins,

mammalian cells, and bacteria. These stable superhydrophobic multilayers worked well to prevent contamination from these materials. The coatings were found to reduce protein adsorption to undetectable levels and completely eliminate the attachment of WT NR6 fibroblasts. In addition, these ultra-thin films eliminated bacterial contamination, which could have many possible applications since this is the first step in preventing biofilm formation. The biological materials could not adsorb or attach to the superhydrophobic multilayers due to the creation of a thin layer of air between the aqueous environment and the film surface. The fact that organic solvents could be used to foul the surface was utilized to selectively pattern superhydrophobic multilayers on the surface. This patterning ability could find use in high through-put screening technology or microarray fabrication.

References for Chapter 6

(1) Costerton, J. W.;Stewart, P. S.;Greenberg, E. P. Bacterial Biofilms: A Common Cause of Persistant Infections *Science* **1999**, *284*, 1318-1322.

(2) Lewis, A. L. Phosphorylcholine-Based Polymers and Their Use in the Prevention of Biofouling *Colloids Surf., B* **2000**, *18*, 261-275.

(3) Tiller, J. C.;Lee, S. B.;Lewis, K.;Klibanov, A. M. Polymer Surfaces Derivatized with Poly(Vinyl-N-Hexylpyridinium) Kill Airborne and Waterborne Bacteria *Biotechnol. Bioeng.* **2002**, *79*, 465-471.

(4) Gray, J. E.;Norton, P. R.;Alnouno, R.;Marolda, C. L.;Valvano, M. A.;Griffiths, K. Biological Efficacy of Electroless-Deposited Silver on Plasma Activated Polyurethane *Biomaterials* **2003**, *24*, 2759-2765.

(5) Ignatova, M.;Labaye, D.;Lenoir, S.;Strivay, D.;Jerome, R.;Jerome, C. Immobilization of Silver in Polypyrrole/Polyanion Composite Coatings: Preparation, Characterization, and Antibacterial Activity *Langmuir* **2003**, *19*, 8971-8979.

(6) Zhang, L.;Yu, J. C.;Yip, H. Y.;Li, Q.;Kwong, K. W.;Xu, A.;Wong, P. K. Ambient Light Reduction Strategy to Synthesize Silver Nanoparticles and Silver-Coated Tio2 with Enhanced Photocatalytic and Bactericidal Activities *Langmuir* **2003**, *19*, 10372-10380.

(7) Rabea, E. I.;Badawy, M. E.-T.;Stevens, C. V.;Smagghe, G.;Steurbaut, W. Chitosan as Antimicrobial Agent: Applications and Mode of Action *Biomacromolecules* **2003**, *4*, 1457-1465.

(8) Baveja, J. K.;Willcox, M. D. P.;Hume, E. B. H.;Kumar, N.;Odell, R.;Poole-Warren, L. A. Furanones as Potential Anti-Bacterial Coatings on Biomaterials *Biomaterials* **2004**, *25*, 5003-5012.

(9) Shi, Z.;Neoh, K. G.;Kang, E. T. Surface-Grafted Viologen for Precipitation of Silver Nanoparticles and Their Combined Bactericidal Activities *Langmuir* **2004**, *20*, 6847-6852.

(10) Kumar, R.;Munstedt, H. Silver Ion Release from Antimicrobial Polyamide/Silver Composites *Biomaterials* **2005**, *26*, 2081-2088.

(11) Yang, S. Y.;Berg, M. C.;Rubner, M. F. Antibacterial Properties of Silver-Loaded Polyelectrolyte Multilayers **In Preparation**.

(12) Chapman, R. G.;Ostuni, E.;Liang, M. N.;Meluleni, G.;Kim, E.;Yan, L.;Pier, G.;Warren, H. S.;Whitesides, G. M. Polymeric Thin Films That Resist the Adsorption of Proteins and the Adhesion of Bacteria *Langmuir* **2001**, *17*, 1225-1233.

(13) Ostuni, E.;Chapman, R. G.;Liang, M. N.;Meluleni, G.;Pier, G.;Ingber, D. E.;Whitesides, G. M. Self-Assembled Monolayers That Resist the Adsorption of Proteins and the Adhesion of Bacterial and Mammalian Cells *Langmuir* **2001**, *17*, 6336-6343.

(14) Prime, K. L.;Whitesides, G. M. Adsorption of Proteins onto Surfaces Containing End-Attached Oligo(Ethylene Oxide): A Model System Using Self-Assembled Monolayers *J. Am. Chem. Soc.* **1993**, *115*, 10714-10721.

(15) Kingshott, P.;Wei, J.;Bagge-Ravn, D.;Gadegaard, N.;Gram, L. Covalent Attachment of Poly(Ethylene Gylcol) to Surfaces, Critical for Reducing Bacterial Adhesion *Langmuir* **2003**, *19*, 6912-6921.

(16) Jon, S.;Seong, J.;Khademhosseini, A.;Tran, T.-N. T.;Laibinis, P. E.;Langer, R. Construction of Nonbiofouling Surfaces by Polymeric Self-Assembled Monolayers *Langmuir* **2003**, *19*, 9990-9993.
(17) Sharma, S.;Popat, K. C.;Desai, T. A. Controlling Nonspecific Protein Interactions in Silicon Biomicrosystems with Nanostructured Poly(Ethylene Glycol) Films *Langmuir* **2002**, *18*, 8728-8731.
(18) Herold, D. A.;Keil, K.;Bruns, D. E. Oxidation of Polyethylene Glycols by Alcohol-Dehydrogenase *Biochem. Pharmacol.* **1989**, *38*, 73-76.
(19) Nelson, C. M.;Raghavan, S.;Tan, J. L.;Chen, C. S. Degradation of Micropatterned Surfaces by Cell-Dependent and -Independent Processes *Langmuir* **2003**, *19*, 1493-1499.
(20) Toes, G. J.;van Muiswinkel, K. W.;van Oeveren, W.;Suurmeijer, A. J. H.;Timens, W.;Stokroos, I.;van den Dungen, J. J. A. M. Superhydrophobic Modification Fails to Improve the Performance of Small Diameter Expanded Polytetrafluoreoethylene Vascular Grafts *Biomaterials* **2002**, *23*, 255-262.
(21) Khorasani, M. T.;Mirzadeh, H. In Vitro Blood Compatability of Modified Pdms Surfaces as Superhydrophobic and Superhydrophilic Materials *J. Appl. Polym. Sci.* **2003**, *91*, 2042-2047.
(22) Chen, W.;Fadeev, A. Y.;Hsieh, M. C.;Oner, D.;Youngblood, J.;McCarthy, T. J. Ultrahydrophobic and Ultralyophobic Surfaces: Some Comments and Examples *Langmuir* **1999**, *15*, 3395-3399.
(23) Oner, D.;McCarthy, T. J. Ultrahydrophobic Surfaces. Effects of Topography Length Scales on Wettability *Langmuir* **2000**, *16*, 7777-7782.
(24) Cassie, A. B. D.;Baxter, S. Wettability of Porous Surfaces *Trans. Faraday Soc.* **1944**, *40*, 546-551.
(25) Wenzel, R. N. Resistance of Solid Surfaces to Wetting by Water *Ind. Eng. Chem.* **1936**, *28*, 988-994.
(26) Wenzel, R. N. Surface Roughness and Contact Angle *J. Phys. Colloid Chem.* **1949**, *53*, 1466-1467.
(27) Morra, M.;Occhiello, E.;Garbassi, F. Contact Angle Hysteresis in Oxygen Plasma Treated Poly(Tetrafluoroethylene) *Langmuir* **1989**, *5*, 872-876.
(28) Shiu, J.-Y.;Kuo, C.-W.;Chen, P.;Mou, C.-Y. Fabrication of Tunable Superhydrophobic Surfaces by Nanosphere Lithography *Chem. Mater.* **2004**, *16*, 561-564.
(29) Feng, L.;Li, S.;Li, Y.;Li, H.;Zhang, L.;Zhai, J.;Song, Y.;Liu, B.;Jiang, G.;Zhu, D. Super-Hydrophobic Surfaces: From Natural to Artificial *Adv. Mater.* **2002**, *14*, 1857-1860.
(30) Lau, K. K. S.;Bico, J.;Teo, K. B. K.;Chhowalla, M.;Amaratunga, G. A. J.;Milne, W. I.;McKinley, G. H.;Gleason, K. K. Superhydrophobic Carbon Nanotube Forests *Nano Lett.* **2003**, *3*, 1701-1705.
(31) Zhai, L.;Cebeci, F. C.;Cohen, R. E.;Rubner, M. F. Stable Superhydrophobic Coatings from Polyelectrolyte Multilayers *Nano Lett.* **2004**, *4*, 1349-1353.
(32) Soeno, T.;Inokuchi, K.;Shiratori, S. Ultra-Water-Repellent Surface: Fabrication of Complicated Structure of Sio2 Nanoparticles by Electrostatic Self-Assembled Films *Appl. Surf. Sci.* **2004**, *237*, 543-547.
(33) Jisr, R. M.;Rmaile, H. H.;Schlenoff, J. B. Hydrophobic and Ultrahydrophobic Multilayer Thin Films from Perfluorinated Polyelectrolytes *Angew. Chem. Int. Ed.* **2005**, *44*, 782-785.

(34) Decher, G.;Hong, J. D.;Schmitt, J. Buildup of Ultrathin Multilayer Films by a Self-Assembly Process: Iii. Consecutively Alternating Adsorption of Anionic and Cationic Polyelectrolytes on Charged Surfaces *Thin Solid Films* **1992**, *210*, 831-835.
(35) Decher, G. Fuzzy Nanoassemblies: Toward Layered Polymeric Multicomposites *Science* **1997**, *277*, 1232-1237.
(36) Caruso, F.;Trau, D.;Mohwald, H.;Renneberg, R. Enzyme Encapsulation in Layer-by-Layer Engineered Polymer Multilayer Capsules *Langmuir* **2000**, *16*, 1485-1488.
(37) Qiu, X.;Leporatti, S.;Donath, E.;Mohwald, H. Studies on the Drug Release Properties of Polysaccharide Multilayers Encapsulated Ibuprofen Microparticles *Langmuir* **2001**, *17*, 5375-5380.
(38) Vazquez, E.;Dewitt, D. M.;Hammond, P. T.;Lynn, D. M. Construction of Hydrolytically-Degradable Thin Films Via Layer-by-Layer Deposition of Degradable Polyelectrolytes *Journal- American Chemical Society* **2002**, *124*, 13992-13993.
(39) Wood, K. C.;Boedicker, J. Q.;Lynn, D. M.;Hammond, P. T. *Tunable Drug Release from Hydrolytically Degradable Layer-by-Layer Thin Films,in Langmuir*Editor. **2005**, Published, 21 1603-1609.
(40) Berg, M. C.;Yang, S. Y.;Hammond, P. T.;Rubner, M. F. Controlling Mammalian Cell Interactions on Patterned Polyelectrolyte Multilayer Surfaces *Langmuir* **2004**, *20*, 1362-1368.
(41) Decher, G.;Lehr, B.;Lowack, K.;Lvov, Y.;Schmitt, J. New Nanocomposite Films for Biosensors - Layer-by-Layer Adsorbed Films of Polyelectrolytes, Proteins or DNA *Biosens. Bioelectron.* **1994**, *9*, 677-684.
(42) Elbert, D. L.;Herbert, C. B.;Hubbell, J. A. Thin Polymer Layers Formed by Polyelectrolyte Multilayer Techniques on Biological Surfaces *Langmuir* **1999**, *15*, 5355-5362.
(43) Mendelsohn, J. D.;Yang, S. Y.;Hiller, J.;Hochbaum, A. I.;Rubner, M. F. Rational Design of Cytophilic and Cytophobic Polyelectrolyte Multilayer Thin Films *Biomacromolecules* **2003**, *4*, 96-106.
(44) Yang, S. Y.;Mendelsohn, J. D.;Rubner, M. F. New Class of Ultrathin, Higly Cell-Adhesion-Resistant Polyelectrolyte Multilayers with Micropatterning Capabilities *Biomacromolecules* **2003**, *4*, 987-994.
(45) Yoo, D.;Shiratori, S. S.;Rubner, M. F. Controlling Bilayer Composition and Surface Wettability of Sequentially Adsorbed Multilayers of Weak Polyelectrolytes *Macromolecules* **1998**, *31*, 4309-4318.
(46) Shiratori, S. S.;Rubner, M. F. Ph-Dependent Thickness Behavior of Sequentially Adsorbed Layers of Weak Polyelectrolytes *Macromolecules* **2000**, *33*, 4213-4219.
(47) Mendelsohn, J. D.;Barrett, C. J.;Chan, V. V.;Pal, A. J.;Mayes, A. M.;Rubner, M. F. Fabrication of Microporous Thin Films from Polyelectrolyte Multilayers *Langmuir* **2000**, *16*, 5017-5023.
(48) Berg, M. C.;Zhai, L.;Cohen, R. E.;Rubner, M. F. Controlled Release from Porous Polyelectrolyte Multilayers **In Preparation**.
(49) Ahn, H.;Cohen, R. E.;Rubner, M. F. *Unpublished Work.*
(50) Hiller, J.;Mendelsohn, J. D.;Rubner, M. F. Reversibly Erasable Nanoporous Anti-Reflection Coatings from Polyelectrolyte Multilayers *Nat. Mater.* **2002**, *1*, 59-63.

(51) Zhai, L.;Nolte, A. J.;Cohen, R. E.;Rubner, M. F. Ph-Gated Porosity Transitions of Polyelectrolyte Multilayers in Confined Geometries and Their Application as Tunable Bragg Reflectors *Macromolecules* **2004**, *37*, 6113-6123.
(52) Zhai, L.;Berg, M. C.;Cebeci, F. C.;Kim, Y.;Milwid, J. M.;Cohen, R. E.;Rubner, M. F. Patterning Hydrophilic Domains on Superhydrophobic Surfaces Using Polyelectrolytes **In Preparation**.
(53) Pirrung, M. C. How to Make a DNA Chip *Angew. Chem. Int. Ed.* **2002**, *41*, 1276-1289.
(54) Orner, B. P.;Derda, R.;Lewis, R. L.;Thomson, J. A.;Kiessling, L. L. Arrays for the Combinatorial Exploration of Cell Adhesion *J. Am. Chem. Soc.* **2004**, *126*, 10808-10809.
(55) Whitesides, G. M. Imaging of Features on Surfaces by Condensation Figures *Science* **1993**, *260*, 647-649.
(56) Tadanaga, K.;Morinaga, J.;Matsuda, A.;Minami, T. Superhydrophobic-Suphydrophilic Micropatterning on Flowerlike Alumina Coating Film by the Sol-Gel Method *Chem. Mater.* **2000**, *12*, 590-592.
(57) Kim, H.-C.;Kreller, C. R.;Tran, K. A.;Sisodiya, V.;Angelos, S.;Wallraff, G.;Swanson, S.;Miller, R. D. Nanoporous Thin Films with Hydrophilicity-Contrasted Patterns *Chem. Mater.* **2004**, *16*, 4267-4272.
(58) Kim, H.-C.;Wallraff, G.;Kreller, C. R.;Angelos, S.;Lee, V. Y.;Volksen, W.;Miller, R. D. Photopatterned Nanoporous Media *Nano Lett.* **2004**, *4*, 1169-1174.
(59) Berg, M. C.;Choi, J.;Hammond, P. T.;Rubner, M. F. Tailored Micropatterns through Weak Polyelectrolyte Stamping *Langmuir* **2003**, *19*, 2231-2237.
(60) Hogt, A. H.;Dankert, J.;Feijen, J. Adhesion of Coagulase-Negative Staphylococci to Methacrylate Polymers and Copolymers *J. Biomed. Mater. Res.* **1986**, *20*, 533-545.
(61) Yang, S. Y.;Rubner, M. F. Micropatterning of Polymer Thin Films with Ph-Sensitive and Cross-Linkable Hydrogen-Bonded Polyelectrolyte Multilayers *J. Am. Chem. Soc.* **2002**, *124*, 2100-2101.
(62) Ladam, G.;Gergely, C.;Senger, B.;Decher, G.;Voegel, J.-C.;Schaaf, P.;Cuisinier, F. J. G. Protein Interactions with Polyelectrolyte Multilayers: Interactions between Human Serum Albumin and Polystyrene Sulfonate/Polyallyamine Multilayers *Biomacromolecules* **2000**, *1*, 674-687.
(63) Ngankam, A. P.;Mao, G.;Van Tassel, P. R. Fibronectin Adsorption onto Polyelectrolyte Multilayer Films *Langmuir* **2004**, *20*, 3362-3370.
(64) Gergely, C.;Bahi, S.;Szalontai, B.;Flores, H.;Schaaf, P.;Voegel, J.-C.;Cuisinier, F. J. G. Human Serum Albumin Self-Assembly on Weak Polyelectrolyte Multilayer Films Structurally Modified by Ph Changes *Langmuir* **2004**, *20*, 5575-5582.
(65) Decher, G.;Lehr, B.;Lowack, K.;Lvov, Y.;Schmitt, J. New Nanocomposite Films for Biosensors: Layer-by-Layer Adsorbed Films of Polyelectrolytes, Proteins or DNA *Biosens. Bioelectron.* **1994**, *9*, 677-684.
(66) Schwinte, P.;Ball, V.;Szalontai, B.;Haikel, Y.;Voegel, J.-C.;Schaaf, P. Secondary Structure of Proteins Adsorbed onto or Embedded in Polyelectrolyte Multilayers *Biomacromolecules* **2002**, *3*, 1135-1143.
(67) Thompson, M. T.;Berg, M. C.;Tobias, I. S.;Rubner, M. F.;Van Vliet, K. J. Quantifying the Role of Compliance in Cell Adhesion and Proliferation: Polyelectrolyte Multilayers as Mechanically Tunable Cell Substrata **Submitted to Biomaterials**.

(68) Wang, T. C.;Rubner, M. F.;Cohen, R. E. Polyelectrolyte Multilayer Nanoreactors for Preparing Silver Nanoparticle Composites: Controlling Metal Concentration and Nanoparticle Size *Langmuir* **2002**, *18*, 3370-3375.
(69) Clark, S. L.;Montague, M.;Hammond, P. T. Selective Deposition in Multilayer Assembly: Sams as Molecular Templates *Supramol. Sci.* **1997**, *4*, 141-146.
(70) Jiang, X.;Hammond, P. T. Selective Deposition in Layer-by-Layer Assembly: Functional Graft Copolymers as Molecular Templates *Langmuir* **2000**, *16*, 8501-8509.
(71) Brandley, B. K.;Schnaar, R. L. Covalent Attachment of an Arg-Gly-Asp Sequence Peptide to Derivatizable Polyacrylamide Surfaces: Support of Fibroblast Adhesion and Long-Term Growth *Anal. Biochem.* **1988**, *172*, 270-278.
(72) Choi, J.;Rubner, M. F. Influence of the Degree of Ionization on Weak Polyelectrolyte Multilayer Assembly *Macromolecules* **2005**, *38*, 116-124.

Chapter 7 Summary and Future Work

7.1. Thesis Summary

The main objective of this thesis was to research possible biomedical or biomaterial applications for weak polyelectrolyte multilayers. Since the assembly of these ultra-thin polymer films is based on aqueous processing, extremely versatile, applicable to many substrates, and mimic biology well, multilayers make excellent candidates as biomaterials. The ability to coat virtually any substrate with a sub-micron thick polymer film and completely change the surface properties of it is extremely powerful. Previous to this thesis work, it was found that polyelectrolyte multilayers could control the surface adhesion of mammalian cells. Interactions with the surface could be turned completely off with only a few layers. This thesis work builds on these findings, and it explores new areas of opportunity where the unique properties of polyelectrolyte multilayers can play an important role.

Patterning weak polyelectrolyte multilayers using polymer-on-polymer stamping was the first application pursued. This patterning technique, which is based on microcontact printing, has many advantages to traditional lithography since it is performed without the use of organic solvents, can be used on a variety of substrates, and can be designed as a parallel process. The goal of the work presented in Chapter 2 was to pattern PAH/PAA multilayer films with PAH when PAA was left as the top layer. This created a multi-functional surface in which chemistry could then be selectively performed in micron-scale regions. In addition, since PAH was used as the patterned polymer, the properties of the patterned region could be tuned through pH adjustments in the ink solution. When the pH of the PAH ink solution was increased, the pattern thickness and number of available functional groups increased due to the change in

polyelectrolyte charge density. This makes it possible to create micro-patterns with predetermined functional density and thickness.

In Chapter 3, the use of PAH patterned surfaces as platforms for creating cell arrays was explored. After stamping the surface of 3.0/3.0 PAA/PAAm multilayers with PAH, the amine groups were then reacted with the heterobifunctional crosslinker, sulfo-LC-SPDP, and later with peptides containing the sequence, RGD. This tri-peptide sequence is a known adhesion ligand for many cell types including the WT NR6 fibroblasts studied. By tuning the pH of the PAH ink and changing the density of amine groups in the patterned regions (as discussed in Chapter 2), the RGD density could also be controlled. The 3.0/3.0 PAA/PAAm multilayers were used as the background due to their ability to resist cell adhesion over long periods of time. It was found that higher RGD density correlated to a greater density of cells on the patterns and a more spread morphology. In addition, the cytoskeletal proteins became more organized with higher RGD density. This technique represents a versatile method to pattern cells onto a variety of substrate, and the cell patterns remained stable for as long as two months.

Besides using the surface of polyelectrolyte multilayers for biological applications, the interior of the thin films can also be useful. Porous polyelectrolyte multilayers made from PAH (pH = 8.5) and PAA (pH = 3.5) were loaded with model drugs, and the release kinetics were studied. The porosity of these multilayers could be controlled by treatment pH, and the pores ranged in size from nanoscale to microscale. Drug release from the microporous films followed Fickian diffusion. However, the nanoporous multilayers showed a zero-order release profile. The zero-order kinetics resulted from the drug being trapped in the nanoporous network that limited the amount of drug capable of release at a given time. Ketoprofen and cytochalasin D were chosen as model drugs because they differ greatly in hydrophobicity. For both drugs, the

time of release was proportional to the number of porous bilayers. In addition, cytochalasin D can be used as a marker for delivery to mammalian cells since it causes cell to take on a much different morphology and become multi-nucleated. All of the porous polyelectrolyte multilayers in the study successfully delivered cytochalasin D to fibroblasts.

The final application that this thesis evaluated was the ability to kill bacteria or resist their adhesion. The 3.0/3.0 PAA/PAAm polyelectrolyte multilayers, which were found to resist mammalian cell adhesion, reduced but did not eliminate bacterial adhesion. To kill bacteria, silver nanoparticles were loaded into the multilayers using an ion exchange with silver acetate and subsequent reduction in DMAB. The silver-loaded multilayers killed gram negative and gram positive bacteria on a level greater than 99.99% for both waterborne and airborne tests. It was also found that the amount of silver released into solution was so small that it was non-toxic to mammalian cells. The cytotoxicity tests were run by growing cells directly on the multilayers after functionalization with RGD, and also by transferring floating cells onto tissue culture polystyrene. Silver released into PBS from the multilayers for over three weeks with just one silver loading and only 3 bilayers.

The antifouling properties of superhydrophobic polyelectrolyte multilayer films were also tested for their ability to prevent the adhesion of bacteria. The superhydrophobic films were formed using porous polyelectrolyte multilayers and subsequent alternate adsorption of SiO_2 nanoparticles and PAH followed by functionalization with a semi-fluorinated silane. The advancing and receding contact angles for these films both exceeded 170°. The multilayer films eliminated protein adsorption and prevented the adhesion of both fibroblasts and bacteria. Protein adsorption was studied by comparing fluorescence intensities of multilayers after immersion in either FITC labeled BSA or FITC labeled lysozyme. NR6 WT fibroblasts could

not attach to the superhydrophobic surface, as could be seen using fluorescent microscopy after staining live and dead cells. For the bacteria experiments, both gram negative Escherichia coli and gram positive Staphylococcus epidermidis were studied. In a waterborne assay, neither was able to attach to the surface. For the airborne assay, colonies were found to grow in the agar placed on the superhydrophobic samples unless the samples were rinsed after the bacteria spray. Superhydrophobic polyelectrolyte multilayers have a great deal of promise as anti-fouling surfaces for long term applications, especially since they do not rely on an agent leaching out of the film.

Although these biological applications may seem very different, they all used the same materials, polyelectrolyte multilayers. In fact, only a few polymers were used for all of these applications. By simply changing the assembly conditions or post-assembly treatment, the properties of the films could be changed drastically. Due to the versatility of these ultra-thin polymer films, the possibilities for polyelectrolyte multilayers seem limitless. Some of the possible future directions will be discussed in the next section.

7.2. Future Directions

Due to the versatility of polyelectrolyte multilayers, there are many directions which can be pursued in the area of biomaterials. Using polyelectrolyte multilayers as a resistant background for patterning mammalian cells has many possibilities. Since the multilayers can be assembled on thin coverslips or other clear materials, this patterning technique makes an excellent candidate for studying cells using confocal microscopy at very high magnification. Studying patterned cells has many implications for learning how cells communicate and behave in relation to other cells. Pattern made of thiols on gold would have much more difficulty with

this application. In addition, the long term stability of the cell patterns lends itself well to studying primary neuron patterns or other cell types that need long culture times.

Drug delivery from porous polyelectrolyte multilayers is another very promising application. This thesis researched small molecule drug delivery, which has potential for delivery of many anti-cancer compounds. The zero-order manner in which the multilayers release drugs is very desirable for sustained release in vivo and for basic drug research. Another future direction for polyelectrolytes is the local delivery of growth factors and proteins. Many of the principles of small molecule delivery from porous polyelectrolyte multilayers could be used for delivering macromolecules. A coating that delivers proteins to cells on the surface has applications for in-dwelling medical devices and in vitro cell culture. Delivery of drugs from an implant surface could signal specific cells or influence cells' phenotypes. This kind of localized drug delivery could either promote or inhibit specific tissue growth around the implant. For studying cells in vitro, protein delivering surfaces have potential for studying dosage effects of drugs or delivering specific growth factors to cells. These types of materials would eliminate the need to inject the compounds and would eliminate spikes in concentration.

Of the applications discussed in this thesis, antibacterial coatings have perhaps the most commercial potential. Killing or eliminating bacterial adhesion is important for medical implants, medical equipment, the food industry, industrial piping, and even household items. Catheters are a class of medical implants that could greatly benefit from antibacterial coatings. They have a high bacterial infection rate and must be replaced frequently due to this problem. Superhydrophobic coatings are particularly interesting for this application because the lifetime of such a coating is theoretically limitless since it does not rely on a finite supply of a compound leaching out of the film. Besides indwelling medical devices, other potential applications for

fouling resistant superhydrophobic multilayers include industrial piping and equipment. Biofilm build-up is a major problem in most industrial processes, and causes many health and product quality problems. However, to be of use in these applications, the long-term antibacterial properties of both the silver-loaded and superhydrophobic multilayers needs to be studied and quantified. This includes studying the silver-ion release from multilayers and biofilm formation. Finally, the properties of silver-loaded/superhydrophobic multilayers need to be characterized since these films combine two very favorable qualities. In addition, polyelectrolyte multilayers could be functionalized with other broad spectrum antibacterial compounds to expand their functionality.